INFORMATION TO USERS

This manuscript has been reproduced from the microfilm master. UMI films the text directly from the original or copy submitted. Thus, some thesis and dissertation copies are in typewriter face, while others may be from any type of computer printer.

The quality of this reproduction is dependent upon the quality of the copy submitted. Broken or indistinct print, colored or poor quality illustrations and photographs, print bleedthrough, substandard margins, and improper alignment can adversely affect reproduction.

In the unlikely event that the author did not send UMI a complete manuscript and there are missing pages, these will be noted. Also, if unauthorized copyright material had to be removed, a note will indicate the deletion.

Oversize materials (e.g., maps, drawings, charts) are reproduced by sectioning the original, beginning at the upper left-hand corner and continuing from left to right in equal sections with small overlaps.

Photographs included in the original manuscript have been reproduced xerographically in this copy. Higher quality 6" x 9" black and white photographic prints are available for any photographs or illustrations appearing in this copy for an additional charge. Contact UMI directly to order.

Bell & Howell Information and Learning
300 North Zeeb Road, Ann Arbor, MI 48106-1346 USA
800-521-0600

PURIFICATION AND CRYSTALLIZATION OF RECOMBINANT PORINS FROM *HAEMOPHILUS INFLUENZAE* TYPE B

by

Alpesh Patel

Department of Microbiology and Immunology
McGill University
Montreal, Québec, Canada

July, 1999

A thesis submitted to the Faculty of Graduate Studies and Research in partial fulfillment of the requirements for the degree of Master of Science

Abstract

M.Sc. **Alpesh Patel** **Microbiology and Immunology**

The major surface-exposed, pore-forming protein in the outer membrane (OM) of *Haemophilus influenzae* type b (Hib) is porin (341 amino acids; M_r 37,782 Da). Porins form water filled channels and allow the diffusion of small hydrophilic solutes up to 1400 Da including nutrients and small antibiotics across the OM. The crystal structures of porins solved to date indicate a conserved motif of a barrel composed of 16 anti-parallel β-strands.

Molecular genetic techniques were used to introduce a hexahistidine tag into surface-exposed loops, loop 4 and loop 8, of Hib porin. Loop 4 was modified by addition of nine amino acids including six consecutive histidine residues following Val-174. Loop 8 was modified by splicing seven amino acids including six consecutive histidines following Thr-321. Plasmids harboring the mutant porins were transformed into a strain of *H. influenzae* deleted for the wild-type *ompP2* gene.

The mutant porins, designated OmpP2.H6(L4) and OmpP2.H6(L8), were purified by metal chelate chromatography using Ni-NTA superflow and POROS 20 MC media. Both recombinant proteins were demonstrated by SDS-PAGE and silver staining to be free of contaminating proteins and lipooligosaccharide. Biophysical analyses by planar lipid bilayer experiments identified their channel forming behavior. OmpP2.H6(L4) showed an increased median single channel conductivity of 1.05 nS. Similarly, the average single channel conductance of OmpP2.H6(L8) was determined to be 1.15 ns; the value for wild-type OmpP2 is 0.85 nS. Preparations of OmpP2.H6(L8) and OmpP2.H6(L4) were detergent exchanged into a variety of non-denaturing detergents. OmpP2.H6 preparations were analysed by dynamic light scattering and the preparations were monodisperse. Crystallization trials of proteins in various detergents using sparse matrix screening solutions (Hampton Research) identified islands of crystallization. Two morphologies of crystals of OmpP2.H6(L8) were observed

following optimization of growth conditions: (i) parallelpiped and (ii) hexagonal bipyramid. X-ray radiation of the parallelpiped crystals resulted in reflections to 8Å. The hexagonal bipyramid crystals did not diffract X-rays.

Abrégé

M.Sc. **Alpesh Patel** **Microbiologie et Immunologie**

La protéine majeure formant un pore dans la membrane externe de *Haemophilus influenzae* type b (Hib) est la porine de 341 acides aminés, 37 782 daltons. Les porines forment des canaux permetant la diffusion jusqu'à une masse moléculaire de 1400 daltons de petites solutés hydrophiliques incluants les antibiotiques, a travers la membrane externe. La structure moléculaire crystale des porines resoluts indiquent un motif conservé de 16 brins β antiparallèles traversant la membrane externe relié par huit longues boucles du coté extérieur et de sept petites boucles du coté periplasmique.

Les techniques de biologie moléculaire furent employées pour introduire une étiquette hexahistidinique dans les boucle éxposées à la surface de porine de Hib. Afin de modifier la quatrième boucle neuf acides aminés dont six histidine consécutives furent inserés après Val-174. La huitième boucle fut modifiée en inserant sept acides aminés, dont six histidines consécutives après Thr-321. Une souche de *Haemophilus influenzae* dont le gène chromosomale de porine a été déleter fut transformée avec des plasmides exprimant les porines mutantes.

Les porines mutantes de Hib, OmpP2.H6(L4) et OmpP2.H6(L8), ont été purifiées par la méthode de "metal-chelate chromatography en utilisant les milieux: Ni^{2+}-NTA Superflow at POROS MC 20. L'analyse par SDS-PAGE des deux prépartions de porines mutantes purifiées démontrerent qu'elles furent dépourvues de toute protéine ou lipooligosaccharide contaminant.

Analyses biophysiques des porines mutantes à l'aide d'expériences de membranes lipidiques planes ont identifié leur comportement de canal. La conductance moyenne d'un canal unique de OmpP2.H6(L4) fut établie à 1,05nS et celle d'un canal unique de OmpP2.H6(L8) à 1,15nS. La conductance moyenne de la protéine native, OmpP2, fut établie à 0,85nS. L'analyse par "dynamic light scattering" des préparations de porines mutantes démontra qu'elles furent monodisperse.

Les préparations de OmpP2.H6(L4) et de OmpP2.H6(L8) furent soumises à une variétés de détergents non-dénaturants suivi d'essaies de crystallization. Ces éssaies ont permis l'identification de conditions permetant la croissance de crystaux de OmpP2.H6(L8) et deux type de morphologie: paralellpiped et bipyramide héxagonale. Des analyse des crystaux par radiation de rayons X au synchrotron ont montré des réflection à 8 Å de résolution pour les crystaux de morphologie de parallelpiped. Les crystaux de morphologie de bipyramide hexagonale n'ont pas réflechi de rayon X.

ACKNOWLEDGEMENTS

Foremost I would like to acknowledge my thesis supervisor, Dr. James W. Coulton, for providing an environment conducive to the execution of academic research. I owe him sincere thanks for the encouragement, support, and expectation of nothing less than the best.

Drs Alice Vrielink and Wolfram Welte eased my transition into their respective laboratories.

The members of the Coulton laboratory past and present are in my debt for their technical assistance, stimulating discussions and making my time in the Coulton lab unforgettable. They are Dr. Francis Arhin, Dr. Greg Moeck, Dr. David Dahan, Andrew Ferguson, Mark Arbing, Francisco Ferreira, Jennifer Wang, Raymond Lee, Wei Sun, Marty Teltscher, Chris Topham, Parinaz Aliahamad, William Hsiao, Sofia Shames, and Nassim Amiali.

I would like to thank Felix Sieder for computer support.

Mark Arbing is acknowledged for performing the single channel conductance experiments on recombinant Hib porins. Sofia Shames and William Hsiao deserve special thanks for their editorial assistance in the preparation of this thesis. I would also like to acknowledge Madani Thiam and Leonie Mikael for their assistance to translate the Abstract into French.

I am indebted the members of the Vreilink laboratory, in particular, Darcy Kohls, Paula Lario, Jaime Cheah, and Dr. Bijan Sobel-Ahvazi for their stimulating discussion and technical assistance.

I am grateful to all members of the Department of Microbiology and Immunology, McGill University for their support.

Finally I would like to express my gratitude to my parents and my sisters for their encouragement and support.

The financial support from the Medical Research Council, Canada and the NATO International Collaborative Research Award (research grants to Dr. Coulton) is gratefully acknowledged.

TABLE OF CONTENTS

List of Table and Figures

List of abbreviations

Å	-	angstrom
cm	-	centimetre
Da	-	dalton
°C	-	degrees Celsius
DNA	-	deoxyribonucleic acid
K	-	Kelvin
kDa	-	kilodalton
kb	-	kilobase-pair
µm	-	micrometre
µM	-	micromolar
µl	-	microlitre
mm	-	millimetre
mM	-	millimolar
mg	-	milligram
ml	-	millilitre
mV	-	millivolt
mS	-	millisiemens
min	-	minute
M	-	molar
OD_x	-	optical density at λ=x nanometres
rpm	-	revolutions per minute
rRNA	-	ribosomal ribonucleic acid
ng	-	nanogram
nS	-	nanosiemen
w/v	-	weight per volume
w/w	-	weight per weight

Literature Review

1. The Gram-negative cell envelope

Three distinct layers form the Gram-negative cell envelope (Fig. 1). They are the outer membrane (OM), the periplasm and the cytoplasmic membrane (CM).

The innermost layer of the envelope is the CM. The CM acts as the true osmotic barrier for bacteria. It is a symmetric lipid bilayer; both the inner and outer leaflets are formed of phospholipids. Interspersed within the CM are integral membrane proteins. They include proteins of the respiratory chain that participate in electron transport and generate a proton gradient resulting in a membrane potential across the CM with the periplasm being acidic relative to the cytoplasm.

The periplasm, also referred to as the periplasmic space, contains two non-proteinaceous polymer species; they are peptidoglycan and membrane derived oligosaccharide (MDO). The periplasm also contains a variety of binding proteins necessary for escorting nutrients imported across the OM to their CM receptors for final transport into the cytoplasm. Peptidoglycan confers shape and rigidity to bacteria. Without peptidoglycan, the hydrostatic pressure across the CM would cause cell lysis in hypoosmotic environments. The peptidoglycan layer is a network of covalently linked glycopeptide strands. In *Escherichia coli*, the glycopeptide or murein strand is a polymer of the aminosugars N-acetylglucosamine and N-acetylmuramic acid. Tetrapeptide branches originate from the N-acetylmuramic acid consisting of L-alanine, glutamic acid, diaminopimelic acid, and a terminal D-alanine. Adjacent murein strands are linked by a covalent bond between the diaminopimelic acid residue of one tetrapeptide and the terminal D-alanine of another tetrapeptide. In *Haemophilus influenzae* the terminal D-alanine of the tetrapeptide may be absent or substituted by glycine, aspartic acid, or serine in the murein monomers. The degree of cross-linkage between murein strands ranges from 23% for *E. coli* to 32% for *Bordetella pertussis*. A value of 27% was observed for *H. influenzae*

Fig. 1. Molecular representation of the Gram-negative cell envelope. Hexagons represent sugar residues and ovals depict phospholipid head-groups.

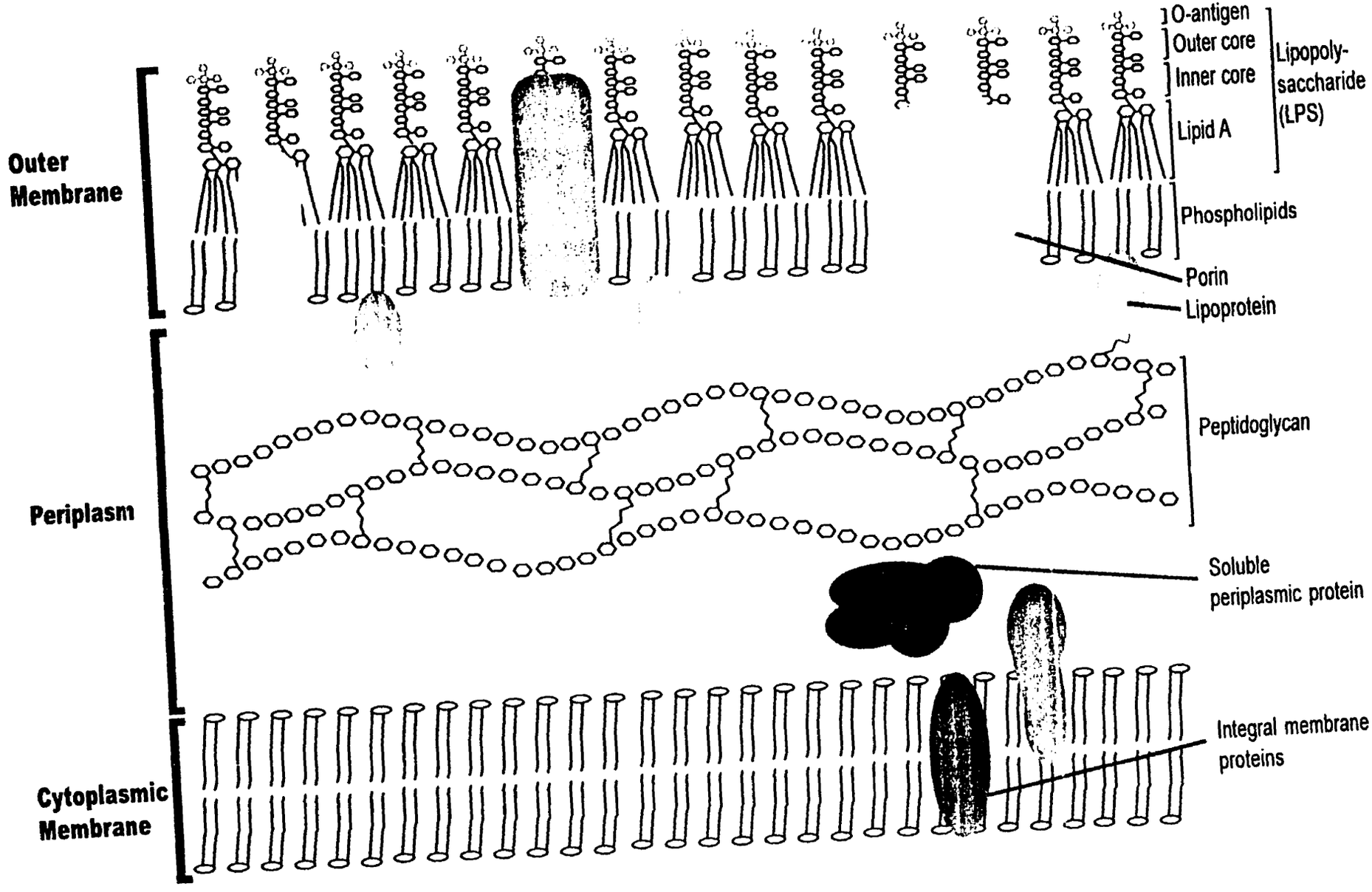
Outer Membrane
Periplasm
Cytoplasmic Membrane
O-antigen
Outer core
Inner core
Lipid A
Lipopoly-saccharide (LPS)
Phospholipids
Porin
Lipoprotein
Peptidoglycan
Soluble periplasmic protein
Integral membrane proteins

(Burroughs *et al.*, 1993). The most external component of the cell envelope is the OM. The OM functions to regulate the flux of solutes between the external environment and the interior of the cell, thus acting as a molecular sieve. It is an asymmetric lipid bilayer; the lipid portion of the outer leaflet is composed exclusively of lipopolysaccharide (LPS) while the lipid portion of the inner or periplasmic leaflet is composed of traditional lipids such as phosphotidylethanolamine or phosphotidylglycerol and cardiolipin (Batley *et al.*, 1982).

Additional layers sometimes surround the OM of Gram-negative bacteria. These can include polysaccharide capsules or S layers composed of protein (Hancock *et al.*, 1991).

2. Outer membrane structure and constituents

2.1. Lipopolysaccharides

Lipopolysaccharide (LPS) is an amphiphilic molecule composed of two or three components that are covalently linked. From the hydrophobic end to the hydrophilic end the components are the lipid A group, the core oligosaccharide, and the O-polysaccharide chain. The lipid A group is composed of six or seven acyl chains linked by ester and amide bonds to a diglucosamine. The core oligosaccharide is subdivided into the inner core comprising 3-deoxy-D-*manno*-octulosonic acid (KDO) molecules linked to a series of heptose sugars followed by the outer core consisting of a series of generally three glucoses branched with a galactose and a N-acetylglucosamine. Distal to the membrane interface is the O-polysaccharide. It is composed of a variable number of identical oligosaccharide subunits that can number from 20 to 30 repeats. Recently the molecular structure of LPS from *E. coli* strain K-12 lacking the repeating O-antigen subunits was solved (Ferguson *et al.*, 1998). The number of repeating O-antigen subunits is significantly less in *H. influenzae* resulting in the lipooligosaccharide (LOS) nomenclature.

2.2. Outer membrane proteins

The OM of Gram-negative bacteria contains numerous proteins. They account for approximately 50% (w/w) of the OM composition (Benz, 1994). Five major outer membrane proteins (OMPs) whose molecular masses vary from 30 kDa to 50 kDa are present in the OM of *E. coli.* These major OMPs number approximately 100,000 copies per cell. They include proteins that are required for bacterial conjugation or that stabilize the outer membrane such as OmpA of *E. coli* (Schweizer and Henning, 1977; Sonntag *et al.*, 1978). Other major OMPs form pores in the OM such as OmpF, OmpC, and PhoE of *E. coli* (Nikaido and Vaara, 1985) while others such as lipoprotein anchor the outer membrane to the peptidoglycan. The lipid portion of the lipoproteins is inserted into the OM on the periplasmic side and approximately one third of lipoproteins are covalently linked to the peptidoglycan (Braun, 1975). In *Haemophilus influenzae* type B (Hib), the five major proteins are P1, 46 kilodaltons (kDa); P2, 38 kDa; P4, 28 kDa; P5, 34 kDa; and P6, 15 kDa. When the five major OMPs of Hib were assayed for pore activity, only the P2 protein displayed channel characteristics (Vachon *et al.*, 1985). Researchers have since referred to protein P2 (OmpP2) as porin. OmpP2 (341 amino acids; M_r 37 782 daltons) is the most abundant protein in the OM of Hib and accounts for 20% of the total outer membrane protein content.

In addition to the major OMPs, many minor OMPs are present and they can number up to 10,000 copies per cell. They include proteins responsible for the export of toxins such as TolC, specific porins such as LamB and Tsx of *E. coli*, and ScrY of *Salmonella typhimurium.* Additionally there are proteins termed active transporters such as FhuA, FepA, and BtuB of *E. coli.*

3. Transport across the OM

3.1. Outer membrane permeability

The OM is impermeable to a variety of solutes. Considering solely the lipid content of the OM, the close packing of the LPS acyl chains, much more densely than can be obtained for glycerol phospholipids restricts the permeability of the OM to hydrophilic permeants (Nikaido and Vaara, 1985). In addition, the

acidic sugar, KDO, and the numerous phosphates of the inner core of the LPS molecule near the membrane surface have been found to associate very strongly with cations resulting in a complex salt bridge network that prevents the permeation of hydrophobic solutes (Lugtenberg and van Alphen, 1983). Mutations that change the structure of LPS or the addition of agents such as EDTA that chelate divalent cations disrupt the ionic bonding network of LPS. Such treatments were demonstrated to make the OM more permeable to hydrophobic compounds (Hancock *et al.*, 1994). The elaboration of LOS on the outer leaflet of the OM by *H. influenzae*, which has a decreased amount of the O-polysaccharide repeating subunits, explains the increased sensitivity of Hib to hydrophobic antibiotics (Hancock and Bell, 1988).

3.2. Solute transport

The selective permeability properties of the OM are imparted by a collection of OMPs. Hydrophilic substances can gain access to the periplasm through channel forming proteins of the OM in one of three pathways. Transport can occur via general channels, specific channels, and active transporters.

Transport via general channels occurs with no energy expense. Solutes that access the periplasm via these protein channels do so along their concentration gradient. OmpC, OmpF, and PhoE of *E. coli* and OmpP2 of Hib form non-specific channels. These channels allow the passive diffusion of solutes below the molecular mass the exclusion limit, which is dictated by the diameter of the pore constriction, into the periplasm. The constriction zone is not simply circular; the shape of the solute and interactions that may occur between the pore wall and the solute also affects solute permeability (Jap and Walian, 1996). Porins of different bacterial species have exclusion limits that range from 600 Da to 5000 Da (Welte *et al.*, 1995). The rate of solute transport showed a linear relationship with solute concentration for these non-specific channels (Schirmer, 1998).

Transport across the OM via specific-porins also occurs independent of energy input powered only by the concentration gradient of solutes. Examples of specific channels include LamB and Tsx of *E. coli*, ScrY of *S. typhimurium*, and

OprB of *Pseudomonas aeruginosa*. The specificity of these channels allows for transport of their substrates at low substrate concentrations.

Active transporters move large compounds that cannot permeate via porins and environmentally limiting compounds that are essential for bacterial metabolism into the periplasm. They include FhuA and BtuB of *E. coli* (Nikaido, 1994). The active transporters utilize energy provided by the cytoplasmic membrane protein TonB and can therefore translocate solutes against their concentration gradient.

Some OMPs are constitutively expressed while others are regulated by environmental signals or physiological signals (Nikaido, 1994). Expression of specific channels is induced by the presence of substrate while the expression of the active transporters is induced by low intracellular concentrations of the nutrient. The expression of non-specific channels from some bacterial species such as OmpC and OmpF of *E. coli* are regulated while other non-specific channels such as OmpP2 of Hib are constitutively expressed.

4. Porin function

4.1. Selectivity

Porins can be classified as general channels or specific channels. Examples of general porins include OmpF, OmpC and PhoE of *E. coli* (Nikaido, 1992), OmpP2 from Hib (Vachon *et al.*, 1985), Omp32 from *Comomonas acidovorans* (Gerbl-Rieger *et al.*, 1992), OprP from *Pseudomonas aeruginosa* (Siehnel *et al.*, 1988), and porins from *Rhodobacter capsulatus* (Schiltz *et al.*, 1991), *Rhodopseudomonas blastica* (Kreusch *et al.*, 1994) and *Paracoccus denitrificans* (Hirsch *et al.*, 1995). Slightly cation selective porins include OmpF and OmpC of E. coli, OmpP2 from Hib (Vachon *et al.*, 1986), and porin from *R. blastica*. Porin from *R. capsulatus* is moderately cation selective. Anion selective porins include PhoE and Omp32. Porin from *P. denitrificans* displayed no ionic selectivity. The ionic selectivity of porins results from the charged cluster of amino acid side chains found at their external mouth (Jap and Walian, 1996). Succinylation of solvent accessible lysine residues of *R. capsulatus* porin altered

ionic selectivity substantially towards cation selectivity compared to native protein (Przybylski *et al.*, 1996). In a different approach, a point mutation that changed Lys-125 to Glu in PhoE also changed the selectivity from anionic to cationic (Bauer *et al.*, 1989)

Specific porins form channels that facilitate the diffusion of specific substrates: LamB for maltose and maltodextrins, Tsx for nucleosides, and ScrY for sucrose (Schmid *et al.*, 1982). Binding sites for substrates have been identified within the channel (Schirmer *et al.*, 1995; Maier *et al.*, 1988; Forst *et al.*, 1998). These specific porins have a lower single channel conductivity and their rate of transport of substrate follows Michaelis-Menten kinetics. The binding sites allow a flux 100 fold greater for specific substrates in comparison to the flux of other small hydrophilic molecules (Freundlieb *et al.*, 1988; Trias *et al.*, 1989).

4.2. *In vivo* assays

The diffusion of compounds via porins from the external environment into the periplasm can be studied in several ways. The uptake of radio-labeled substrates into the cell (Sonntag *et al.*, 1978) is one method. Another method to study diffusion via porins *in vivo* is the growth of bacteria on defined substrates that are the only source of an essential nutrient; and finally measuring the susceptibilities of bacteria to several antibiotics (Capobianco and Goldman, 1994). Comparison of these measurements among different bacterial species is not possible due to differences in the types and number of porins expressed by different species of bacteria. The growth conditions under which the experiments are performed can also have an effect as the expression of some porins is regulated by environmental conditions. Point mutations enable the analysis of the role of specific amino acid residues. During analysis of mutated porins, it may not be clear if the mutation also changes the cellular physiology in addition to channel properties. Transport of the solute across the CM can also be modified in response to alterations in the periplasmic concentration of solutes.

Porin-deficient, antibiotic-resistant mutants have been isolated from several Gram-negative bacteria. Examples include *E. coli* mutants deficient for OmpF and OmpC porins that displayed resistance to cefazolin and moxolactam

(Jaffé *et al.*, 1983), *S. typhimurium* mutants deficient in OmpC porin that showed resistance to cephalexin (Medeiros *et al.*, 1987), and *Serratia marcescens* mutants deficient in the 41 kDa porin that showed resistance to β-lactams (Goldstein *et al.*, 1983). β-lactam resistant *H. influenzae* isolates from cystic fibrosis patients that had altered OmpP2 permeability were also characterized (Regelink *et al.*, 1999).

4.3 *In vitro* analysis

Analysis of purified porins by sodium dodecylsulfate-polyacrylamide gel electrophoresis (SDS-PAGE) revealed, in many cases, a very high molecular mass species that was approximately three times the mass of a porin monomer. The high molecular mass species was no longer visible when samples were boiled prior to SDS-PAGE suggesting a trimeric association of porins under native conditions (Reid *et al.*, 1988). Similar results were not obtained for Hib porin. Hib porin trimers were only detected by SDS-PAGE when the porin sample was cross-linked prior to electrophoretic separation (Vachon *et al.*, 1988).

A variety of *in vitro* techniques are used to study pore function. One method measures the efflux of radiolabelled solutes from proteoliposomes reconstituted from lipids and purified porins (Nakae, 1975). Using this method, the molecular mass exclusion limits of OmpF, OmpC and PhoE porins from *E. coli* were calculated to approximately 600 Da (Jap and Walian, 1996) while the exclusion limit for Hib porin was calculated to approximately 1400 Da (Vachon *et al.*, 1985).

Another method is the liposome-swelling assay (Nikaido and Rosenberg, 1983). Reconstituted liposomes are prepared such that they contain a large molecular weight dextran (20 to 40 kDa) unable to permeate through the porins. These liposomes scatter light and exhibit high optical density. The reconstituted liposomes are then diluted into a solution containing dextran (isotonic with respect to the lumen of the liposomes) and a test sugar. If the sugar is able to enter the liposomes via the porins, then water will follow the solutes into the liposomes to correct for the different osmotic pressure within the liposomes. The resultant swelling of liposomes can be detected as a decrease in optical density.

Measurements are taken for 10 seconds after mixing the liposomes in the test sugar solution. The initial rate of swelling corresponds to the rate of solute permeation. Using the Renkin equation (Renkin, 1954), the effective diameter of the OmpF pore was estimated to be 1.1 nm (Nikaido and Rosenberg, 1983) and the effective diameter of the pore formed by Hib porin was estimated to be 1.8 nm (Vachon *et al.*, 1988). This method is considered more informative than measuring the efflux of radio-labelled solutes as it determines the relative rates of diffusion of a series of sugars.

The third method measures the conductivity of ions through porin channels in planar lipid bilayer (Benz *et al.*, 1978). The planar lipid bilayer or black lipid membrane apparatus consists of a chamber separated by a teflon sheet. An aperture in the teflon sheet connects the two (*cis* and *trans*) sides of the chamber, each containing an electrode. The chamber is filled with an electrolyte solution and lipids are painted onto the aperture. Lipid bilayer formation is indicated by the field turning optically black when viewed through a microscope. Purified protein sample is added to the *cis* side of the chamber and this is followed by the application of a voltage at the *cis* electrode (10 to 100 mV), which permits porins and other membrane proteins to insert into the bilayer. If the inserted proteins form channels, ions flow through the pores in response to the potential difference. The flux of ions across the pore is detected as current and can be measured by electrodes connected to an amplifier in series with an analog to digital converter. Analog to digital conversion of the data allows it to be stored digitally.

The readout for single channel conductances appears as a stepwise increase of the measured current. For classical bacterial porins each step corresponds to the insertion of a porin trimer. Hib porin, however, inserts into the lipid bilayer as monomers so the calculated conductance does not need to be divided by three. A possible explanation is that during purification Hib porin trimers dissociate into monomers. After many measurements (400 insertions), one arrives at a mean single channel conductivity measurement for the tested porin.

The single channel conductivity of monomers of OmpF porin of *E. coli*, *R. capsulatus* porin, and Hib porin in 1M KCl electrolyte solution were reported as 0.8 nS (Benz *et al.*, 1979), 1.1 nS (Benz, 1994), and 0.85 nS (Dahan *et al.*, 1994), respectively. It was proposed that the higher conductance of *R. capsulatus* porin compared to OmpF porin from *E. coli* reflects the larger diameter of the pore formed by *R. capsulatus* porin (Cowan *et al.*, 1992; Weiss *et al.*, 1991a). The larger diameter proposed for porin from *R. capsulatus* by the single channel conductance results correlates with the higher exclusion limit that ranges from 1000 to 2000 Da for this protein (Jap and Walian, 1996). Almost identical single channel conductance values for Hib porin and OmpFfrom *E. coli*, however, does not correlate with the significantly larger exclusion limit found of 1400 Da for Hib porin. These discrepancies illustrate the inability to correlate the flux of monatomic ions with pore diameters.

5. Structure of porins

5.1 Primary structure

The amino acid sequences of many Gram-negative bacterial porins are known including those from the following genera: *Escherichia, Klebsiella, Salmonella, Neisseria, Bordetella, Chlamydia, Comomonas, Haemophilus, Rhodobacter, Rhodopseudonmonas, Pseudomonas*. The primary sequences indicate that the molecular mass of porin monomers range from 30 kDa to 50 kDa (Jap and Walian, 1990). DNA sequences also show the presence of a 20-30 amino acid N-terminal signal sequence, which targets the nascent porin polypeptides to the OM. The primary amino acid sequence of porins indicates these proteins to be more polar than some water-soluble proteins. As well, the sequences do not contain long stretches of hydrophobic amino acids that arrange themselves as α-helices as observed in cytoplasmic membrane proteins. The primary sequences show stretches of amino acids whose side chains alternate from hydrophobic character to hydrophilic character. This amphipathic character is required to form β-strands able to span the OM.

Comparison of the porin sequences from Gram-negative bacteria showed the absence of significant similarities. Porin sequences from the same species (OmpC, OmpF, and PhoE of *E. coli*), from the same genus (class 3 porin from *Neisseria meningitidis* and porin PIA from *N. gonorrhoeae*), and from related organisms (OmpC from *E. coli* and OmpC from *Salmonella typhimurium*), however, do show sequence similarities (Jeanteur *et al.*, 1994). The similarity among porin sequences is in agreement with the phylogenetic relationships derived from 16S rRNA analyses.

5.2. Secondary and tertiary structure

Spectroscopic analyses employing circular dichroism (CD) and Fourier transformed infrared spectroscopy (FTIR) are used to probe the secondary structure of proteins. These tests revealed that 50% to 60% of porin secondary structure was composed of β-sheets. The remaining 40% to 50% of the secondary structures were unidentifiable (Eisele and Rosenbusch, 1990; Nabedryk *et al.*, 1988). The predicted secondary structure of β-sheets also suggested these proteins to be highly polar in contrast to the α-helices of most other membrane proteins (Schulz, 1996).

The secondary structure of porins has also been predicted by computer algorithms (Jeanteur *et al.*, 1994). The predictions showed 16 amphipathic (alternating hydrophilic-hydrophobic) membrane-spanning β-strands for the non-specific porins and 18 amphipathic membrane-spanning β-strands for the specific porins with adjacent strands connected by loops. Together, the β-strands and loops could form β-barrels in the OM. The amphipathic character of the β-strands would be responsible for their stability in the hydrophobic environment of the OM. The hydrophilic side chains were proposed to face the water-filled lumen of the pore while the hydrophobic side chains are believed to be in contact with the acyl chains of lipopolysaccharide and phospholipids of the OM.

The predicted secondary structures of OMPs can be experimentally tested in several ways. Antigenic determinants of porin can be mapped (Klebba *et al.*, 1990). Alternatively proteoliposomes made with lipids and the OMP in question can be subjected to limited proteolysis. Peptides can be purified and identified

allowing identification of surface accessible cleavage sites (Goldshleger *et al.*, 1995). Foreign epitopes can also be inserted into proteins followed by epitope localization (Charbit *et al.*, 1991). These experiments allow the discrimination of surface exposed regions from buried regions thus providing information regarding the topology of porins.

β-barrels composed of antiparallel β-sheets were predicted to be the tertiary structure of porins. Adjacent β-strands that form the β-barrel were predicted to be linked by short stretches of amino acid residues called turns on the periplasmic side and connected by longer stretches of amino acid residues termed loops on the exterior side. Hydrophobic residues of the membrane-spanning β-strands were proposed to face the hydrophobic environment of the lipid acyl chains. The β-strands were subsequently found to be inclined 20 to 40° relative to the normal of the OM.

5.3. High resolution structures

High resolution structure of porin from *R. capsulatus* was solved to 1.8 Å (Weiss *et al.*, 1991b). Molecular structures at atomic resolution of the general porins OmpF and PhoE porins from *E. coli* (Cowan *et al.*, 1992), *Rhodopseudomonas blastica* porin (Kreusch and Schulz, 1994), and *Paracoccus denitrificans* porin (Hirsch *et al.*, 1997) followed. These seminal achievements (Fig. 2) contributed greatly to our knowledge of porins. Given the high structural similarities of porins for which crystal structures had been solved, one could then construct some homology-derived scaffold for porins of unknown structure (Srikumar *et al.*, 1997). Preliminary crystallization of OmpC from *E. coli* showed substantially different crystallization conditions and crystal packing as compared to OmpF, despite high amino acid sequence homology (Kim, 1998). Common features among the solved structures include a β-barrel arrangement of 16 anti-parallel β-strands connected by long loops on the extracellular side and short turns on the periplasmic side. The crystal structure of general porins shows that loop 3 is folded into the channel lumen. Crystal structures of the specific porins LamB of *E. coli* (Schirmer *et al.*, 1995) and ScrY of *S. typhimurium* (Forst *et al.*, 1998) show a β-barrel arrangement consisting of 18 anti-parallel β-strands.

Fig. 2. Ribbon representaion of porin structures. Monomer of (A) *Rhodobacter capsulatus* porin, (B) *Rhodopseudomonas blastica* 37b4 porin, and (C) *E. coli* OmpF/PhoE porin are shown viewed from the trimer axis to the trimer perimeter. Arrows represent the 16 β-strands and coils represent the α-helices. Diagrams are oriented such that the periplasmic face is below. (Reproduced with permission from Welte *et al.*, 1995.)

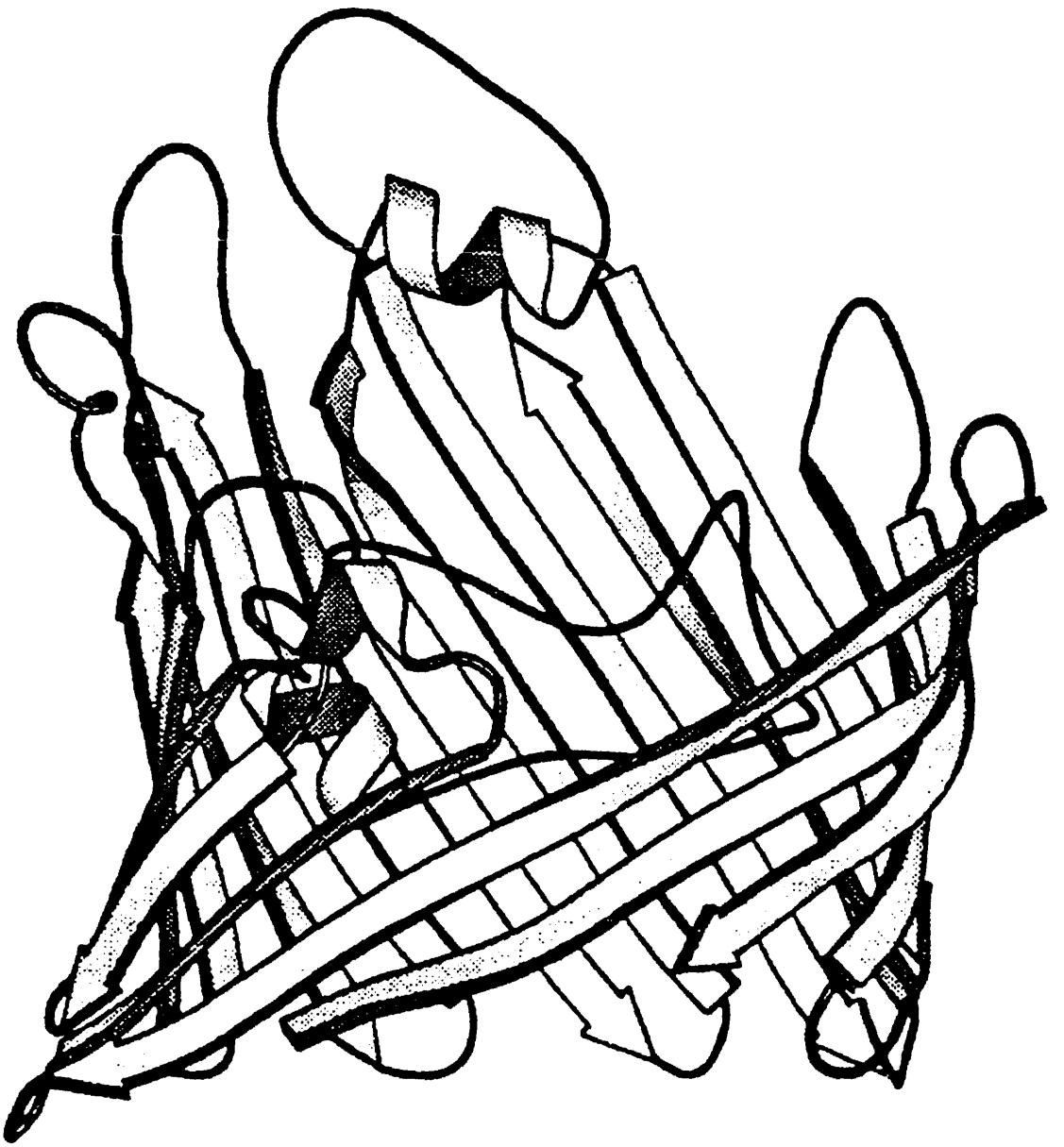

A

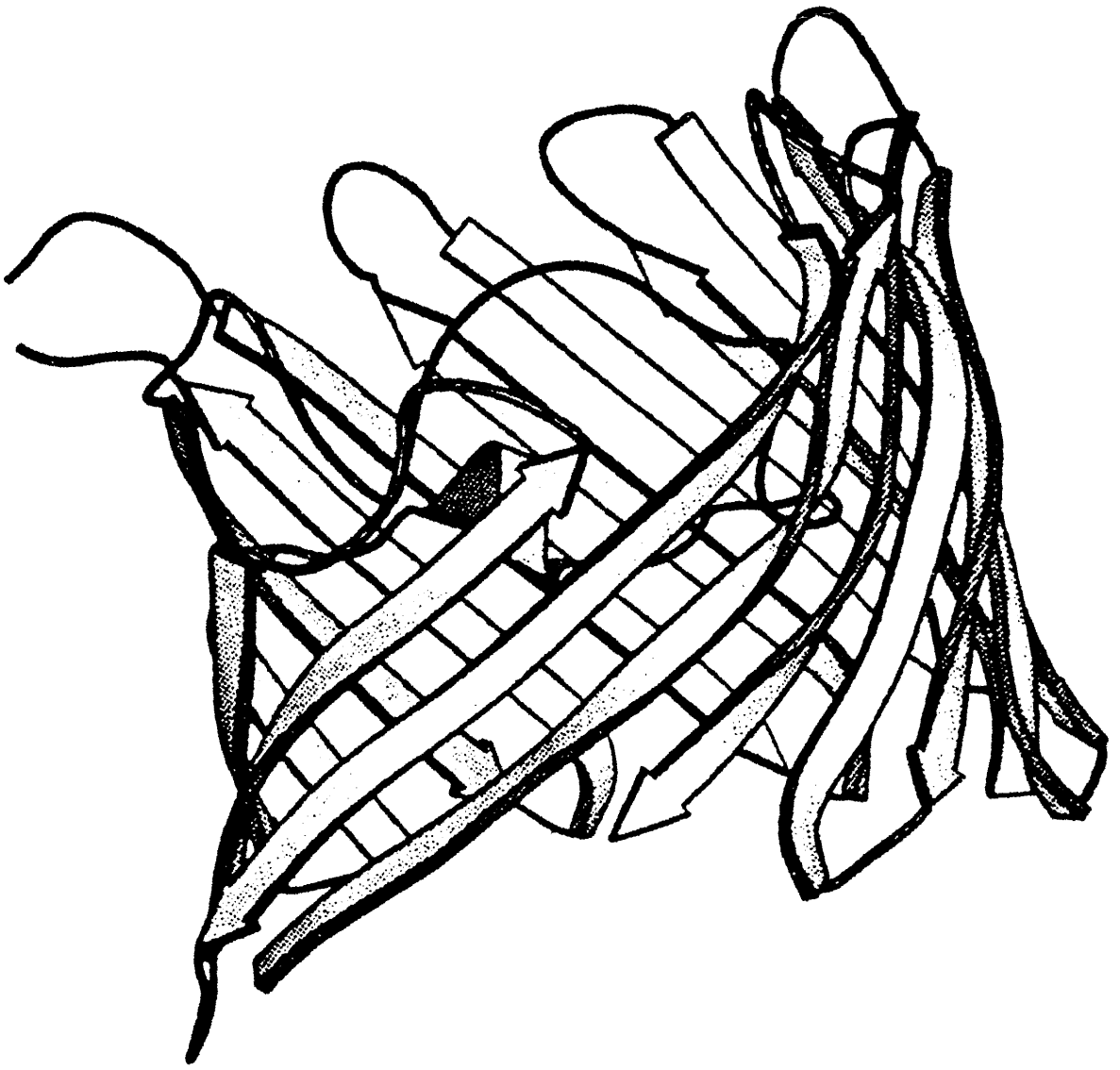

B

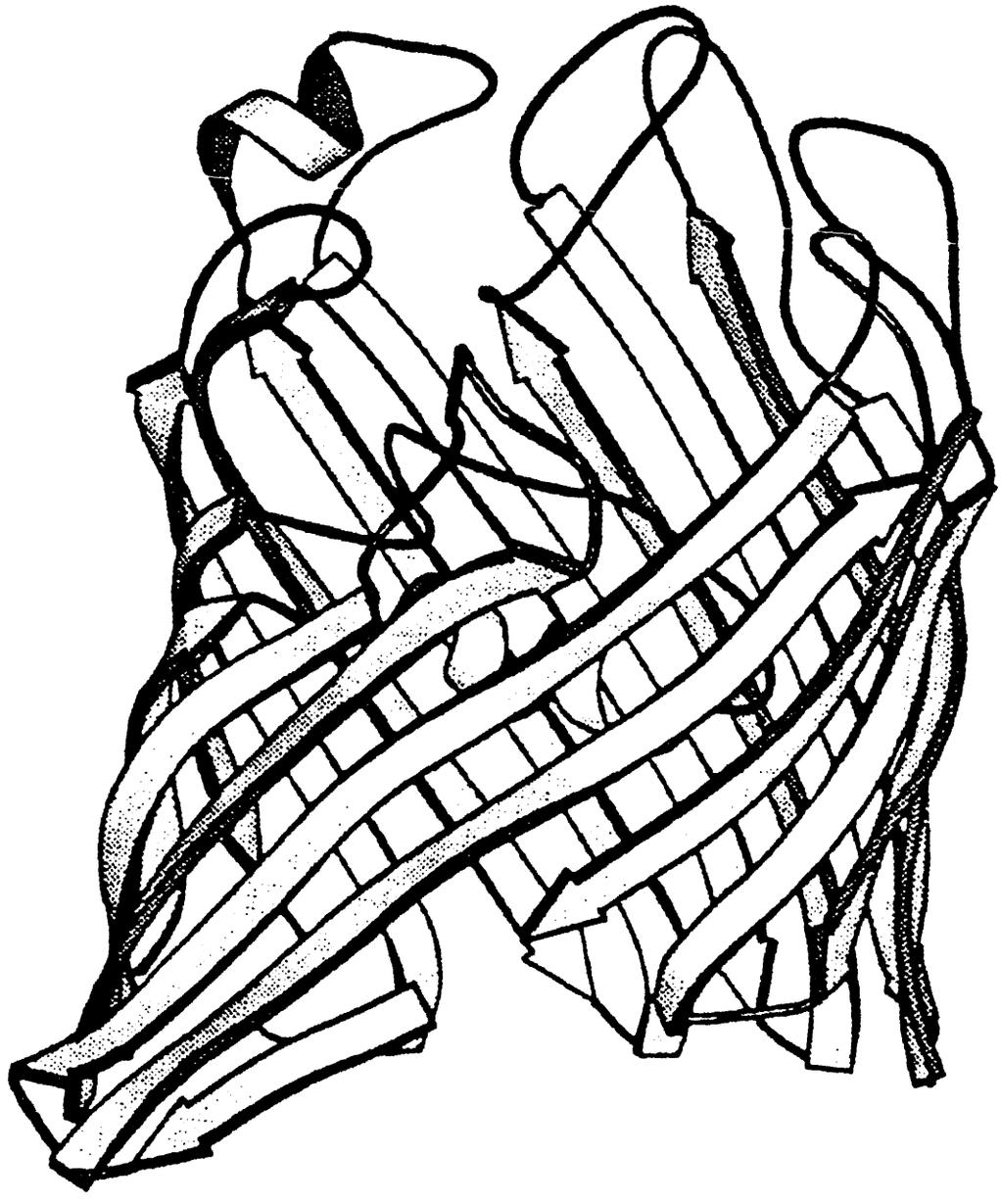

C

These structures are in agreement with the secondary structure predictions using computer algorithms (Schirmer and Cowan, 1993). Unique to specific porins is that three of the nine loops on the extracellular side were folded into the pore lumen. Barrels of both general and specific porins are comprised of β-strands that are inclined 30-40° with respect to the barrel axis. The high-resolution structures of porins and other proteins that form β-barrels in the OM of bacteria show a unique and distinguishing feature. Two belts of aromatic amino acids circumscribe β-strands near the hydrophobic-hydrophilic interfaces of the lipid bilayer (Fig. 3). It was recently proposed that this motif acts to anchor OMPs in the OM (Ferguson *et al.*, personal communication).

6. Structures of other classes of bacterial OMPs

Recently the atomic structures of some other OMPs were elucidated. The crystal structure FhuA of *E. coli*, an iron-siderophore receptor that actively transports ferrichrome-iron in an energy dependent manner (Schoffler and Braun, 1989) was solved (Ferguson *et al.*, 1998; Locher *et al.*, 1998). The carboxy-terminal residues (161 to 723) of FhuA form a 22-stranded β-barrel while the amino-terminal residues (1 to 160) form a four-stranded mixed β-sheet that folds into a cork that occludes the channel formed by the barrel (Ferguson *et al.*, 1998; Locher *et al.*, 1998). The transmembrane domain of OmpA (amino acids 1-171) was also solved at high resolution (Pautsch and Schulz, 1998); the structure showed that it did not form a water-filled channel. The crystal structure of OmpA171 revealed that the amino-terminal residues were arranged as eight anti-parallel β-strands that form a β-barrel. The carboxy-terminal residues (172 to 325) were suggested to provide a binding site for peptidoglycan to anchor it to the OM (Pautsch and Schulz, 1998). OmpA was previously considered to be a porin due to its ability to allow slow diffusion of solutes (Sugawara and Nikaido, 1992). The OmpA homologue in *P. aeruginosa*, OprF, was also shown to have channel-forming properties (Nikaido *et al.*, 1991). OprF allows diffusion of larger solutes in comparison to the *E. coli* porins and could be purified as an active monomer. Both OmpA and OprF were originally assigned to a new class of

Fig. 3. Ribbon diagram of *Rhodobacter capsulatus* porin viewed from the trimer perimeter to the trimer axis. Aromatic amino acid side chains are accentuated by ball and stick representation. They emphasize the upper and lower aromatic belts. (Reproduced with permission from Welte *et al.*, 1995.)

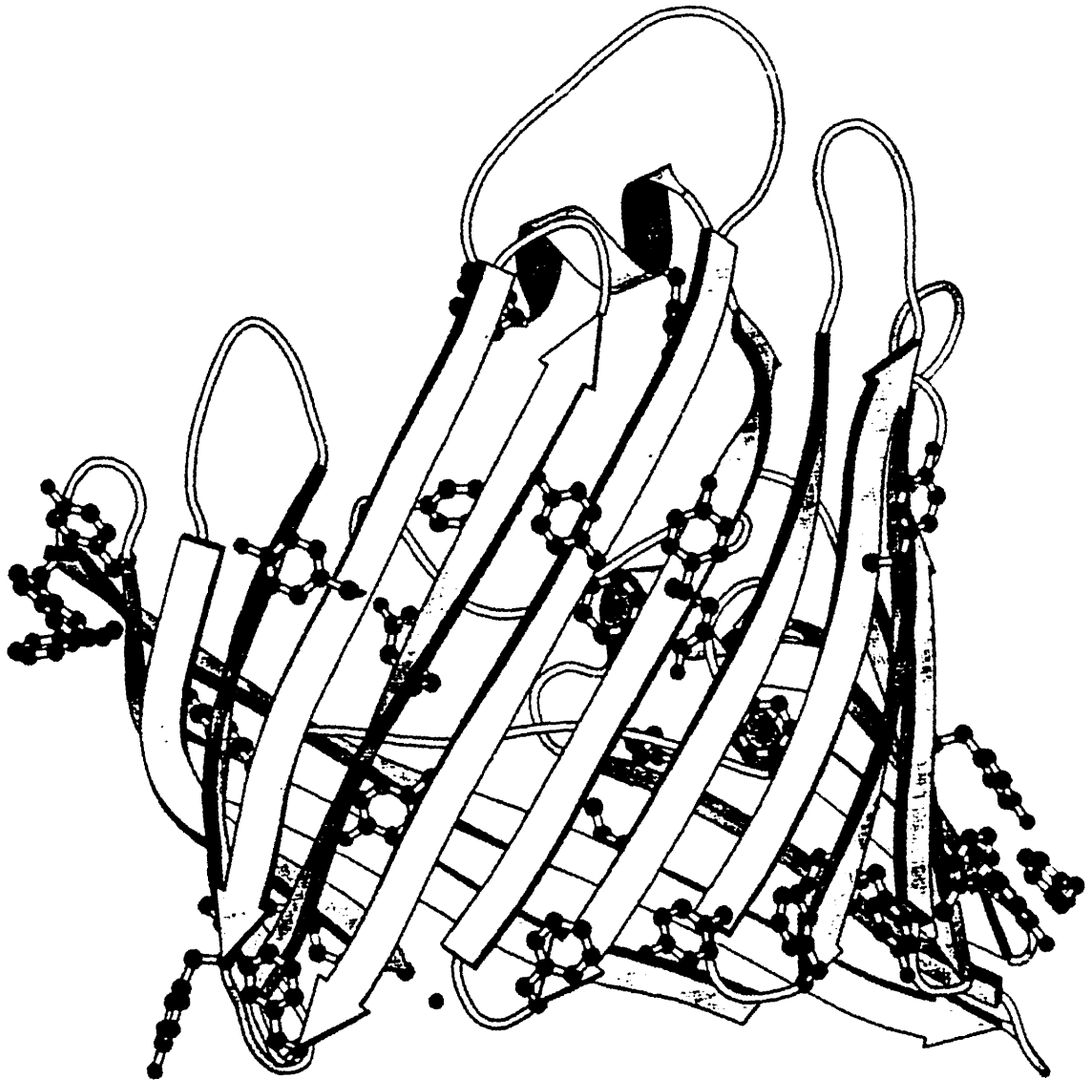

monomeric porins (Nikaido, 1993). Both FhuA and OmpA form β-barrels although neither acts as a general or a specific porin (Locher *et al.*, 1998; Pautsch and Schulz, 1998). In summary, bacterial outer membrane proteins have as their hallmark a β-barrel structure and the barrels have 8, 16, 18 or 22 anti-parallel β-strands.

7. Non-bacterial porins

Mitochondria and plastids are eukaryotic organelles that possess a bimembranous envelope similar to the Gram-negative cell envelope. In contrast to Gram-negative bacteria, both the inner membrane and OM of these organelles are composed of phospholipids. The OM of mitochondria and plastids were observed to be porous membranes (Wojtczak, 1974). Large general diffusion pores were identified in mitochondrial outer membranes; they were termed mitochondrial porins. The mitochondrial porins, formerly known as voltage dependent anion channels have many similar features with the bacterial porins but have much larger pores evident from their measured exclusion limit of 4000 Da to 5000 Da. Porins were also identified in the OM of colourless plastids called leucoplasts. These porins have a molecular mass exclusion limit of approximately 10,000 Da (Fischer *et al.*, 1994). Both, mitochondrial and leucoplast porins appear to have structural similarity with the bacterial porins but lack sequence similarity. The identification of porins in the OM of mitochondria and leucoplasts supports the endosymbiotic hypothesis regarding the evolutionary relationship between bacteria and the cellular organelles.

Another class of porins that can only be permeated by water, carbon dioxide and glycerol are termed aquaporins. They are structurally quite different from the bacterial porins. The topology of aquaporin1 (AQP1) protein, formerly referred to as CHIP28, from red blood cell membranes was determined by FTIR analysis to lack β-structure and contain α-helices. The secondary structure confirmed by electron diffraction experiments revealed AQP1 tetramers with individual subunits composed of six transmembrane α-helices (Agre *et al.*, 1998). The aquaporins are not limited to the red cell membranes. Other members of the

aquaporin family are expressed in a large range of tissues including the eyes, the lungs, and the kidneys. Homologs have also been identified in insects (Beuron *et al.*, 1995), plant roots (Weig *et al.*, 1997), frog skin (Abrami *et al.*, 1995) and *E. coli* (Calamita *et al.*, 1998).

8. X-ray crystallography

8.1. Properties and Uses

X-ray crystallography has proven useful in elucidating the three-dimensional structure of soluble proteins. The use of aqueous systems to generate X-ray quality crystals has enabled the growth of many soluble protein crystals. Growth of X-ray quality crystals of membrane proteins was impeded due to the instability of membrane proteins in aqueous systems. In the absence of a hydrophobic environment provided by membrane lipids, membrane proteins quickly precipitate out of solution. A breakthrough occurred in 1980 when X-ray quality crystals of bacteriorhodopsin (Michel and Oesterhelt, 1980), and OmpF of *E. coli* (Garavito and Rosenbusch, 1980) were finally grown. Although a high-resolution structure of bacteriorhodopsin derived from electron microscopy existed (Henderson and Unwin, 1975), researchers wanted to confirm the equivalence of X-ray and electron microscopic structures. Preliminary moderate-resolution structural information for OmpF derived from X-ray crystallography followed (Garavito *et al.*, 1983). This was superseded by the crystallization and structure determination of photosynthetic reaction centers from *Rhodopseudomonas viridis* (Deisenhofer *et al.*, 1984) and *Rhodobacter sphaeroides* (Allen *et al.*, 1987). The addition of surfactants such as detergents or lipids to membrane protein purification was crucial for applying the classical crystallization techniques devised for soluble proteins in the context of membrane proteins. The first three-dimensional structure of porin was obtained from the phototrophic bacterium *Rhodobacter capsulatus* (Nestel *et al.*, 1989)

8.2. Crystallization requirements

Extensive studies by membrane protein crystallographers have shown three major criteria necessary for the successful crystallization of membrane

proteins. The first criterion is based on experimental observation that extramembranous surfaces must be sufficiently abundant to allow stable crystal contacts. Membrane surfaces protected by detergent molecules are too fluid to participate in forming a stable crystallization contact. Proteins with larger extramembranous surfaces have more accessible surfaces for crystal contacts. However, they are also believed to be much more flexible. Although such proteins might crystallize in a manner similar to soluble proteins, there is no evidence that proteins with small extra-membranous surfaces would crystallize less readily with delicate manipulation in a detergent environment (Garavito and Picot, 1991). The second criterion deals with the association of integral membrane proteins with the lipid bilayer, in particular the nature of the transmembrane segments. The presence of extramembranous regions on both sides of the macromolecule to promote growth of three-dimensional crystals is an essential crystallization requirement (Garavito and Picot, 1991). The final criterion deals with protein preparation. An absolute requirement for undertaking crystallographic experiments is large amounts of homogeneous protein free of any other contaminating species. Factors that may introduce chemical heterogeneity including genetic variability and post-translational modification must be removed. Post-translational modification is a concern when working with eukaryotic proteins and can be ignored when working with bacterial proteins. Over-expression of the protein of interest in a genetically defined system is achieved by cloning the protein encoding DNA sequences in a high copy plasmid downstream of a bacterial promoter sequence. The resultant plasmid can be introduced into competent *E. coli*. Homogeneity of the protein preparation is maintained by purification from a clonally derived bacterial culture. Although post-translational modification of eukaryotic proteins is not be maintained by expression in *E. coli*, all protein molecules will be identically synthesized satisfying a prerequisite to commence crystallization trials. The absence of post-translational modification such as glycosylation may however prevent correct folding of the nascent polypeptide and give rise to the incorrect crystal structure.

A eukaryotic expression system would be required for correct post-translational modification.

Overexpression of soluble proteins in non-homologous hosts is generally successful; however overexpression of membrane proteins results in some difficulties due to their targeting to membranes by specific signal sequences. Overexpression of the desired protein can result in accumulation in inclusion bodies, which are aggregates of denatured protein. The harsh detergent treatment required to extract proteins from inclusion bodies normally results in denaturing the protein of interest. Refolding of proteins may result in misassembly and conformational heterogeneity, which will prevent successful crystallization of diffraction quality crystals. Membrane protein samples cannot be stored at -20°C, since they will denature as a result. Hence storage of membrane protein preparations is only possible at 4°C. However, long-term storage at 4°C should be avoided since it can result in proteolysis and introduce further heterogeneity to the sample. Protein preparations can be tested for their physical heterogeneity by dynamic light scattering (DLS). DLS will determine whether macromolecule preparations are monodisperse. Monodispersity is indicated if all molecules in the sample have a molecular mass extrapolated by the DLS instrument confined to statistically reasonable range. The extrapolated mass is derived from the calculated physical size of proteins. DLS analysis of protein preparations has become an indispensable tool to measure sample homogeneity and predisposition to form crystals (Ferré-D'Amaré and Burley, 1994). To avoid long purification protocols of membrane proteins that contribute to chemical and physical heterogeneity, a rapid purification strategy is required. A purification protocol that yields large amounts of homogeneous protein in four to six days is preferable to the classical protocols that approached three weeks due to the multiple chromatography steps required to deplete all undesirable species of proteins and LPS from the preparation.

Introduction to conducted research

Haemophilus influenzae is a Gram-negative bacterium that was responsible for invasive disease in North America for several decades (Ward *et al.*, 1982). *H. influenzae* is the causative agent for bacterial meningitis, septicemia, epiglottitis, cellulitis, arthritis, osteomyelitis, pericarditis, and pneumonia (Turk, 1982). *H. influenzae* can be serologically typed into a series of serotypes (a through f) based on differing antigenicity of polysaccharide capsules (Sikkema and Murphy, 1992).

Infections due to Hib are more serious than infections caused by other serotypes of *H. influenzae*. Studies in the 1970s and 1980s showed that 1 out of 200 children contracted Hib disease by age 5 (Broome, 1987). Peak rates of Hib infection occur in infants 6 to 11 months old (Wenger *et al.*, 1990) and 60% to 70% of all invasive disease occurred in children aged <18 months. Hib disease typically manifests itself as bacterial meningitis (up to 60%), epiglottitis (15% to 30%) and a small fraction as arthritis. Three to six per cent of all children with invasive Hib disease died as a result of the infection while up to 25% of meningitis survivors suffered long term consequences, commonly as hearing loss or more seriously in the form of mental retardation (Wenger, 1998).

Prior to introduction of Hib conjugate vaccines 10 000 to 20 000 cases of serious Hib disease including meningitis were reported in Canada and the United States (U.S.) annually. Hib disease levels fell by more than 95% in 1995 compared to the pre-vaccine levels of 1988 (Wenger, 1998) following the widespread introduction of the Hib conjugate vaccines. The vaccines are composed of the capsular polysaccharide polyribosylribitol phosphate (PRP) conjugated to immunogenically active proteins (Decker and Edwards, 1998). The decrease in Hib disease was attributed to herd immunity apparent by the decreased rate of nasopharyngeal carriage of Hib in children from 3-7% to 0.2% (Mohle-Boetani *et al.*, 1993). Public health officials insist that the elimination of the remaining incidence of Hib disease in both the U.S. and Canada can be achieved by pursuing a stronger vaccination effort. The effort should be directed to underprivileged populations that previously received inadequate immunization

coverage. Nevertheless, antibiotics were a part of treatment for children who had active Hib infection. Currently however, treatment of Hib and other pathogenic bacteria with antibiotics has become less effective due to the development of multidrug-resistant bacteria (Seki *et al.*, 1999; Dominguez and Pallares, 1998).

Porins from Gram-negative bacteria are outer membrane proteins that contribute to the selective permeability properties of the OM. They form aqueous channels that permit the non-specific diffusion of small molecules such as sugars, amino acids, nucleosides, and hydrophilic antibiotics into the periplasm. Porins also allow the diffusion of toxic metabolites from the periplasm to the external environment. Porins are arranged in the OM as trimers although the pore-forming activity of porin monomers was also identified. The molecular mass exclusion limit is defined as the maximum size of solute that can freely diffuse through the water-filled channel formed by porins. Exclusion limits for different porins vary between the bacterial genera.

Examination of the available complete gene sequence of *H. influenzae* strain Rd identified 1,743 putative open reading frames in the chromosome (Fleischmann *et al.*, 1995). Due to the similarities of porin sequences within genera, the *ompP2* gene was found to encode the unique porin in *Haemophilus* strains. Hib porin allows the non-specific diffusion of solutes up to an exclusion limit of 1400 Da with a slight preference for cations. It is expressed at high levels independent of bacterial culture conditions (Loeb and Smith, 1982). A genetically modified Hib strain unable to express OmpP2 was rendered avirulent in the animal model of infection (Cope *et al.*, 1990).

The molecular architecture of Hib porin is not resolved to atomic resolution. Since hydrophilic antibiotics use porin to enter the periplasm, information on the molecular structure at atomic resolution will enable researchers to design novel antibiotics against Hib. High-resolution structural information of Hib porin may also explain certain differences that exist between the classical porins and Hib porin. First, the channel formed by Hib porin has a molecular mass exclusion limit of 1,400 Da, much higher than the exclusion limit of 600 Da for the *E. coli* porins: OmpF, OmpC, and PhoE. Despite this

difference, the structure of Hib porin identified by molecular modeling of its amino acid sequence onto the homology-derived structural scaffold of the porin family was shown to be very similar to OmpF of *E. coli* (Srikumar *et al.*, 1997). Secondly, unlike classical porins whose trimeric organization is disrupted only by boiling protein sample in SDS prior to SDS-PAGE, the trimeric organization of Hib porin was only disclosed by SDS-PAGE when protein was cross-linked prior to electrophoresis. Only high-resolution structural information would provide the necessary information to explain these unique features of Hib porin biochemistry and function.

The secondary structure model of Hib porin (Fig. 4) shows transmembrane β-strands connected at the exterior surface by eight long loops and at the periplasmic face by seven short turns. Monoclonal antibody (mAb) reactivities in flow cytometry revealed loop 4 and loop 8 to be exposed at the cell surface (Srikumar *et al.*, 1992). Homology mapping of OmpP2 found that loop 3 is critical in forming the constriction loop. This constriction loop, alternatively termed the eyelet region, apparently limits the size and shape of solutes able to permeate the channel. Molecular modeling of Hib porin identified its structural similarities to OmpF of *E. coli* and disclosed a shorter length of loop 3 and a longer length of loop 4 (Srikumar *et al.*, 1997).

Mutant Hib porin containing six or 12 amino acid deletions independently in loop 3 or in loop 4 were generated (Srikumar *et al.*, 1997). The mutant porins were purified in the same manner as wild type porin and reconstituted into planar lipid bilayers to test for channel formation. The single channel conductance measurements were compared to wild type Hib porin. Mutant Hib porin possessing a six amino acid deletion in loop 3 displayed a broad distribution of single channel conductance values, while deletions of 12 amino acids from the same loop destabilized the porin channel preventing the collection of useful data. By comparison, deletion of six or 12 amino acids from loop 4 of Hib porin resulted in an increased single channel conductance compared to wild type Hib porin. It was proposed that loop 4 of Hib porin, although surface-accessible, is oriented

Fig. 4. Secondary structure representation of OmpP2 from *Haemophilus influenzae* type b based on epitope mapping of surface exposed determinants, hydropathy predictions, and amino acid sequence alignment to OmpF porin of *E. coli* and the family of *H. influenzae* porins. Amino acids are identified by their single letter abbreviation. Hydrophilic amino acids are circled. Amino acids comprising transmembrane β-strand are shown within rectangles.

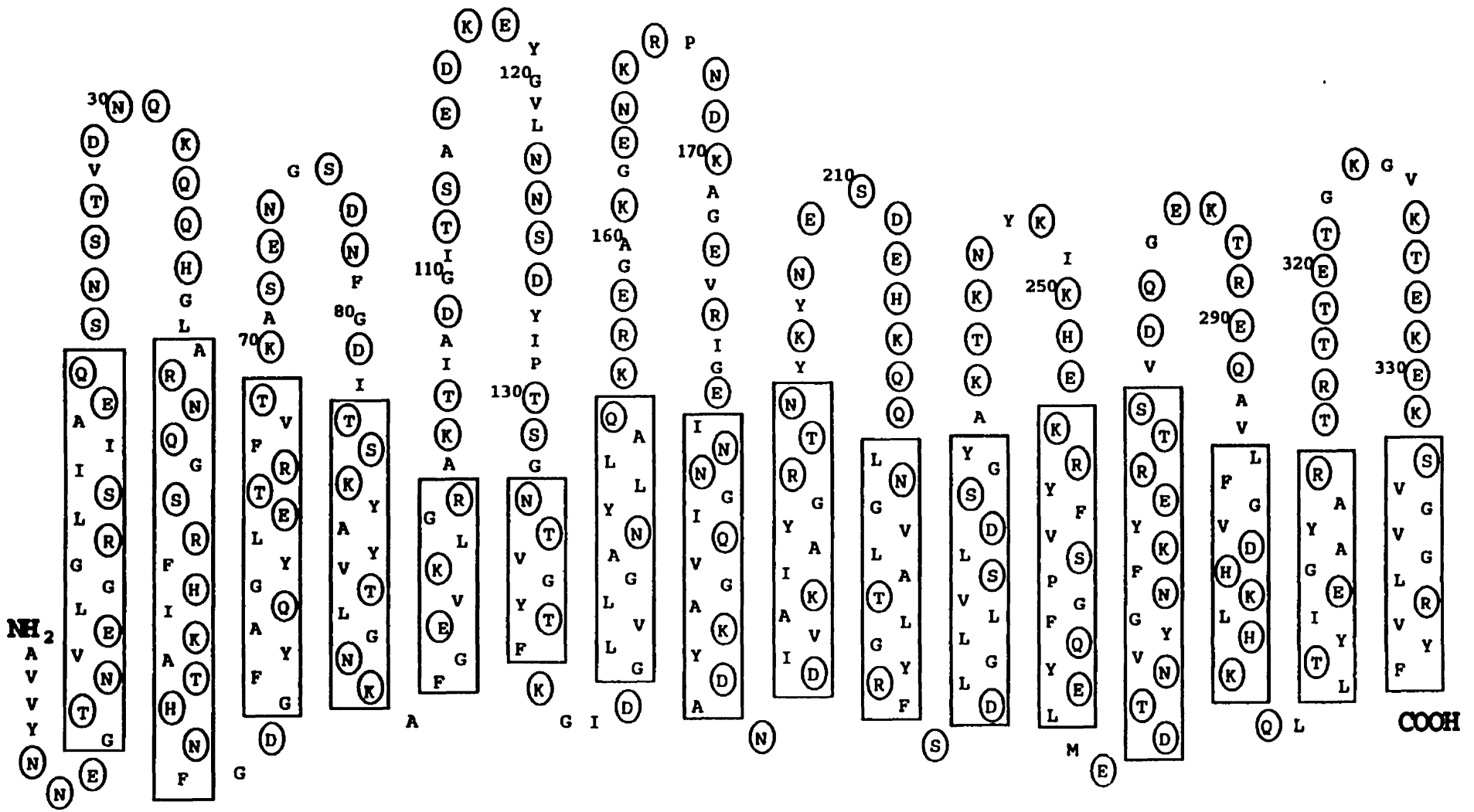
NH2
COOH

toward the central axis of the pore. Therefore, deletions in this loop could increase the single channel conductance by widening the pore entrance.

With the emergence of X-ray crystallography as the most powerful technology to probe the atomic structure of membrane proteins, its application to investigate the structure of OmpP2 becomes compelling. A prerequisite to initiate structural studies of a protein is a well-defined purification protocol. The purification must produce large quantities of approximately 100 mg of pure, homogeneous protein, free of contaminating substances.

Presented in this thesis are experiments designed to purify large amounts of homogeneous Hib porin. This material was then used to grow X-ray quality crystals.

The established purification protocol (Srikumar *et al.*, 1997) yields 100 mg amounts of Hib porin, mostly free of contaminating proteins. Crystals grown from these preparations produced X-ray diffraction, which extended to between 4 and 5 Å resolution (Coulton and Welte, personal communication). Evaluation of the long-established purification protocol identified steps that might have been injurious to maintaining native conformation of OmpP2. Based on the success of purifying FhuA.H6 from *E. coli* by affinity purification on Ni^{2+}-nitrolotriacetate (Ni^{2+}-NTA; QIAGEN) (Moeck *et al.*, 1996), the same procedure was advocated for Hib porin purification. This chromatographic technique requires the introduction of a hexahistidine affinity tag into OmpP2. Appropriate selection of sites for the introduction of hexahistidine tags included consideration of the molecular structures of other bacterial porins (Weiss *et al.*, 1991; Weiss *et al.*, 1991). Amino acid alignments of the porin sequences from several *H. influenzae* strains and Hib strains revealed that amino acid sequences varied maximally in loop 2, loop 4, loop 5 and loop 8 (Dajani *et al.*, 1979; Munson and Tolan, 1989; Sikkema and Murphy, 1992). Variation of amino acid sequences of OmpP2 in clinical isolates of non-typable *H. influenzae* are highest in surface exposed loops compared to the amino acid sequences correspoding to the β-strands. Because these loops are exposed at the cell surface, they would be predisposed to antigenic drift. The observed sequence divergence at these locations was

attributed to immune pressure indicating that sequence conservation in these loops was not essential to maintain the function and structure of porin. In addition, loop 4 and loop 8 in the OmpF crystal structure do not participate in the crystal contacts (Cowan *et al.*, 1992). Loop 4 and loop 8 of Hib porin were therefore targeted for molecular genetic incorporation of a hexahistidine affinity tag.

Materials and methods

Insertion of hexahistidine affinity tags into OmpP2 of Hib

Bacterial strains, plasmids, and growth conditions.

The strains and plasmids utilized in this project are listed in Table 1. *H. influenzae* strain DB117 is a recombination-deficient strain derived from KW20 (Setlow *et al.*, 1972). *H. influenzae* strain RSFA21 was generated by replacement of the chromosomal *omp*P2 gene from *H. influenzae* strain DB117 with a kanamycin resistance cassette (Srikumar *et al.*, 1997). *H. influenzae* strains were grown on chocolate agar plates or in brain heart infusion (BHI; Oxoid) broth supplemented with 1 mg•ml^{-1} of haemin and 10 mg•ml^{-1} of NAD^{+} (sBHI) at 37°C. Media for *E. coli* strains have been described (Sambrook *et al.*, 1989). Antibiotic concentrations used for the selection of chromosomal and plasmid markers after transformation and for propagation of *H. influenzae* and *E. coli* strains were 20 mg•ml^{-1} of kanamycin and 10 mg•ml^{-1} of tetracycline in solid medium. Selection of plasmid-encoded resistance in *E. coli* was achieved with 125 mg•ml^{-1} of ampicillin on solid medium. Antibiotic concentrations were halved for growth in liquid medium.

Gene cloning

The entire *ompP2* gene together with upstream and downstream sequences is contained in the shuttle vector pEJH39-1-35 (12.6 kb) as an *Eco*RI-*Pst*I fragment. The 1.1 kb *Pvu*II-*Ssp*I fragment of the coding region was excised by restriction endonuclease digestion and cloned into pBluescript SK (-) that had been digested with *Pvu*II. The resulting plasmid was termed pFFA02 (Srikumar *et al.*, 1997).

Molecular biology

Restriction endonuclease digestions, ligation and DNA manipulations were performed as described elsewhere (Sambrook *et al.*, 1989). *E. coli* strain DH5α and *H. influenzae* strains DB117 and RSFA21 were used as hosts for large scale isolation of plasmid DNA using the Plasmid Midi or Maxi Kit (QIAGEN). DNA was

TABLE 1

Bacterial strains, phages, and plasmids used in this study

Strain, phage, or plasmid	Relevant characteristics	Source or reference
E. coli strains		
DH5α	*supE44 ΔlacU169 (ϕ80 lacZΔM15) hsdR17 recA1 endA1 gyrA96 thi-1 relA1*	Bethesda Research Laboratories
CJ236	*dut1 ung1 thi-1 relA1*/pCJ105(*cam*^{r} F')	BIO-RAD
MV1190	Δ(*lac-proAB*) *thi supE* Δ(*srl-recA*)*306*::Tn*10*(*tet*^{r}) F' [*traD36 proAB lacI*^{q} *lacZΔM15*]	BIO-RAD
Haemophilus strains		
ATCC9795	Wild type Hib subtype 1H *ompP2*$^+$	(Vachon *et al.*, 1985)
KW20	Wild type Hi Rd *ompP2*$^+$ *rec-1*$^+$	(Barcak *et al.*, 1991)
DB117	KW20 *rec-1*	(Setlow *et al.*, 1972)
RSFA21	KW20 Δ*ompP2 kan*^{r}	(Srikumar *et al.*, 1997)
Phage		
M13K07	M13 carrying a mutation in gene II	BIO-RAD
Plasmids		
pBluescript SK(-)	Phagemid *bla*$^+$	Stratagene
pEJH39-1-35	pGB103 Ω(*Pst*I::*Eco*RI-*Pst*I DL42 2.5-kb *ompP2*$^+$) ColE1 Hi Rep	(Cope *et al.*, 1990)
pFFA02	pBluescript SK(-) Ω(*Pvu*II::*Pvu*II-*Ssp*I pEJH39-1-35 1-kb sequences coding for mature Hib porin)	(Srikumar *et al.*, 1997)
pAP04	pFFA02 Ω (*Sna*BI::annealed sna.hisA and sna.hisB)	This study
pAP14	pFFA02 Ω 5'-ATG CAT CAC CAT CAC CAT CAC-3' after nucleotide 1256	This study
pAP25	pEJH39-1-35 *ompP2*	This study
pAP36	pEJH39-1-35 *ompP2*	This study

extracted from agarose gels using the QIAEX II Gel Extraction kit (QIAGEN). *E. coli* was transformed by rendering the cells competent to DNA uptake using calcium chloride (Sambrook *et al.*, 1989). *Haemophilus* strains were rendered competent for DNA uptake using calcium chloride (Barcak *et al.*, 1991).

Construction of hexahistidine derivative in loop 4 of OmpP2.

The plasmid pFFA02 (3.6 kb) was linearized with *Sna*BI (New England Biolabs). A double-stranded oligonucleotide encoding six consecutive histidine residues and containing an internal *Nsi*I site (underlined) was generated by annealing (80°C, followed by slow cooling) two single-stranded oligonucleotides: 5'-GT ATG CAT CAC CAT CAC CAT CAC GGG C-3' (sna.hisA) and 5'-G CCC GTG ATG GTG ATG GTG ATG CAT AC-3' (sna.hisB). This introduced Arg-Met-His6-Gly after Val174; the extra amino acids were required to maintain the reading frame. The linearized pFFA02 was ligated using T4 DNA ligase (overnight at 16°C) with this double-stranded oligonuceotide, thereby introducing a novel *Nsi*I site and eliminating the *Sna*BI site. The incorporation of a methionine preceding the His6 tag allowed incorporation of a novel *Nsi*I restriction endonuclease site in the DNA sequence. This permitted screening of DNA constructs by differential *Nsi*I sensitivity compared to parental plasmids. The ligation mixture was used to transform competent *E. coli* strain DH5α; selection was for ampicillin resistance. Plasmids from 15 transformants were isolated and were screened for their sensitivity to *Nsi*I and their resistance to *Sna*BI. Five plasmids (pAP01 to pAP05) were selected that were sensitive to *Nsi*I. These five plasmids were subjected to DNA sequencing using as oligonucleotide Por.6 (5'-T583-GAAGTAAAACTTGGTCGT-G603-3') as a primer to determine the orientation of insertion of the double-stranded oligonucleotide: the numbers correspond to the published sequence of *ompP2* (Munson and Tolan, 1989). Plasmid pAP04 contained the insertion in the desired orientation without anomalous cloning artifacts. Restriction endonuclease cleavage using *Pvu*II and *Mlu*I allowed retrieval of the recombinant *ompP2* gene from pAP04. Digestion products were separated by electrophoresis on an agarose gel (0.8%); the *Pvu*II-*Mlu*I fragment (1.1 kb) was isolated.

To recombine the mutagenized fragment, the parental plasmid pEJH39-1-35 was linearized with *Pvu*II as confirmed by agarose gel electrophoresis. Due to the presence of two *Mlu*I sites in pEJH39-1-35, the *Pvu*II-linearized pEJH39-1-35 was partially digested with *Mlu*I in order to generate the desired cloning vector. The digestion products were again resolved by agarose gel electrophoresis and the 11.5 kb *Pvu*II-*Mlu*I fragment was isolated. The 11.5 kb *Pvu*II-*Mlu*I fragment of pEJH39-1-35 and the 1.1 kb *Pvu*II-*Mlu*I fragment from pAP04 were then ligated using T4 DNA ligase (overnight at 16°C). The post-ligation mixture was transformed into *H. influenzae* strain RSFA21 with selection for both tetracycline and kanamycin resistance. Plasmids were isolated from some transformants. The desired recombinant plasmid was predicted to have an additional *Nsi*I site compared to parental plasmid pEJH39-1-35. Plasmid DNA was sequenced using oligonucleotide Por.6 and Por.7.1 (5'-G776-GGTGAAAATAAGCGGCC-T794-3') as primers to determine the fidelity of cloning of the recombinant *ompP2*-containing fragment.

Construction of his6 derivative in loop 8 of OmpP2.

Using the Muta-Gene Phagemid In Vitro *Mutagenesis* kit (BIO-RAD) plasmid pFFA02 was transformed into *E. coli* strain CJ236 (BIO-RAD) (Fig. 5). Negative strand phagemid DNA from plasmid pFFA02 was generated in *E. coli* strain CJ236 upon coinfection with phage M13K07. A 50 base oligonucleotide 5'-AGA ACA CTG GAG ACA *ATG CAT CAC CAT CAC CAT CAC* GGT AAA GGC GTA AA-3', designed to introduce six consecutive histidine residues into OmpP2 of Hib was annealed to the pFFA02 single-stranded DNA. A methionine codon followed by six consecutive histidine codons (italics) were incorporated as part of the oligonucleotide allowing the introduction of a novel *Nsi*I site (underlined). The novel *Nsi*I site again permitted screening of constructs by differential *Nsi*I sensitivity. The mixture was transformed into competent cells of *E. coli* strain MV1190 with selection for ampicillin. Plasmids were isolated from 20 transformants and screened for *Nsi*I sensitivity. Five candidate plasmids (pAP11 to pAP15) were subjected to DNA sequencing using oligonucleotide Por.9 (5'-A1184-GATCATAAACTTCACAAA-C1203-3') as a primer. Plasmid pAP14 was

Fig. 5. Mutagenesis protocol from Muta-Gene Phagemid In Vitro *Mutagenesis* kit (BIO-RAD). Phagemid pFFA02 was transformed into *E. coli* strain CJ236 followed by isolation of negative strand phagemid upon helper phage infection of cells. Mutagenic 50-mer oligonucleotide was annealed to negative stranded pFFA02 and the positive strand was synthesized using the 50-mer as a primer. The mixture was transformed into strain MV1190 and mutagenic phagemid was isolated.

confirmed as containing the desired insertion. To recombine the mutant gene into the parental plasmid pEJH-39-1-35, plasmid pAP14 was doubly digested with *Pvu*II and *Mlu*I. The DNA fragments were electrophoresed on an agarose gel and the 1.1 kb fragment isolated. This *Pvu*II-*Mlu*I fragment of pAP14 was ligated to the 11.5 kb *Pvu*II-*Mlu*I fragment of pEJH39-1-35 isolated as described above. The post-ligation mixture was transformed into *H. influenzae* strain DB117. Transformants were selected for tetracycline resistance. Plasmid DNA was isolated from transformants and tested for altered sensitivity to *Nsi*I as compared to pEJH39-1-35. The differentially *Nsi*I-sensitive plasmids were then sequenced to confirm the introduction of the mutation in the loop 8 coding sequence. Plasmid with correct sequence was thereafter used to transform *H. influenzae* strain RSFA21 to express recombinant porin in a porin-deleted background.

Purification to homogeneity of OmpP2.H6s

Extraction of membranes and associated proteins

H. influenzae strain RSFA21 harboring plasmid pAP25 or pAP36 encoding recombinant Hib porin with His6 tag in loop 4 [OmpP2.H6(L4)] and recombinant Hib porin with His6 tag in loop 8 [OmpP2.H6(L8)] was transferred from the glycerol stock to a chocolate plate containing kanamycin and tetracyline for overnight growth. The following morning, a single colony was transferred from the plate to a tube containing 5 ml of prewarmed sBHI with appropriate antibiotics. The starter culture was monitored until the OD_{600} reached 1.00, at which time the 5 ml starter culture was transferred into a flask containing 295 ml of prewarmed sBHI plus antibiotics. This culture was again monitored until the OD_{600} reached 1.00. The 300 ml culture was equally distributed to six 2.8 litre fernbach flasks each containing 950 ml of sBHI plus antibiotics. The culture was again monitored until the OD_{600} reached 1.00, at which time the cells were harvested. Cells were collected by centrifugation at 5,500 x *g*. The cell pellet was then stored at -20°C until needed.

The frozen cell pellet was thawed prior to beginning the extraction process. The bacterial pellet derived from one litre of culture was resuspended in 5 ml of 200 mM Tris-HCl, pH 8.0. To the suspended cells 10 ml of 200 mM tris (hydroxymethyl) aminomethane-HCl (Tris-HCl) pH 8.0, 1 M sucrose and 80 µl of 100 mM phenylmethylsulfonyl fluoride (PMSF) was added. 100µl of 100 mM EDTA pH 8.0, 150µl of lysozyme 12 $mg \cdot ml^{-1}$, 32 ml double distilled water (ddH_2O) and 50µl 100 mM PMSF was further added. The cell suspension was mixed and incubated at room temperature for 30 minutes. 50 ml of 50 mM Tris-HCl pH 8.0, 10 mM $MgCl_2$, 0.5% lauryldimethylamine oxide (LDAO) was further added followed by 500µl of DNase I (1 $mg \cdot ml^{-1}$) and 500 µl of RNase A (1 $mg \cdot ml^{-1}$). The cell suspension was incubated at room temperature for an additional 30 minutes with vigorous shaking. Membranes were collected by centrifugation of the mixture at 15000 × *g* for 30 minutes at 4°C. The supernatant was discarded and the pellets was resuspended in 10 ml ddH_2O and 0.5 ml of 100 mM PMSF. After complete resuspensionof the membrane pellet, 140 ml ddH_2O of was added. This membrane suspension was mixed vigorously for 5 minutes and centrifuged again at 15000 × *g* for 30 minutes at 4°C. The membrane pellet resuspension and centrifugation step was repeated. The supernatant was discarded and the pellet was resuspended in 4 ml ddH_2O. Protein was quantified using the Bradford dye-binding assay (BIO-RAD). Double distilled water was added to bring the protein concentration to 2.5 $mg \cdot ml^{-1}$. An equal volume of 50 mM Tris-HCl pH 8.0, 1% LDAO, 20 mM EDTA and 100 µM PMSF was added. This mixture was stirred at room temperature for 30 minutes and then centrifuged at 8000 × *g* for 30 minutes at 4°C. The supernatant was filtered through a 0.45 µm filter and subsequently concentrated by ultrafiltration at 4°C using a YM10 membrane with a MWCO of 10,000 (Amicon). The resulting solution was dialyzed by transferring the protein solution into dialysis tubing (MWCO of 12,000 to 14,000; Fisher Scientific) against 1 litre of 50 mM Tris-HCl pH 8.0, and 0.1% LDAO at 4°C for 12 hours. The dialysis buffer was changed to 1 litre of 50 mM Tris-HCl pH 8.0, 200 mM NaCl, 0.1% LDAO, and 20 mM

imidazole. Dialysis continued in this buffer for 12 hours. The final dialysate was filtered through a 0.45 μm acetate filter prior to metal-chelate chromatography.

Ni^{2+}-NTA affinity chromatography

All chromatography was performed by coupling all columns to a Biologic HR FPLC (BIORAD) that measured the OD_{280} and conductivity of exiting solution. The first chromatographic step employed a XK26/20 column (Amersham Pharmacia Biotech) that was filled with 45 ml Ni^{2+}-NTA Superflow (QIAGEN). The Ni^{2+}-NTA medium in the column was cleaned and charged by passing one column volume of 0.1% LDAO, 200 mM acetic acid, 100 mM $NiSO_4$ through the column. Excess Ni^{2+} was removed by applying one column volume of buffer B (elution buffer) whose composition is 50 mM Tris-HCl pH 8.0, 200 mM NaCl, 0.1% LDAO, and 500 mM imidazole. The column was then equilibrated with buffer A (equilibration buffer) whose composition is 50 mM Tris-HCl pH 8.0, 200 mM NaCl 0.1% LDAO and 20 mM imidazole until the conductivity and OD_{280} readings were constant. The protein concentration of the sample was diluted with buffer A to 5 $mg \cdot ml^{-1}$. The sample was loaded onto the column at a flow rate of 2.5 $ml \cdot min^{-1}$. Immobilized protein was washed with four column volumes of buffer A during which the flow-through was collected. A linear gradient of buffer was applied with imidazole concentration increasing from 20 mM to 500 mM over four column volumes to elute the affinity bound proteins. Throughout the chromatography the flow rate was maintained at 2.5 $ml \cdot min^{-1}$ and all buffers were maintained at 25°C. Fractions of 8 ml were collected during the elution step. To identify proteins in each of the chromatography fractions, 10 μl aliquots were collected from the starting material, the flow-through fractions, and fractions spanning the chromatography peak corresponding to OD_{280}. They were analyzed by 12% SDS-PAGE adapted from (Laemmli, 1970) followed by silver staining for proteins (Morrissey, 1981) and silver staining for LPS (Tsai and Frasch, 1982). Fractions containing purified OmpP2.H6 were pooled and concentrated to < 20 ml by ultrafiltration at 4°C. The resulting protein solution was transferred to dialysis tubing and dialyzed against 500 ml of 50 mM ammonium acetate pH 8.0, 200 mM NaCl, 0.1% LDAO and 25 mM imidazole at

4°C for 4 hours to remove excess imidazole. Dialysis buffer was replaced with fresh buffer and dialysis continued overnight. Ni^{2+}-NTA-purified OmpP2.H6 was subjected to a second chromatographic step employing a different medium to remove residual amounts of contaminating proteins and lipooligosaccharide.

Poros MC 20 affinity chromatography

A Poros HP glass 16mmD/250mmL column (PerSeptive Biosystems) was filled with 15 ml of rehydrated Poros MC 20 medium (PerSeptive Biosystems). The interaction between deoxycholate and LPS reportedly allowed the regeneration of Detoxi-Gel Endotoxin Removing Gel (Pierce) resin composed of polymyxin B immobilized to agarose particles. Although the molecular interaction between deoxycholate and LPS is not characterized, deoxycholate is used to remove endotoxin adsorbed to the polymyxin B resin. To take advantage of the interaction between deoxycholate and LPS, a novel step in the perfusion chromatography protocol was introduced. It included washing the POROS-immobilized protein with solution containing deoxycholate in order to remove LOS from the preparation. In addition, to exploit the weak interaction between OmpP2.H6 and LOS that cannot be abolished in buffer containing 200 mM NaCl, a second step was added to the perfusion chromatography protocol, in which the POROS-immobilized OmpP2.H6(L8) was washed with buffer containing 500 mM NaCl. Such concentrations of NaCl are known to disrupt the weak ionic interaction between macromolecules and allow the separation of one molecular species from another. The POROS MC 20 column was prepared for use by a cleaning-regeneration step. The procedure consisted of sequentially applying: one column volume of 50 mM EDTA, 1 M NaCl; two column volumes of ddH_2O; two column volumes of 1 M NaOH, 1 M NaCl; two column volumes 1 M acetic acid; and two column volumes ddH_2O. The cleaned column was then charged with divalent nickel by applying one column volume of 1 M $NiSO_4$ to the column. Excess Ni^{2+} was removed by applying two column volumes of elution buffer (buffer B): 50 mM ammonium acetate pH 8.0, 200 mM NaCl, 0.1% LDAO and 500 mM imidazole, through the column. The column was equilibrated with buffer A, 50 mM ammonium acetate pH 8.0, 200 mM NaCl, 0.1% LDAO and 25 mM

imidazole, until the conductivity and OD_{280} readings were constant. All solutions that were applied to the POROS MC 20 column to clean and prepare the medium were applied at a flow rate of 10.0 ml•min^{-1}. Chromatographic purification of proteins on the POROS MC 20 column proceeded at a flow rate of 5 ml•min^{-1}. Ni^{2+}-NTA-purified protein sample was applied to the POROS MC 20 followed by two column volumes of buffer A to remove any unbound proteins. Flow-through fractions were collected for analysis. 1.5 column volumes of high salt buffer consisting of 50 mM ammonium acetate pH 8.0, 500 mM NaCl, 0.1% LDAO and 25 mM imidazole was applied to the column. Flow-through was collected for SDS-PAGE analysis. Two column volumes of buffer A were again passed through the column which was followed by passing three column volumes of deoxycholate wash buffer consisting of 50 mM ammonium acetate pH 8.0, 200 mM NaCl, 0.1% LDAO, 25 mM imidazole and 0.3% sodium deoxycholate. Flow-through was collected for analysis. One column volume of buffer A was applied to the column followed by specific elution of immobilized protein from the POROS MC 20 column by applying a linear gradient of imidazole increasing from 25 to 500 mM over four column volumes. 5 ml fractions were collected and those spanning the chromatographic peak were analyzed. Fractions containing only OmpP2.H6 were pooled, concentrated and dialyzed against 50 mM ammonium acetate pH 8.0, 50 mM NaCl, 0.06% LDAO.

Detergent exchange chromatography

To prepare purified OmpP2 in a wide variety of detergents for sparse matrix crystallization screening, the purified OmpP2.H6 was exchanged from LDAO to a series of other detergents by anion exchange chromatography. Non ionic detergents such as N,N-dimethyldecylamine-N-oxide (DDAO) (Fluka), N,N-dimethylundecylamine-N-oxide (UDAO) (Fluka), n-decyl-β-D-maltopyranoside (DM) (Calbiochem), n-dodecyl-β-D-maltoside (DDM) (Calbiochem), n-octyl-β-D-glucoside (β-OG) (Bachem), octylpolyoxyethylene (C_8E_N) (Bachem) and methyl-6-O-(N-heptylcarbamoyl)-α-D-glucopyranoside (HECAMEG) (Calbiochem) were selected. Detergent exchange was achieved using 10 ml Q-sepharose ion exchange media (Amersham Pharmacia Biotech) packed into a XK 16/20 column

(Amersham Pharmacia Biotech). The column was equilibrated in buffer A consisting of 50 mM ammonium acetate pH 8.0, 2 X critical micelle concentration (CMC) of detergent (Table 2), 50 mM NaCl. Purified and dialyzed protein solutions in 50 mM ammonium acetete pH 8.0, 50 mM NaCl, 0.06% LDAO were mixed with an equal volume of equilibration buffer. This mixture was applied to the ion exchange column at 2 ml•min^{-1}. The column was washed with three column volumes of equilibration buffer and flow-through was collected. OmpP2.H6 was specifically eluted by applying a linear gradient (50 to 500 mM) of NaCl over two column volumes. 5 ml fractions were collected spanning the chromatographic peak. Flow-through fractions and elution fractions were analyzed by 12% SDS-PAGE followed by silver staining. Fractions containing OmpP2.H6 were pooled and concentrated.

Gel Filtration

Purified and detergent-exchanged protein preparations were subjected to gel filtration to separate aggregates from monomers with the goal of removing any high molecular mass species that contribute to the heterogeneity. 30 ml of Superdex 200 Prep grade (Amersham Pharmacia Biotech) was filled in a XK 16/20 column (Amersham Pharmacia Biotech) to undertake the gel filtration. All gel filtration steps proceeded at 1 ml•min^{-1}. The gel was first equilibrated in equilibration buffer: 50 mM ammonium acetate pH 8.0, 2 x CMC detergent of choice, and 200 mM NaCl. The column was calibrated with standards of Blue Dextran 2000 (2000 kDa), BSA and Ovalbumin (Amersham Pharmacia Biotech). The purified OmpP2.H6 was concentrated then dialyzed into equilibration buffer and applied to the gel filtration column. The column was washed with equilibration buffer and fractions spanning the chromatographic peak were collected. The fractions corresponding to the main peak were pooled, concentrated, and dialyzed.

OmpP2.H6(L8) Purification in DDAO

To exclude the possibility that the low CMC value of LDAO is responsible for disrupting the trimeric association of Hib porin, a preparation of OmpP2.H6(L8) was extracted and purified by Ni^{2+}-NTA, POROS MC 20 and gel

Table 2

Detergents and their respective CMC used in this study

Detergent	CMC (mM)	CMC (%) (w/v)
Dimethylundecylamine-N-oxide (UDAO)	6.0	0.13
Dimethyldodecylamine-N-oxide (DDAO)	10.4	0.21
Dodecylmaltoside (DDM)	0.6	0.03
Decylmaltoside (DM)	1.6	0.082
β-Octylglucoside (β-OG)	22	0.65
Octylpolyoxyethylene (C_8E_N)	17	0.6
Methyl-6-O-(N-heptylcarbamoyl)-glucoside (HECAMEG)	19.5	0.654
Dimethyldodecylamine-N-oxide (LDAO)	2.0	0.046

filtration exclusively in the presence of DDAO by substituting the relative concentration of LDAO with respect to CMC with the corresponding value for DDAO. The higher CMC value of DDAO is expected prevent dissociation of Hib porin trimers into monomers.

Protein Analysis

Monoclonal antibody reactivity of surface exposed determinants

Purified OmpP2.H6(L4) and OmpP2.H6(L8) preparations were tested for reactivities to monoclonal antibodies (mAbs) Por.1 and Por.6 that react specifically with determinants on Hib porin mapped to amino acids 118-Glu to 123-Asn and amino acids 318-Thr to 325-Val, respectively (Srikumar *et al.*, 1992). These amino acid sequences are predicted to form loop 4 and loop 8, respectively according to the proposed molecular structure derived from modeling the Hib porin sequence onto the structural scaffold of the porin family (Srikumar *et al.*, 1997). Following 12% SDS-PAGE of wild-type and recombinant Hib porins, proteins were transferred electrophoretically (Towbin *et al.*, 1992) to nitrocellulose membranes (Schleicher & Schuell, Inc.). Prestained markers (BIO-RAD) were resolved on the same SDS-polyacrylamide gel and cotransferred to the membranes to estimate the sizes of reactive species. The nitrocellulose membranes were blocked with Tris-HCl saline pH 7.3 solution containing 1% bovine serum albumin and immobilized proteins were reacted with primary antibodies, Por.1 or Por.6. Membranes were reacted with developing antibody, goat anti-mouse antibody coupled to alkaline phosphatase (187-AP), and alkaline phosphatase activity was detected by addition of NBT and BCIP (BIO-RAD). Duplicate SDS-polyacrylamide gels were silver stained for protein.

Planar lipid bilayer

Purified protein samples were tested for their ability to form channels in planar lipid bilayers. As previously described (Benz *et al.*, 1978), a lipid bilayer was formed over an aperture 250 μm in diameter by applying monoolein (Sigma-Aldrich) from the *cis* side of the chamber. After applying a potential difference

between the *cis* and the *trans* chambers, the current was monitored to ensure a stable bilayer was formed. Aliquots of 5ng of protein were introduced into the *cis* side of the bilayer chamber and current was monitored for a stepwise increase in current corresponding to the insertion of channel forming proteins. Approximately 400 upward rectifying steps of current were measured and the average single channel conductance was determined for both preparations of OmpP2.H6(L4) and OmpP2.H6(L8).

Dynamic Light Scattering

Crystallizability of protein preparations was assessed by dynamic light scattering (DLS) on a DynaPro801 instrument (Protein Solutions Inc.). Protein samples in the buffer for crystallization screening were diluted to a final protein concentration of 2 $mg \cdot ml^{-1}$. The analysis cuvette was washed until background counts went below 7000 counts per minute. Prior to taking the measurement of the protein samples, a background measurement of the buffer was obtained. All samples were filtered using a Whatman Anotop Plus syringe filter of 0.1 μm porosity while injecting samples into the analysis cuvette. Data returned by the instrument are scattering amplitude, translational coefficient, particle radius, estimated molecular weight, polydispersity, per cent mass, temperature of the cell, counts per minute, baseline, and sum of squares (SOS) error. The SOS error measurement compares the fit between the experimental data and an autocorrelation function generated from the analysis results.

Crystallization Trials

Protein samples were all concentrated between 10 and 20 $mg \cdot ml^{-1}$ followed by extensive dialysis with a minimum of three changes of dialysis buffer: 20 mM ammonium acetate pH 8.0, 2 x CMC detergent, 100 mM NaCl, prior to crystallization trials. Protein solutions were filtered using a 0.1 μm eppendorf filter (Millipore) by centrifugation at 14000 rpm in a bench top centrifuge immediately before crystallization trials. Crystallization trials were performed using solutions from Crystal screen, Crystal screen 2, and Membfac sparse

matrix crystallization screening kits (Hampton Research). A total of 146 commercially available solutions were tested. The sitting drop vapour diffusion technique was employed using the CrystalClear strips (Hampton Research). Reservoirs were filled with 100 μl of crystallization solution followed by mixing equal volumes (3-5 μl) of protein solution and crystallization solution as a droplet. The reservoir and adjacent droplet were sealed with CrystalClear tape (Hampton Research) to form a closed system thereby allowing the droplet conditions to equilibrate to reservoir conditions. Once islands of crystallization were identified using this setup, the conditions were repeated in larger scale sitting drop vapour diffusion technique to confirm the crystallization growth conditions employing VDX plates (Hampton Research) and Micro-Bridges (Hampton Research) to hold the droplet. Hanging drop vapor diffusion technique using VDX plates (Hampton Research) as reservoirs and 22 mm siliconized glass cover slips (Assistent) from which to hang the droplet was also tested. For both setups, 22 mm circular glass cover slips were used to seal the reservoirs using immersion oil B as a sealing agent. Crystallization solutions have three components: precipitant, salt and buffering agent. After crystal growth conditions were confirmed, the concentration of the precipitant of the crystallization solution was permuted *versus* varying pH values. This was followed by the salt concentration permutation *versus* precipitant concentration to increase the qualities of crystals in both morphology and size. All crystals were grown at 290 K. Crystals of sufficient size were mounted in a capillary tube with mother liquor to prevent crystal desiccation and sealed at both ends with wax. Crystallization conditions were also modified from initial conditions to include a cryoprotectant that facilitates data collection at low temperatures and eliminates crystal decay as a result of X-ray exposure. Crystals grown in these conditions were scooped into a Cryoloop (Hampton Research) and immediately transferred to a nitrogen stream whose temperature was maintained at 93 K.

X-Ray Irradiation of Crystals

Crystals that were tested for diffraction at room temperature were mounted in a capillary tube in a column of mother liquor whereas those tested at low temperatures were mounted in a cryoloop. Mounted crystals were X-ray irradiated at a locally available X-ray setup consisting of a Rigaku RU 200 rotating anode generator and a 30 cm MAR image plate detector (Biotechnology Research Institute; Montreal). Cryo-irradiation of crystals was performed by maintaining the crystal in a nitrogen stream at 93 K during X-ray irradiation. The image plate detector was set at a distance of 262 mm from the crystal such that the outer edge of the image plate corresponded to a resolution limit of 3.6 Å. Each test crystal was exposed for 30 minutes with a 1° rotation. Crystals with obvious diffraction patterns were then rotated 90 degrees for a second exposure to assess crystal anisotropy.

Results

His6 tag insertion into surface exposed loops

Generation of his6 insertion in loop 4 of OmpP2.

The mutagenic sequence (annealed sna.hisA and sna.hisB oligonucleotides) was ligated to *Sna*BI-linearized pFFA02 and transformed into *E. coli* strain DH5α. More than 20 transformants were detected on antibiotic (ampicillin) selection plates. Ten of these plasmids (pAP01 to pAP10) were isolated and pAP01 to pAP05 were found to be sensitive to *Nsi*I, the novel restriction site that was introduced within the annealed oligonucleotide. These plasmids were subjected to DNA sequencing using primer Por.6, which annealed 5' to the mutagenized region. Plasmids, pAP02 and pAP04, were confirmed to contain the insertion in the desired orientation. The remaining plasmids contained the mutagenic insertion in the opposite orientation. No anomalies were detected across the ligation regions (Fig. 6a). The 1.1 kb *Pvu*II-*Mlu*I fragment from plasmid pAP04, was ligated to the 11.5 kb *Pvu*II-*Mlu*I fragment derived from plasmid pEJH39-1-35. Recombinant plasmid was transformed into *H. influenzae* strain RSFA21. Due to a very low transformation efficiency (250 colonies•μg^{-1} DNA), two colonies were detected on the antibiotic selection plates which contained kanamycin and tetracycline. One of the doubly-antibiotic resistant colonies did not yield plasmid. Plasmid DNA was isolated from the second colony and designated pAP25. It was linearized by *Pvu*II restriction endonuclease digestion, indicating the presence of one *Pvu*II site. Plasmid pAP25 contained two *Mlu*I sites, identical to the parental plasmid pEJH39-1-35. As expected, plasmid pAP25 displayed altered sensitivity to *Nsi*I; one additional restriction site was detected as compared to the parental plasmid pEJH39-1-35. Double digestion of pAP25 with *Pvu*II and *Nsi*I yielded four fragments, indicative of three *Nsi*I sites within the recombinant plasmid. Double digestion of pEJH39-1-35 employing *Nsi*I and *Pvu*II yielded three fragments indicative of two *Nsi*I sites

Fig. 6. Plasmid pFFA02 was mutagenized to give (A) plasmid pAP04 by linker insertion and (B) plasmid pAP14 by annealing a mutagenic primer described in Materials & Methods. The 1.1 kbp *Pvu*II-*Mlu*I fragments were cloned back into the parental plasmid pEJH39-1-35 cleaved also with *Pvu*II and *Mlu*I resulting in plasmid pAP25 and plasmid pAP36, respectively.

A

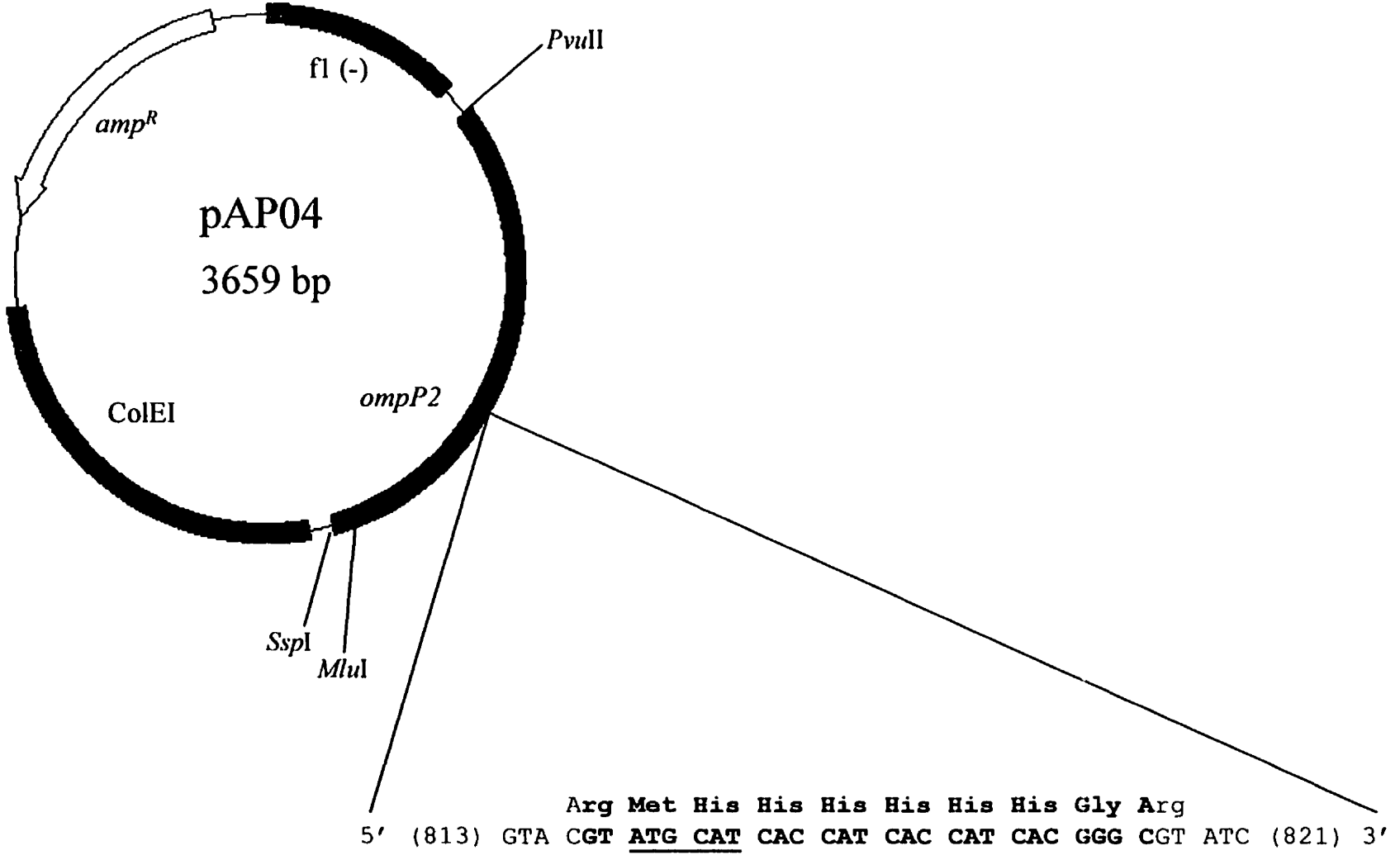
f1 (-)
PvuII
ampR
pAP04
3659 bp
ColEI
ompP2
SspI
MluI
Arg Met His His His His His His Gly Arg
5′ (813) GTA CGT ATG CAT CAC CAT CAC CAT CAC GGG CGT ATC (821) 3′

B

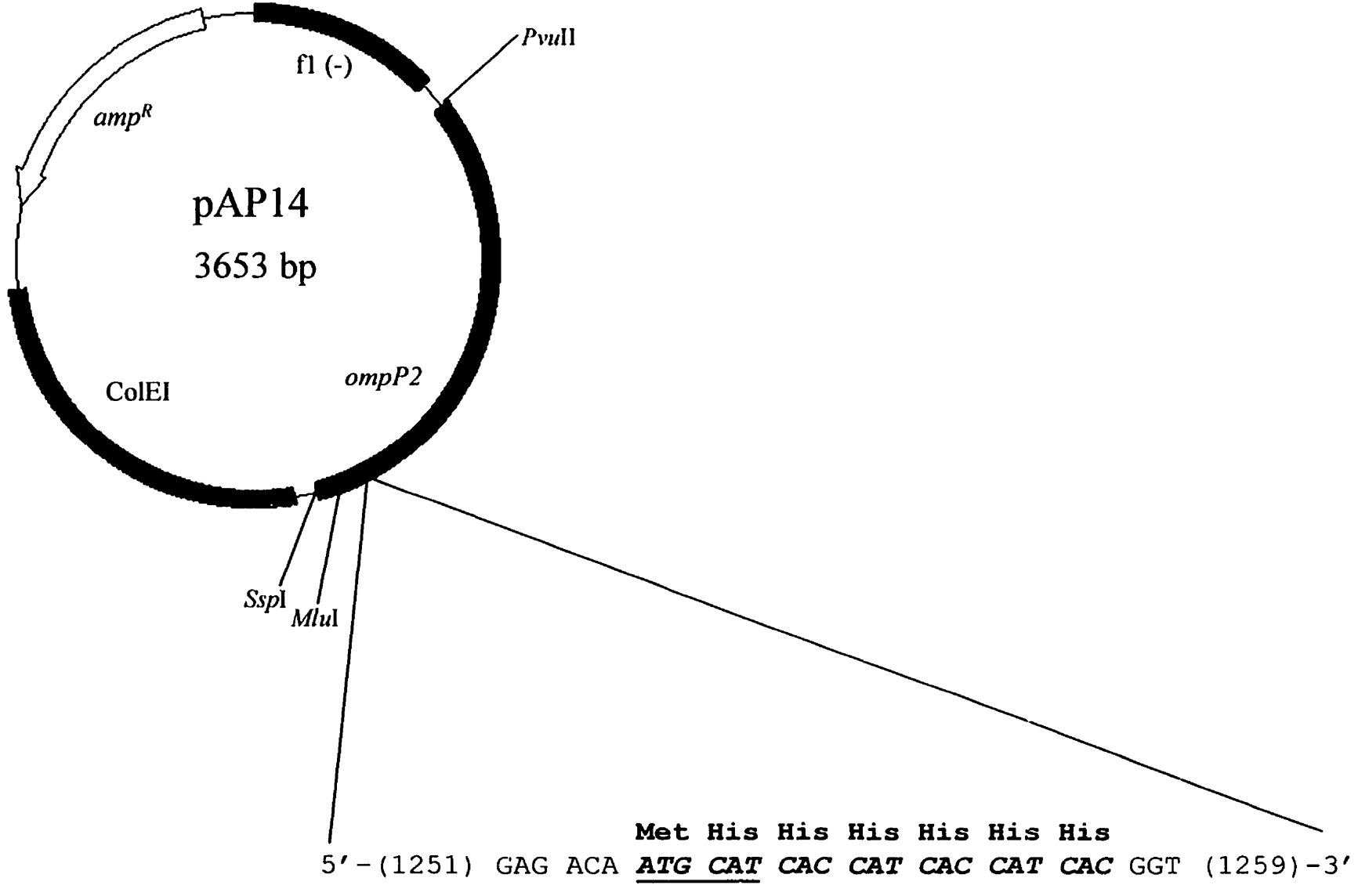
f1 (-)
PvuII
ampR
pAP14
3653 bp
ColEI
ompP2
SspI
MluI
Met His His His His His His
5′-(1251) GAG ACA ATG CAT CAC CAT CAC CAT CAC GGT (1259)-3′

in the parental plasmid. Sequencing of the mutation region using oligonucleotide Por.6 as a primer confirmed the fidelity of the hexahistidine coding sequences.

Generation of his6 insertion in loop 8 of OmpP2

Negative-sense single-stranded pFFA02 was annealed to the mutagenic oligonucleotide (50-mer). Following synthesis of the positive-sense strand of plasmid pFFA02 incorporating the mutation, the mixture was transformed into *E. coli* strain MV1190. Over 20,000 transformants appeared on the antibiotic selection plates. Plasmids were isolated from ten transformants. These plasmids were designated pAP11 to pAP20. Plasmids, pAP11 to pAP15, were sensitive to *Nsi*I restriction endonuclease digestion. These plasmids were expected to contain the desired mutation. DNA sequencing of the target region showed that plasmid pAP14 contained the insertion in the desired orientation and without any anomalous sequence alterations of molecular cloning (Fig. 6b). The 1.1 kb *Pvu*II-*Mlu*I fragment from pAP14 was ligated to the 11.5 kb *Pvu*II-*Mlu*I fragment of plasmid pEJH39-1-35. Due to extremely low transformation efficiency for *H. influenzae* strain RSFA21, recombinant plasmid was rescued by transformation into competent *H. influenzae* strain DB117. Seven transformants grew on the Chocolate agar plates containing tetracycline after incubation for 24 hours at 37°C in a 5% CO_2 atmosphere. Plasmid DNA from transformants was isolated and *Nsi*I sensitivity was assessed. Four of the seven plasmids had a digestion pattern virtually identical to the *Nsi*I digestion pattern of pAP25. The dissimilarity of the migration pattern of the *Nsi*I digested plasmids with respect to pAP25 was a result of relative location of the novel *Nsi*I site. The four plasmid samples were used to independently transform competent *H. influenzae* strain RSFA21 with selection for both tetracycline and kanamycin. Twenty-eight transformants appeared following incubation of the chocolate plates for 24 hours at 37°C in a 5% CO_2 atmosphere. Seven transformants were grown to OD_{600} value of 1.00 in 300 ml of sBHI with tetracycline and kanamycin overnight. Plasmid DNA from large cultures of these seven transformants was isolated, digested with *Nsi*I, and resolved by agarose gel electrophoresis (0.8%). The

digestion pattern of each plasmid DNA sample following *NsiI* digestion was indistinguishable from the others. Plasmid DNA was sequenced using oligonucleotide Por.9, which annealed 5' to the target site. It confirmed that no artifacts of mutagenesis were introduced. One of the purified plasmid samples had DNA sequence data across the mutation region that was identical to the homologous region in plasmid pAP14; it was named plasmid pAP36. The three remaining DNA sequencing results contained multiple ambiguities that did not confirm the desired mutation. *H. influenzae* strain RSFA21 harboring plasmid pAP36 was grown in large quantities as the source of recombinant Hib porin with hexahistidine tag in loop8 termed OmpP2.H6(L8).

Expression and purification of OmpP2.H6s

H. influenzae strain RSFA21 containing plasmid pAP25 or pAP36 possessed growth phenotype similar to that of wild type *H. influenzae* strain DB117. Outer membrane preparations indicated the presence of a major OMP migrating at 38 kDa corresponding to recombinant porin.

Small-scale pilot experiments were performed to determine the ability of OmpP2.H6 to bind efficiently Ni^{2+}-NTA agarose. Purification of OmpP2.H6 in Zwittergent Z-3,14 was not successful using a Ni^{2+}-NTA agarose equilibrated with LDAO. However, purification of OmpP2.H6 was achieved when the Zwittergent Z-3,14- solubilized preparation was exchanged into LDAO and then applied to the LDAO-equilibrated Ni^{2+}-NTA agarose. Affinity-bound OmpP2.H6 was eluted from the Ni^{2+}-NTA agarose using a 500 mM imidazole solution. A minor population of OmpP2.H6 appeared in the flow-through. Significant enrichment of OmpP2.H6 was observed in the protein fraction that was displaced from the gel slurry using imidazole.

An established protocol that allowed for efficient purification of FhuA.H6 from *Escherichia coli* K-12 (Ferguson *et al.*, 1998) was adapted for large-scale purification of OmpP2.H6. The elution profile showed a single symmetrical peak, indicative that one molecular species was eluted (Fig. 7). Elution of OmpP2.H6(L4) occurred at a lower imidazole concentration when compared to

Fig. 7. Chromatogram of Ni^{2+}-NTA Superflow purification of OmpP2.H6(L8). Lower X-axis indicates time (Hr:Min:Sec). Outer left Y-axis measures absorbance at OD_{280} (Absorbance Units), inner left Y-axis measures per cent buffer B (%) applied to column, right Y-axis measures conductivity (mS/cm). Buffer A (50 mM Tris-HCl pH, 8.0, 200 mM NaCl, 0.1 % LDAO, 20 mM imidazole) is applied until time index of 00:50:00. A linear gradient of buffer B (50 mM Tris-HCl pH, 8.0, 200 mM NaCl, 0.1 % LDAO, 500 mM imidazole) 0-100 % is applied from time index 00:50:00 to time index 01:30:00. The absorbance trace increased from a baseline value of 0 AU to a peak value of 1.70 AU at time index 00:15:00 corresponding to flow through following application of membrane extract to column medium at time index 00:00:00. The absorbance trace returns to a baseline value of 0 AU while the column is washed with 2 column volumes of Buffer A. The absorbance trace forms a single symmetric peak reaching an OD_{280} value of 0.93 AU corresponding to eluted protein. Fractions spanning the elution peak are indicated on the upper X-axis. The conductivity trace does not significantly fluctuate from its starting value of 0.45 mS/cm.

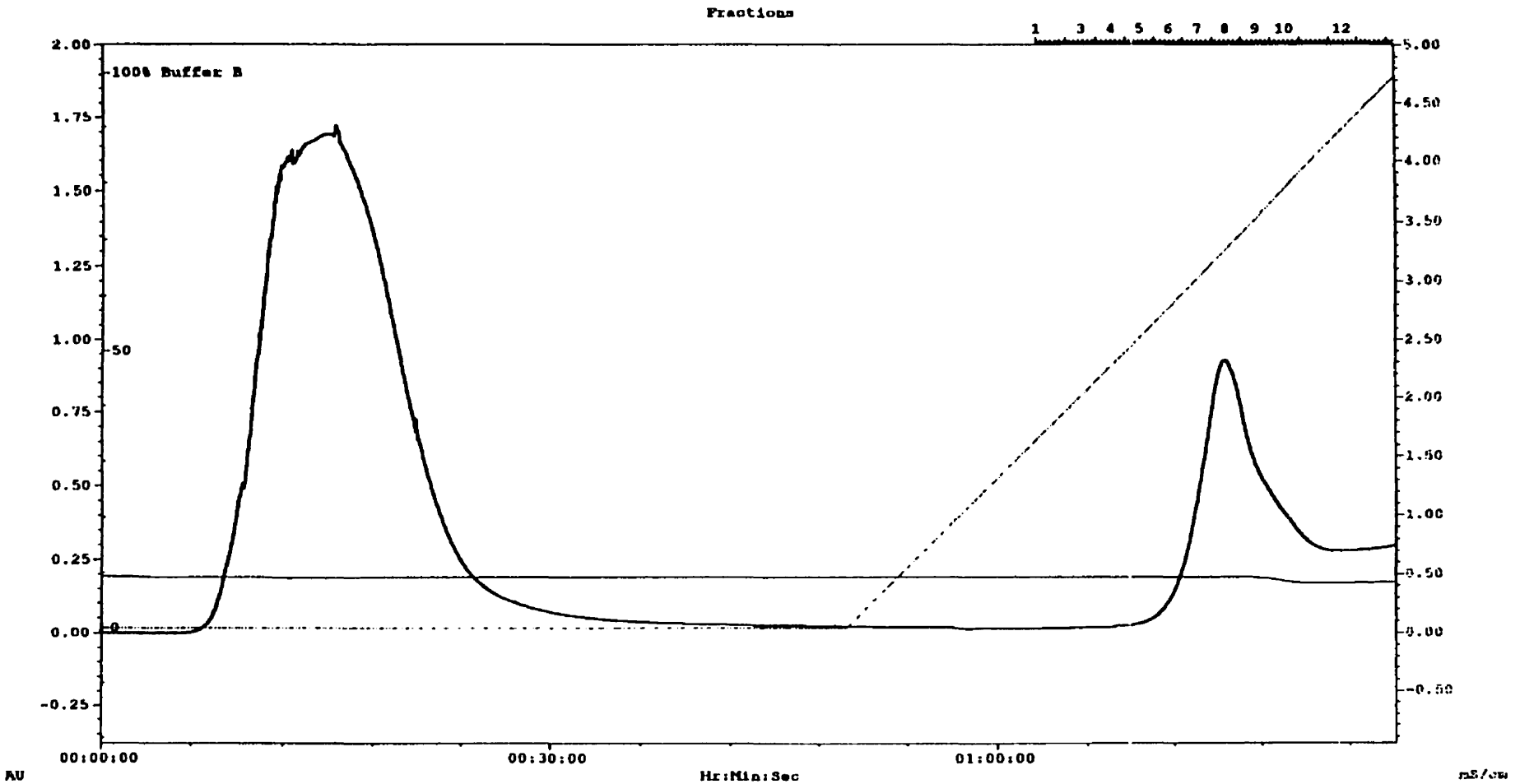
Fractions
1 3 4 5 6 7 8 9 10 12
100% Buffer B
50
0
2.00
1.75
1.50
1.25
1.00
0.75
0.50
0.25
0.00
-0.25
5.00
4.50
4.00
3.50
3.00
2.50
2.00
1.50
1.00
0.50
0.00
-0.50
00:00:00
00:30:00
01:00:00
AU
Hr:Min:Sec
mS/cm

the concentration of imidazole required to elute OmpP2.H6(L8). Ni^{2+}-NTA-purified OmpP2.H6 samples were virtually free from contaminating proteins. LOS, however, remained a contaminant as displayed both on 12% SDS-polyacrylamide gel silver stained for proteins and 12% SDS-polyacrylamide gel silver stained for LPS (Fig. 9). Following concentration of purified proteins by ultrafiltration, the protein sample was dialyzed in appropriate buffer for POROS MC 20 chromatography. Chromatogram of POROS MC 20 purification of OmpP2.H6(L8) shows a unique elution peak (Fig. 8). Flow-through fractions, fractions corresponding to wash steps, and elution fractions were analyzed by 12% SDS-PAGE. Duplicate gels were silver-stained for protein and LPS (Fig. 9). The gels revealed specific removal of contaminating lipooligosaccharide in the high salt and deoxycholate wash steps. The elution fractions spanning the chromatographic peak showed significant or complete removal of contaminating LOS. These fractions were pooled, concentrated, and dialyzed to prepare for crystallization trials or for detergent exchange by anion-exchange chromatography.

Purified OmpP2.H6(L4), OmpP2.H6(L8), and OmpP2 were resolved by SDS-PAGE, transferred to nitrocellulose membranes, and probed with mAbs Por.1 and Por.6. The immunoblot showed abrogation of mAb Por.6 reactivity to OmpP2.H6(L8) while no alteration of reactivity was observed against OmpP2.H6(L4) with respect to the reactivity seen against wild-type Hib porin. Reactivity to mAb Por.1 was identical for recombinant and wild type Hib porins (Fig. 10).

Ion-exchange chromatography permitted the transfer of OmpP2.H6(L8) preparations from buffer containing LDAO to a variety of buffers containing different detergents. The chromatography protocol called for mixing equal volumes of protein solution in 50 mM ammonium acetate pH 8.0, 50 mM NaCl, and 0.06% LDAO with equilibration buffer. The protein remained in solution after mixing with equilibration buffer from each of the different detergent experiments indicating stability in solutions containing LDAO and other detergents. The chromatogram of OmpP2.H6(L8) detergent-exchange into DDAO shows a unique

Fig. 8. Chromatogram of POROS MC 20 purification of OmpP2.H6(L8). Lower X-axis indicates time (Hr:Min:Sec). Outer left Y-axis measures absorbance at OD_{280} (Absorbance Units), inner left Y-axis measures per cent buffer B (%) applied to column, right Y-axis measures conductivity (mS/cm). Buffer A (50 mM ammonium acetate pH 8.0, 200 mM NaCl, 0.1% LDAO, 25 mM imidazole) is applied until time index of 00:22:00. A linear gradient of buffer B (50 mM ammonium acetate pH 8.0, 200 mM NaCl, 0.1% LDAO, 500 mM imidazole) 0-100 % is applied from time index 00:22:00 to time index 00:26:00 followed by 100% buffer B until time index 00:29:00. Ni^{2+}-NTA-purified OmpP2.H6(L8) was applied at time index 00:02:00. The absorbance trace did not significantly fluctuate from a baseline value of 0 AU during flow-through and buffer A wash steps. The conductivity trace began at a baseline value of 0.52 mS/cm and increases at time index 00:11:00 to a value of 1.05mS/cm corresponding to the high salt wash. The conductivity trace returns to baseline at time index 00:15:00 corresponding to the end of the high salt wash. Application of buffer containing deoxycholate lowered the conductivity trace to 0.48 mS/cm at time index 00:18:00. The conductivity trace returned to baseline at time index 00:22:00 following deoxycholate wash. The absorbance trace forms a symmetric peak with a maximum value of 1.4 AU corresponding to elution of OmpP2.H6(L8). Fractions spanning the elution peak are indicated on the upper X-axis.

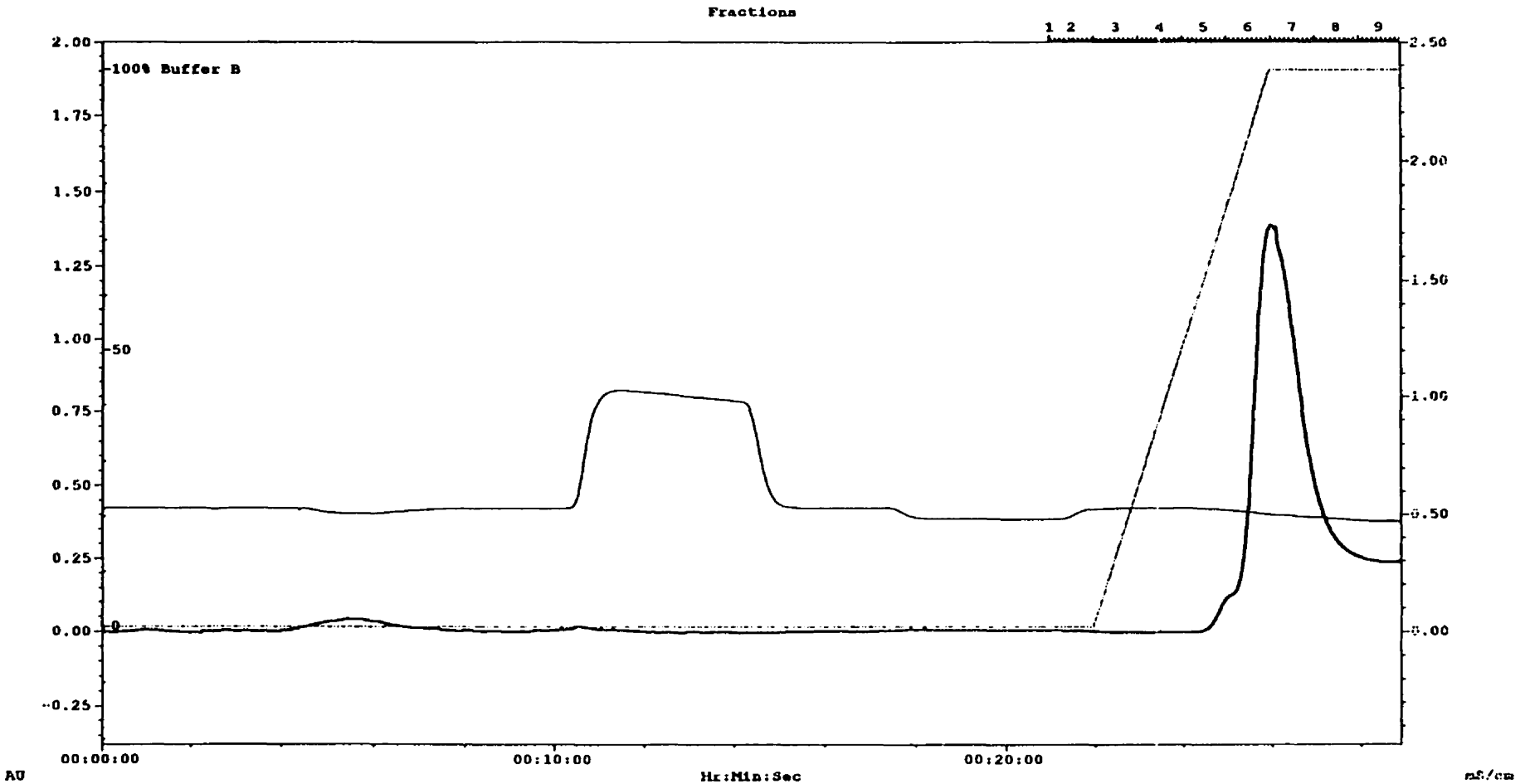
Fractions
1 2 3 4 5 6 7 8 9
100% Buffer B
50
0
2.00
1.75
1.50
1.25
1.00
0.75
0.50
0.25
0.00
-0.25
2.50
2.00
1.50
1.00
0.50
0.00
00:00:00
00:10:00
00:20:00
AU
Hr:Min:Sec
mS/cm

Fig. 9. Analysis of extraction and purification steps. Samples were resolved by 12% SDS-PAGE followed by silver staining for protein (A) or silver staining for LOS (B). Lane contents are : (1) broad range molecular weight markers (BIO-RAD), masses indicated at side, or 50 ng Hib LOS standard; (2) aqueous fraction of cell lysate; (3) detergent-soluble membrane fraction (starting material for Ni^{2+}-NTA column); (4) detergent-insoluble membrane fraction; (5) Ni^{2+}-NTA flow-through fraction; (6) pooled Ni^{2+}-NTA elution fractions/ starting material for POROS MC 20 column; (7) POROS MC 20 flow through; (8) POROS MC 20 high salt wash fraction; (9-10) consecutive POROS MC 20 deoxycholate wash fractions; (11-14) consecutive POROS MC 20 elution fractions.

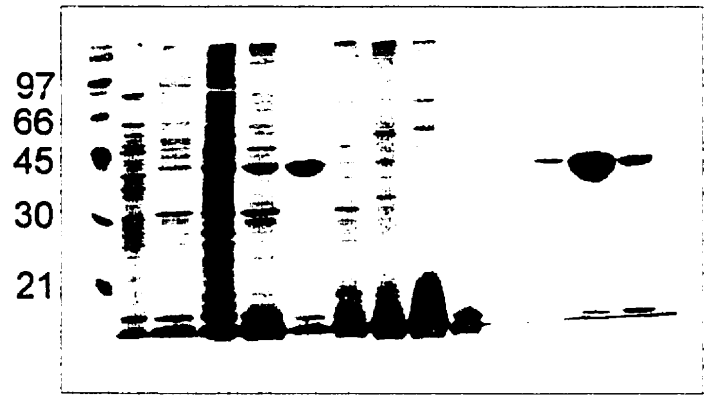

1 2 3 4 5 6 7 8 9 10 11 12 13 14

Fig. 10. Immunoblot of wild type and recombinant Hib porins to surface reactive mAbs. 12% SDS-PAGE transferred to nitrocellulose membranes. Lane contents are: (M) prestained molecular mass markers (masses indicated at side); (1-3) 0.5, 1.0, 2.0 μg OmpP2; (4-6) 0.5, 1.0, 2.0 μg OmpP2.H6(L4); (7-9) 0.5, 1.0, 2.0 μg OmpP2.H6(L8). Membranes were probed with Por.1 (A) or Por.6 (B).

A

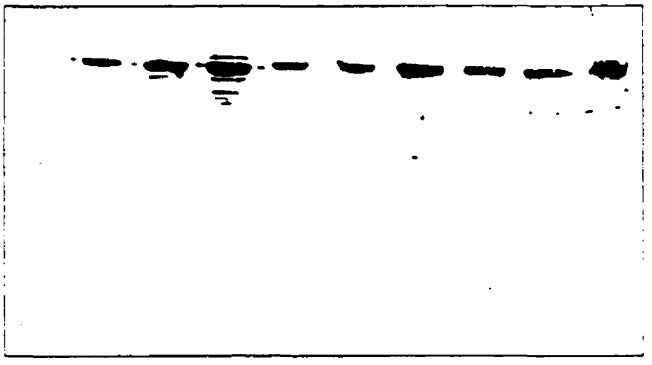

M 1 2 3 4 5 6 7 8 9

B

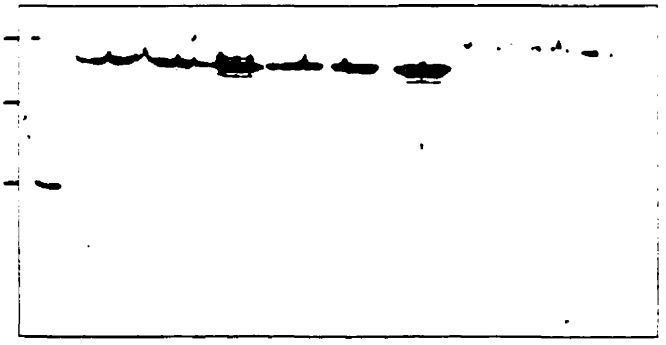

peak (Fig. 11). Flow-through and elution fractions were analyzed by 12% SDS-PAGE. Duplicate gels were silver stained for protein or lipooligosaccharide detection. Flow-through fractions of detergent-exchange chromatographies did not contain any significant quantity of OmpP2.H6. The elution fractions spanning the chromatographic peak of the detergent-exchange chromatographies uniquely contained OmpP2.H6. Exchange into buffers containing C_8E_N or HECAMEG was successful despite precipitation of OmpP2.H6(L8) in the elution fractions. Protein stability in buffers containing C_8E_N or HECAMEG deteriorated upon concentration as indicated by further protein precipitation. Elution fractions from detergent exchange chromatographies into C_8E_N and HECAMEG contained precipitated protein. Precipitated protein was resolubilized by addition of NaCl to a final concentration of 200 mM. The elution fractions were pooled, concentrated to between 10 $mg \cdot ml^{-1}$ and 20 $mg \cdot ml^{-1}$, and dialyzed against appropriate buffer for crystallization trials. Protein preparations that were detergent exchanged into C_8E_N and HECAMEG continued to precipitate throughout the concentration steps. This prevented optimal concentration. Therefore, these samples were not subjected to crystallization trials. Exchange into buffers containing UDAO, DDAO, DDM, DM, or β-OG was successful. These protein preparations of OmpP2.H6(L8) were concentrated to between 10 $mg \cdot ml^{-1}$ and 20 $mg \cdot ml^{-1}$ and extensively dialyzed to equilibrate the detergent concentration to 2 x CMC.

Metal-chelate-purified and detergent-exchanged OmpP2.H6 samples were subjected to gel filtration to exclude any high molecular mass aggregates that might contribute to sample heterogeneity. The gel filtration column was calibrated with three molecular mass species and tested with a sample of previously purified OmpP2.H6 to determine approximate elution volume. Void volume of gel filtration column was determined to be 12 ml. The protein sample was applied to the gel filtration column previously equilibrated with equilibration buffer. Conductivity and OD_{280} of the exiting solution from the gel filtration column was measured. These measurements showed a unique peak eluting from the column (Fig. 12). The fractions spanning the chromatographic peak were pooled, concentrated, and dialyzed in preparation for crystallization trials.

Fig. 11. Chromatogram of Q-Sepharose detergent exchange of OmpP2.H6(L8). Lower X-axis indicates time (Hr:Min:Sec). Outer left Y-axis measures absorbance at OD_{280} (Absorbance Units), inner left Y-axis measures per cent buffer B (%) applied to column, right Y-axis measures conductivity (mS/cm). Buffer A (50 mM ammonium acetate pH 8.0, 50 mM NaCl, 2 x CMC detergent of choice) is applied until time index of 00:22:00. A linear gradient, 0-100%, of buffer B (50 mM ammonium acetate pH 8.0, 50 mM NaCl, 2 x CMC detergent of choice) is applied from time index 00:18:00 to time index 00:30:00 followed by 100% buffer B until time index 00:34:00. POROS-purified OmpP2.H6(L8) was applied at time index 00:02:00. The absorbance trace fluctuated from a baseline value of 0 AU up to 0.08 AU during flow-through and buffer A wash steps. The absorbance trace peaked to a maximum value of 0.8 AU corresponding to elution of OmpP2.H6(L8). The conductivity trace began at a baseline value of 0.24 mS/cm and increased from time index 00:26:00 to a maximum value of 1.05mS/cm corresponding to application of buffer B, which contained a higher NaCl concentration. Fractions spanning the elution peak are indicated on the upper X-axis.

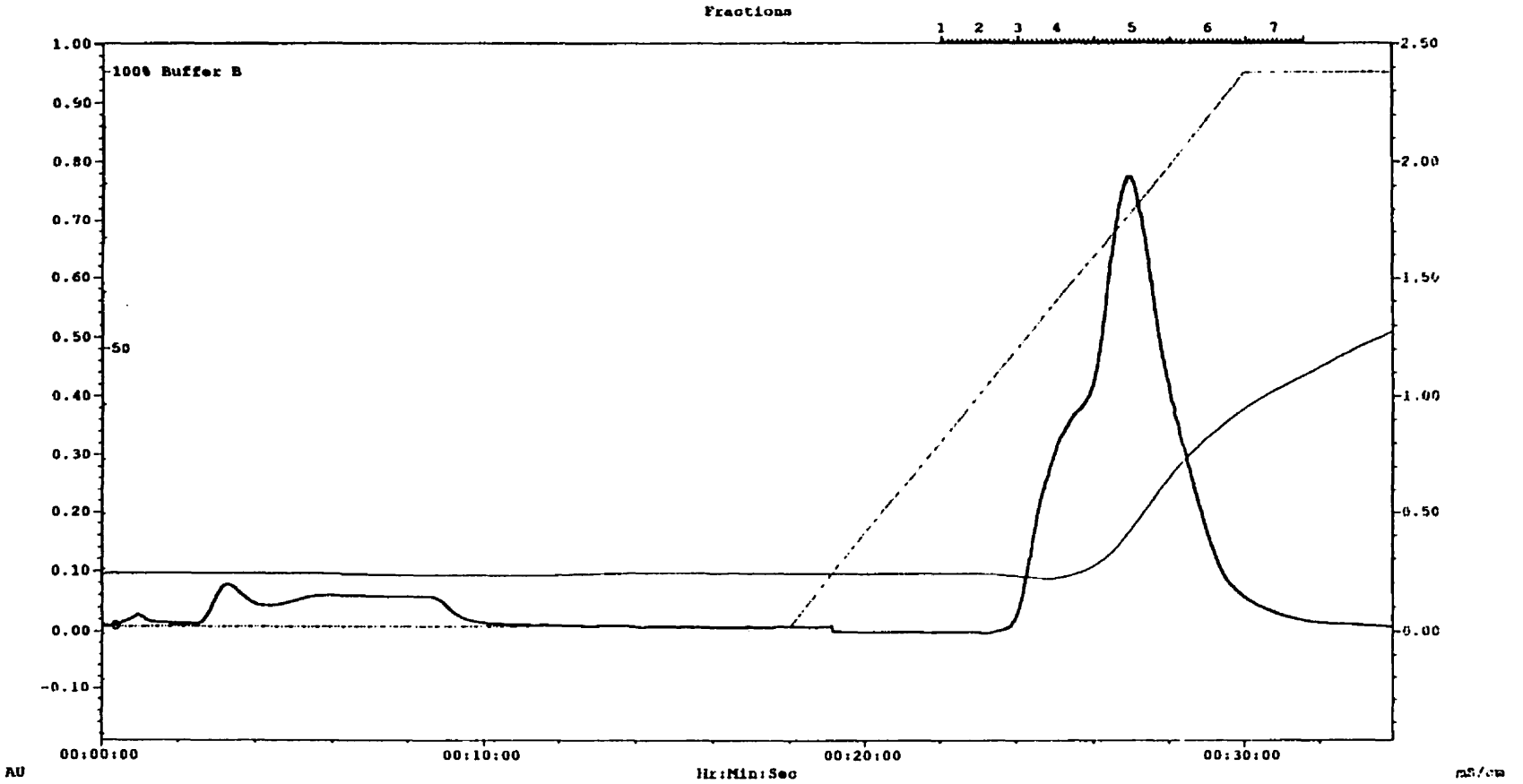
Fractions
1 2 3 4 5 6 7
100% Buffer B
50
1.00
0.90
0.80
0.70
0.60
0.50
0.40
0.30
0.20
0.10
0.00
-0.10
2.50
2.00
1.50
1.00
0.50
0.00
00:00:00
00:10:00
00:20:00
00:30:00
AU
Hr:Min:Sec
mS/cm

Fig. 12. Chromatogram of gel filtration of OmpP2.H6(L8). Lower X-axis measures time (Hr:Min:Sec). Outer left Y-axis measures absorbance at OD_{280} (Absorbance Units), inner left Y-axis measures per cent buffer B (%) applied to column, right Y-axis measures conductivity (mS/cm). Buffer A (50 mM ammonium acetate pH 8.0, 200 mM NaCl, 2 x CMC detergent of choice) is constantly applied. Purified OmpP2.H6(L8) was applied at time index 00:01:00. The conductivity trace did not significantly fluctuate from a baseline value of 0.52 mS/cm. Protein eluted from time index 00:11:00 to time index 00:22:00. The absorbance trace peaked to a maximum value of 0.76 AU corresponding to elution of OmpP2.H6(L8). Fractions spanning the elution peak are indicated on the upper X-axis.

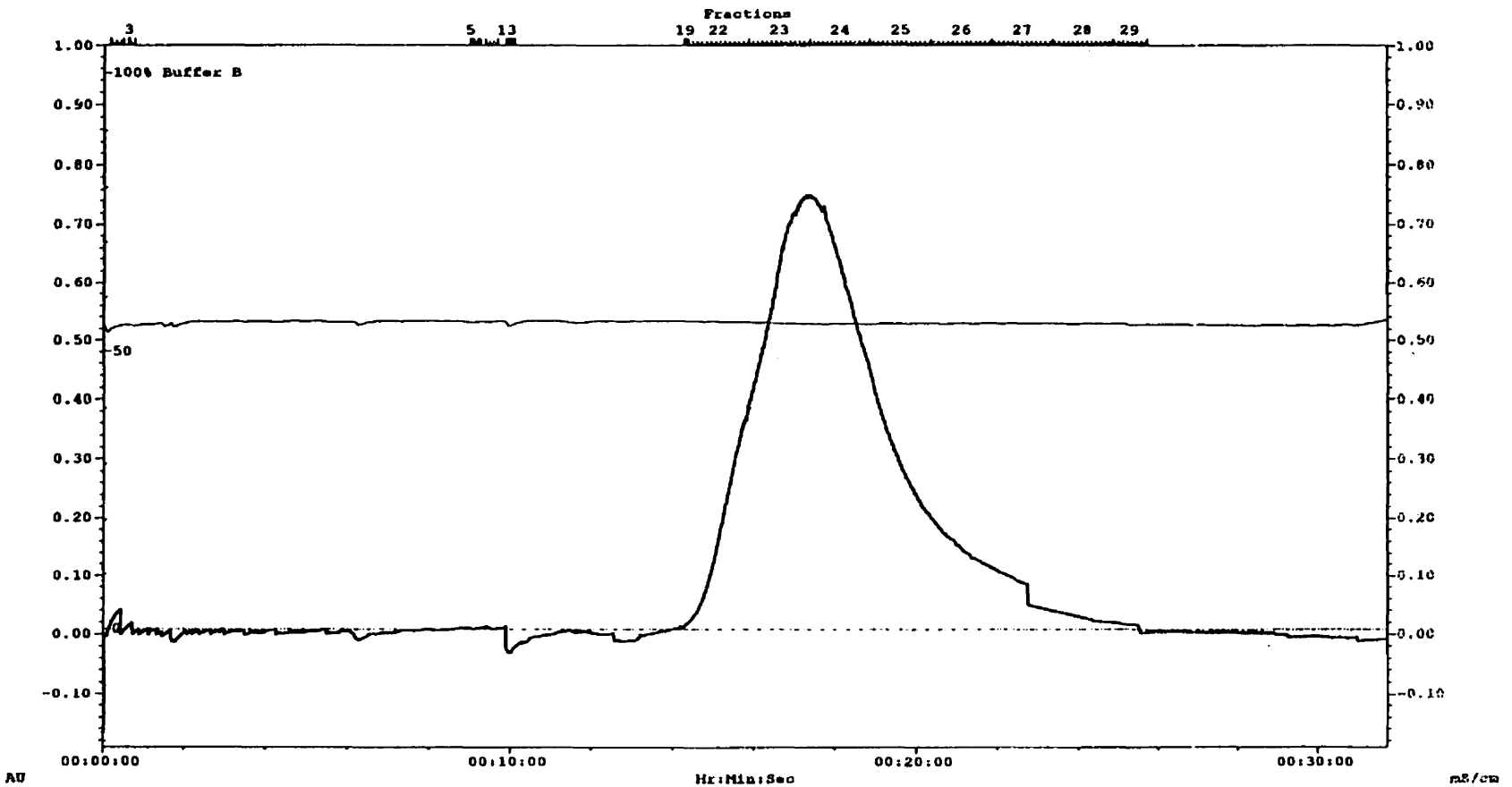
Fractions
3
5
13
19
22
23
24
25
26
27
28
29
100% Buffer B
50
1.00
0.90
0.80
0.70
0.60
0.50
0.40
0.30
0.20
0.10
0.00
-0.10
00:00:00
00:10:00
00:20:00
00:30:00
Hr:Min:Sec
AU
mS/cm

Functional analysis of purified OmpP2.H6s

Single channel conductance experiments were carried out on many preparations of recombinant Hib porin using the planar lipid bilayer setup. Ni^{2+}-NTA-purified OmpP2.H6(L4) and OmpP2.H6(L8) preparations were assessed for their channel forming ability. The median single channel conductance of OmpP2.H6(L4) was determined to be 1.05 nS while the average single channel conductance of OmpP2.H6(L8) was measured to be 1.15 nS (Fig. 13). The same measurements were obtained for POROS MC 20-purified preparations and for detergent exchanged preparations. The median single channel conductance of OmpP2.H6(L8) purified only in the presence of DDAO was also 1.15 nS.

Assessment of homogeneity of OmpP2.H6 preparations

Monodispersity of the protein preparations was determined immediately before proceeding to crystallization trials. Protein samples in buffer for crystallization trials were analyzed by a DLS for monodispersity. Measurements were recorded for 10 to 15 time windows. Samples were measured to be monodisperse and have a molecular mass distribution centered at 39 kDa for preparations of both OmpP2.H6(L4) (Table 3) and OmpP2.H6(L8). Bimodal DLS analysis of a preparation of OmpP2.H6(L8) that was extracted and purified exclusively using DDAO showed a major species with a molecular mass centered at 98 kDa and a second species with a molecular mass centered at 1134 kDa (Table 4). All samples were then subjected to crystallization screening using sparse matrix screening kits using the sitting drop method.

Crystallization trials

Preliminary crystallization trials of OmpP2.H6(L4) in buffer containing LDAO or β-OG using the three sparse matrix screening kits yielded no islands of crystallization. Further investigation of OmpP2.H6(L4) was therefore not pursued. Preliminary crystallization screening of LOS-depleted and LOS-undepleted

Fig. 13. Single channel conductance of OmpP2.H6(L4) (A) and OmpP2.H6(L8) (B) displayed in histogram format after recording in excess of 400 insertions. The median single channel conductance of OmpP2.H6(L4) and OmpP2.H6(L8) is 1.05 nS and 1.15 nS, respectively.

A

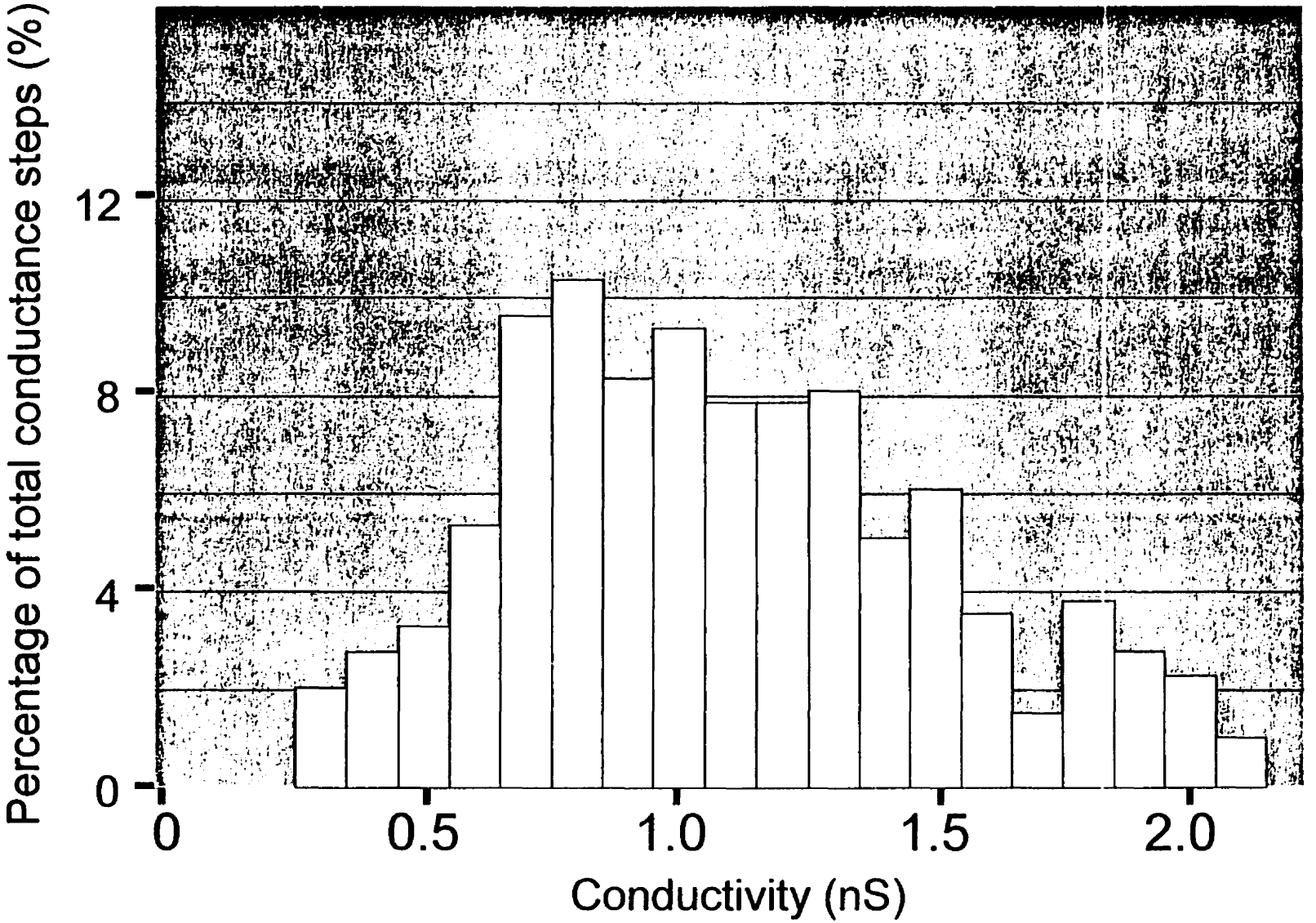
Percentage of total conductance steps (%)
0
4
8
12
0
0.5
1.0
1.5
2.0
Conductivity (nS)

B

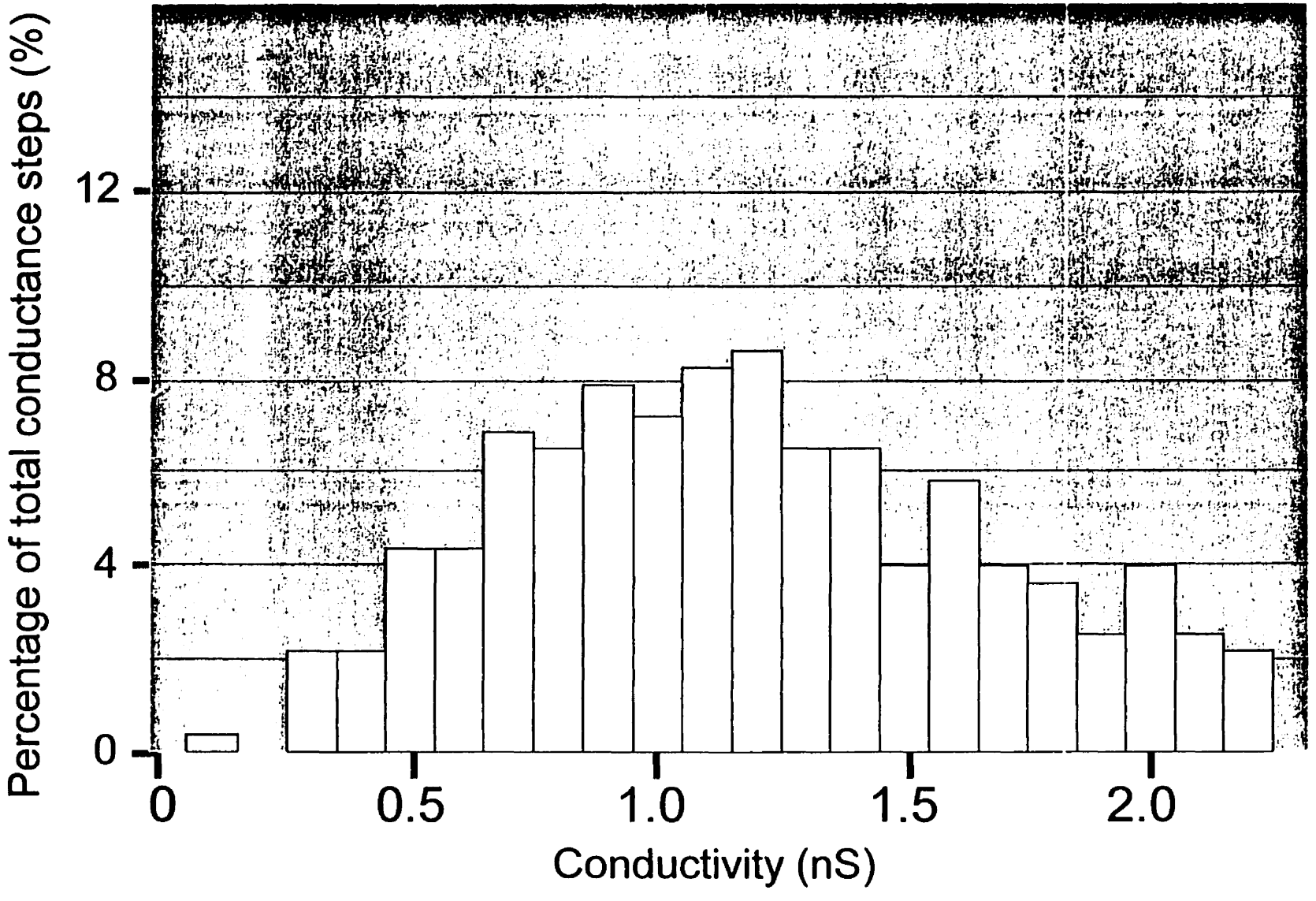
Percentage of total conductance steps (%)
12
8
4
0
0
0.5
1.0
1.5
2.0
Conductivity (nS)

Table 3

Dynamic light scattering
OmpP2.H6(L4)

Meas #	Time (s)	Ampl ()	Diffn Coeff	Radius (nm)	Polyd (nm)	Estd MW	Temp (°C)	Count (cnts/s)	Base Line	SOS Error
1	0	0.753	686	2.8	----	37	17.2	127531	1.000	0.366
2	21	0.765	679	2.8	----	37	17.1	124815	1.001	0.273
3	65	0.749	675	2.9	0.5	38	17.3	123516	1.000	0.287
4	110	0.737	669	2.9	0.4	39	17.3	121650	0.999	0.206
5	153	0.732	661	2.9	----	40	17.3	117909	1.000	0.174
6	199	0.725	656	3.0	----	41	17.4	111625	1.000	0.108
7*	246	0.720	574	3.4	1.0	57	17.3	112336	1.019	1.975
Mean Values:										
6 Mono		0.744	671	2.9	0.2	39	17.3	121174	1.000	0.236
0 Bi 1st		0.000	0	0.0	----	0	0.0	0	0.000	0.000
2nd		0.000	0	0.0		0				

* - measurement was not included when determining mean values

Meas # - measurement number
Time - starting time of respective measurement
Ampl - amplitude of scattered photons
Diffn Coeff - diffraction coefficient of scattered photons relative to incident photons
Radius diffraction - mean hydrodynamic radius of macromolecules derived from the coefficient
Polyd mean - polydispersity, deviation of the hydrodynamic radius values from
Estd MW - molecular weight estimated from hydrodynamic radius
% Mass - %age fraction of mass per measurement in bimodal analysis
Temp - temperature of cell
Count - scattered photons detected per second

Parameters associated with completeness of fit and residual error in regression analysis of the autocorrelation.

BaseLine - a baseline value of 1.000 indicates no difference in the calculated and measurable baselines, the data can be resolved in a single Gaussian distribution.
SOS Error - Sum of squares error, measure of unresolved noise due to low photon signal, noisy solvents or polydispersity. A value less than 5.000 is acceptable.

Table 4

Dynamic light scattering
OmpP2.H6(L8)

Msr #	Time (s)	Ampl ()	Diff Coef	Rad (nm)	Polyd (nm)	Est MW	% Mass	Temp (.C)	Count (cts/s)	Base Line	SOS Error
1	0	0.507	553	4.0	----	85	97	22.3	259663	1.000	0.304
		0.224	227	9.8	----	741	3				
2	12	0.464	574	4.0	----	82	96	23.1	260938	1.004	0.568
		0.289	235	9.7	----	715	4				
3	52	0.511	572	4.0	----	82	97	23.0	250792	0.999	0.275
		0.264	234	9.7	----	721	3				
4	66	0.484	588	3.9	----	77	94	23.1	247613	1.000	0.248
		0.314	268	8.5	----	521	6				
5	81	0.486	581	3.9	----	80	94	23.1	247819	1.001	0.392
		0.312	270	8.5	----	512	6				
6	96	0.610	526	4.3	----	101	98	23.1	253914	0.999	0.516
		0.185	194	11.8	----	1143	2				
7	110	0.511	545	4.2	----	93	95	23.1	258171	1.005	0.392
		0.285	240	9.5	----	682	5				
8	180	0.551	546	4.2	----	93	97	23.1	251003	1.001	0.692
		0.236	225	10.1	----	799	3				
9	194	0.405	614	3.7	----	70	92	23.2	256272	1.000	0.415
		0.355	281	8.1	----	467	8				
10	209	0.448	403	5.7	----	193	99	23.1	390115	1.032	0.575
		0.170	107	21.2	----	4797	1				
11	222	0.563	526	4.4	----	102	98	23.2	258762	1.004	0.189
		0.210	204	11.2	----	1011	2				
12	244	0.595	503	4.6	----	114	99	23.2	259722	1.001	0.545
		0.110	174	13.1	----	1493	1				
Mean Values:											
Mono		0.739	403	5.7	2.5	205	100	23.1	266232	1.009	7.289
Bi-1		0.511	544	4.2	----	98	96	23.1	266232	1.004	0.426
Bi-2		0.246	222	10.9		1134	4				

Refer to legend of Table. 3

OmpP2.H6(L8) in buffers containing various detergents yielded some islands of crystallization (Table 5). Crystal growth conditions were optimized as described in Materials and Methods to yield crystals sufficiently large for X-ray examination. Hexagonal bipyramid and cubic morphology crystals resulted from crystallization of LOS-undepleted OmpP2.H6(L8) in buffer containing LDAO and DDAO, respectively (Fig. 14). Crystals were grown to sufficient size to be mounted for X-ray examination. The same crystallization conditions previously allowed growth of wild-type OmpP2 crystals in our laboratory that diffracted to between 4 and 5 Å (Coulton and Welte, personal communication). X-ray radiation of the hexagonal bipyramid crystal for 30 minutes with a 1° rotation did not result in a diffraction pattern. Similarly, cubic crystals grown in identical conditions with detergent in the buffer replaced with DDAO did not yield any diffraction pattern. Examination of the hexagonal bipyramid and cubic crystals under polarized light revealed them not to be birefringent. As birefringence of crystals is a good indication that the crystals are ordered well enough to diffract X-rays, the hexagonal bipyramid and cubic crystals were not expected to yield diffraction spots. OmpP2.H6(L8) crystals of parallelpiped morphology were grown from protein preparations exchanged into buffer containing DDAO (Fig. 14). X-ray radiation of these crystals showed diffraction to 8 Å resolution (Fig. 15). The parallelpiped crystals were macroseeded to increase crystal thickness. These attempts, however, proved unsuccessful at producing larger crystals. The preparation of OmpP2.H6(L8) purified exclusively in the presence of DDAO did not result in any islands of crystallization when tested against the 146 commercially available screening solutions.

Table 5

Initial crystallization conditions of OmpP2.H6(L8) in this study.

Preparation in LDAO	
Crystallization Condition	**Crystal Morphology and dimensions**
30% PEG 400, 0.2 M $MgCl_2$, 0.1M HEPES pH 7.5 *	Hexagonal bipyramids 200 x 200 x 200 μm
12% MPD, 0.1 M ADA pH 6.5	Rods: 50 x 20 x 10 μm
12% MPD, 0.1 M HEPES pH 7.5, 0.1 M sodium citrate	Oblong spheres: 40 x 30 x 30 μm
35% Dioxane	Plates: 300 x 100 x 5 μm
10% Ethanol, 1.5 M NaCl	Irreg. cubes: 40 x 40 x 40 μm
30% MPD, 0.1 M $NaCH_3COO$ pH 4.6	Plates: 150 x 100 x 5 μm
2.5 M 1,6-Hexanediol, 0.1 M sodium citrate pH 5.6	Rods: 100 x 20 x 20 μm
Preparations in DDAO	
Crystallization Conditions	**Crystal morphology and dimensions**
30% PEG 400, 0.2 M $MgCl_2$, 0.1M HEPES pH 7.5 *	Cubic 100 x 100 x 100 μm
12% PEG 6000, 0.1 M ADA pH 6.5, 0.1 M $MgCl_2$	Rods: 300 x 40 x 40 μm
12% PEG 6000, 0.1M MES pH 6.5	Irreg. rods: 300 x 30 x 20 μm
Preparations in β-OG	
Crystallization Conditions	**Crystal morphology and dimensions**
20% PEG 8000, NaCacodylate pH 6.5, 0.2 M Mg Acetate	Rods: 300 x 50 x 60 μm

* indicates preparation was not depleted of LOS

Fig. 14. Crystals of OmpP2.H6(L8). (A) Hexagonal bipyramid crystals grown from protein preparation in 20 mM ammonium acetate pH 8.0, 100 mM NaCl, 0.10% LDAO against crystallization solution containing 30% PEG, 100 mM $MgCl_2$, 100 mM HEPES pH 7.5 after 21 days. Dimensions: *circa* 400 x 200 x 100 μm (B) Parallelpiped crystals grown from protein preparation in 20 mM ammonium acetate pH 8.0, 200 mM NaCl, 0.5% DDAO against crystallization solution containing 12% PEG 6000, 100 mM $MgCl_2$, and 100 mM ADA pH 6.5 after 10 days. Dimensions: *circa* 400 x 50 x 50 μm.

A

B

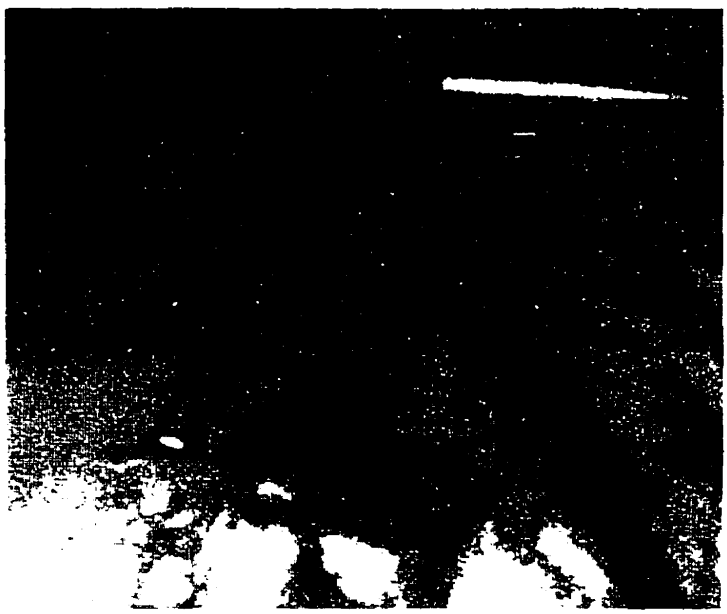

Fig. 15. X-ray diffraction image from parallelpiped OmpP2.H6(L8) crystal exposed for 30 minute over 1° rotation using a Rigaku RU 200 rotating anode generator in combination with a 30 cm MAR image plate detector. Image edge corresponds to a diffraction limit of 3.6 Å. Dashed circle corresponds to a diffraction resolution of 7 Å. Outermost reflections are visible at 8 Å.

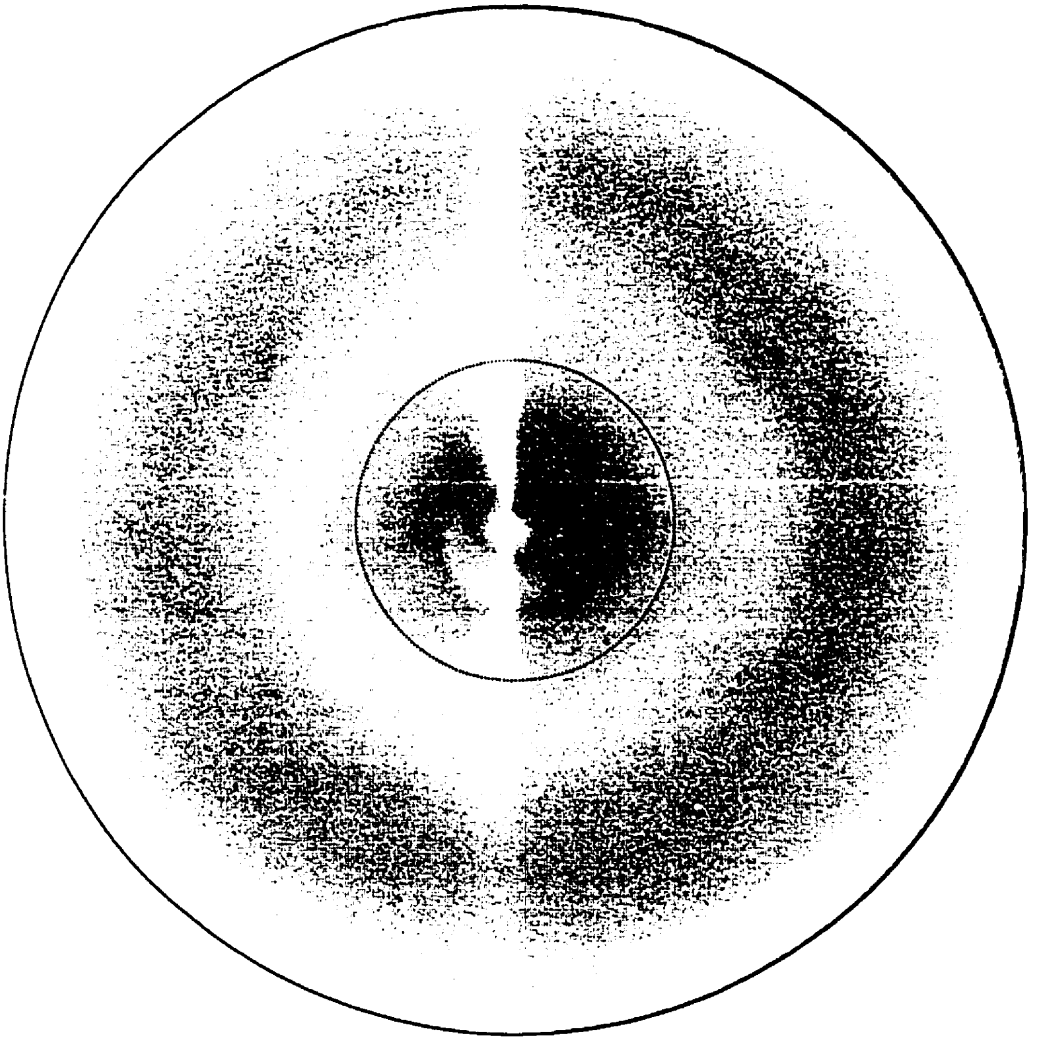

Discussion

Immobilized metal-chelate affinity chromatography (IMAC) is a powerful technique used to purify large homogeneous preparations of crystallographic quality protein. The technique takes advantage of the strong affinity of consecutive histidine residues for immobilized transition metal with two free coordination sites. The first generation of IMAC media employed the iminodiacetate functional group to chelate transition metal ions at three of six possible coordination sites. Leaching of immobilized metal ions into protein preparations due to the affinity of proteins or peptides in the mobile phase with comparable chelating character to bind transition metal ions was a disadvantage. The current generation of IMAC media has overcome this problem. Ni^{2+}-NTA (QIAGEN), Talon (Clontech) and POROS MC (PerSeptive Biosystems) are chromatographic media with a stronger affinity for transition metal ions. Ni^{2+}-NTA medium consists of agarose particles with nitrolo-triacetate functional groups that have the ability to chelate four of the six coordination sites of Ni^{2+}. Metal ion binding to the agarose particle is therefore much stronger and the remaining two coordination sites are left accessible to imidazole side chains of histidine residues. Talon medium particles have a tetradentate functional group that can also chelate four of the six coordination sites of transition metal ions. Charging with cobalt is prescribed for optimal performance of Talon. POROS MC particles are conjugated to imidodiacetate functional groups. The imidodiacetate group is also capable of chelating four of the six coordination sites of a transition metal ion. POROS medium particles are used in perfusion chromatography, which is a chromatographic advance that permits high flow rates combined with high-resolution separation of macromolecules.

A final consideration for the use of IMAC is the site of hexahistidine affinity tag insertion. Insertion of the affinity tag at the amino- or carboxy-terminus offers convenience when purifying soluble proteins. If the tag is not buried, then it can be removed by specific protease digestion following protein purification to homogeneity. High efficiency protein purification is strongly indicative of surface-exposed affinity tags. The same, however, is not true for membrane proteins.

The amino- and carboxy-termini of membrane proteins are not necessarily surface exposed, hence knowledge of the gross topological organization is required and care must be taken to preserve protein secondary structure. The high-resolution atomic structures of the porins solved to date show that the amino- and carboxy-termini are not surface exposed and occasionally interact with each other by salt bridge to complete the 16^{th} β-strand. Insertion of affinity tags in porins therefore must be restricted to extramembranous regions that are surface-exposed. Potential sites of insertion should not be in regions that are essential for the normal functioning of the protein. Loop 3 constitutes such a region in porins. High-resolution crystal structures of porins show that loop 3 is folded into the pore lumen and, therefore, plays an important role to screen on the basis of size solutes that can cross the pore. A final consideration when choosing the affinity tag insertion site is to avoid regions of possible crystal contacts. This, however, requires that proteins with moderate sequence homology to the protein under study have been successfully crystallized to solve the high-resolution X-ray crystal structures. Loop 4 and loop 8 of the OmpF porin structure were observed not to participate in crystal contacts. A unique *Sna*BI site was found in the transfer vector, pFFA02, in the sequence corresponding to loop 4 of OmpP2. Restriction endonuclease digestion followed by insertion of a linker encoding six consecutive histidine codons allowed for mutagenesis of loop 4. Since there was no unique restriction site found in the DNA sequence of plasmid pFFA02 that corresponded to loop 8 of OmpP2, we decided to insert the hexahistidine codons by oligonucleotide-directed mutagenesis at this location.

Both recombinant hexahistidine-tagged Hib porins were expressed to high levels in strain RSFA21. SDS-PAGE analysis of lysed RSFA21 harboring recombinant plasmids revealed a significant enrichment of porin in the membrane extract. The level of expression is equivalent or surpasses the chromosomal expression of porin in strain DB117. Despite the predicted membrane-proximal location of the His6 tag following Val174 in loop 4, the tag was sufficiently exposed to allow successful purification of OmpP2.H6(L4). Immobilized OmpP2.H6(L4) was eluted from Ni^{2+}-NTA medium at an imidazole concentration

of 150mM. Loop 8, in contrast, was proposed to be most surface-exposed according to the topology map of Hib porin (Srikumar *et al.*, 1992). Since construction of OmpP2.H6(L8) was achieved by oligonucleotide-directed mutagenesis, there was no necessity to add flanking nucleotides to compensate for codon breakage due to endonuclease cleavage of DNA. Mutagenesis, therefore, consisted of the introduction of nucleotides encoding Met-His6 immediately after Thr321. Purification of OmpP2.H6(L8) was also successful using Ni^{2+}-NTA as the primary purification medium. Elution of immobilized OmpP2.H6(L8) occurred at an imidazole concentration of 180 mM.

The difference in imidazole concentration required to elute OmpP2.H6(L4) compared to OmpP2.H6(L8) offers some insight to the binding affinity of the two recombinant proteins. The membrane-proximal location of the His6 tag in OmpP2.H6(L4) may prevent its optimal surface exposure due to steric blockage by flanking amino acids 155-173. This may explain the moderate association between the His6 tag and Ni^{2+}-NTA. The location of the His6 tag in OmpP2.H6(L8) is proposed to be maximally surface exposed, thus explaining the very strong association between the His6 tag and Ni^{2+}-NTA. The higher imidazole concentration required to elute OmpP2.H6(L8) as compared to the imidazole concentration required to elute OmpP2.H6(L4) correlates with the predicted relative surface exposure of the two His6 tags.

Acidification of the buffer is another means to elute immobilized proteins. The interaction of consecutive histidine residues with Ni^{2+}-NTA is mediated by the lone pair electrons of the nitrogen on the imidazole ring of histidine. Lower pH conditions protonate the nitrogen of the imidazole ring of histidine side chains converting its lone pair electrons to bonding pair electrons. Since bonding pair electrons are unable to bind the chelate Ni^{2+} in the context of NTA, the interaction of His6 affinity tags with Ni^{2+}-NTA is abrogated in acidic conditions resulting in protein elution. This procedure, however, is likely to denature OmpP2.H6 preparations making them unsuitable for structural studies. Another method for eluting Ni^{2+}-NTA-immobilized proteins is the addition of divalent cation chelators such as EDTA. Since Ni^{2+} is required to mediate the interaction between the

NTA functional group and His6-tagged proteins, addition of chelating agents that bind Ni^{2+} with very sufficient affinity to remove it from NTA will also promote elution of immobilized His6-tagged proteins. Elution of immobilized OmpP2.H6's was not attempted by pH reduction or addition of strong chelators.

The purification results for OmpP2.H6 are similar to the results obtained with FhuA.H6 (Ferguson *et al.*, 1998). The mutant FhuA.H6 had an insertion of six consecutive histidine residues with three additional amino acids to maintain the reading frame of the *fhuA* gene. The inserted sequence introduced Ser-His6-Gly-Ser after Pro-405 in a region previously proposed to form loop 10 (Koebnik and Braun, 1993). Recent elucidation of the structure of FhuA (Ferguson *et al.*, 1998; Locher *et al.*, 1998) assigned amino acid 405 to constitute loop 5 of the carboxy-terminal 22-stranded β-barrel.

Immunoblot with mAbs Por.1 and Por.6 demonstrated that the location of His6 affinity tag insertion at Val174 did not prevent recognition by mAb Por.1 of its cognate determinant. The ability of OmpP2.H6(L4) to be purified by metal-chelate chromatography indicates that the region around Val174 is surface exposed. Recognition of OmpP2.H6(L8) by mAb Por.6 was abolished confirming the location of the His6 tag in loop 8 immediately following Thr321.

SDS-PAGE analysis followed by silver staining for proteins and lipooligosaccharide revealed preparations of both OmpP2.H6(L4) and OmpP2.H6(L8) following purification by Ni^{2+}-NTA to be nearly homogeneous (Fig. 9). A protein species migrating to about 25 kDa and significant amounts of lipooligosaccharide were evident contaminants. Removal of these two contaminating species was proposed by a second step of IMAC that employed perfusion chromatography. Perfusion chromatography allows improved chromatographic separation of macromolecules at high flow rates using both low- and high-pressure systems. Perfusion chromatography particles contain "through pores", which are channels that traverse the particles. Additionally the pockets on the particles are shallower than the pockets found on conventional chromatographic particles. This enables macromolecules to diffuse to and from

their binding sites on the particles at very high rates, permitting chromatographic separation at high flow rates without a loss of resolution.

POROS MC 20 was selected for the second chromatographic purification of OmpP2.H6. POROS MC 20 purification proceeded using the same buffers as for Ni^{2+}-NTA purification substituting Tris-HCl with ammonium acetate as the buffering agent to avoid the incompatibility of Tris-HCl with the perfusion chromatography medium. Removal of the contaminating protein species was evident by SDS-PAGE analysis of the POROS-purified preparations of OmpP2.H6.

The high affinity of LPS to OMPs has been documented. LPS association to FhuA was demonstrated to be very specific and strong (Locher and Rosenbusch, 1997). Depending on the detergent used for extraction, different species of FhuA were identified by SDS-PAGE that associated to one, two or no molecules of LPS. FhuA strongly associated with one LPS molecule migrated slower than FhuA unassociated with LPS while FhuA associated to two molecules of LPS migrated least rapidly. Unassociated LPS was identified at the dye front of the SDS-polyacrylamide gels indicating weak interaction of FhuA with many LPS molecules. The weak interaction was disrupted by preparation for SDS-PAGE analysis. Strong association between LPS and FhuA in a one to one stoichiometry allowed cocrystallization and determination of the X-ray crystal structure of FhuA and LPS (Ferguson *et al.*, 1998). Complexes of OmpF-LPS suitable for structure-function studies by X-ray crystallography were also isolated. Free-flow electrophoresis (FFE) of outer membrane extracts of *E. coli* B^E in the presence of C_8E_N above the CMC (0.5% to 1.0%) allowed isolation of OmpF trimers with a full complement of associated LPS (Holzenburg *et al.*, 1989). The same FFE experiments carried out in the presence of EDTA allowed the isolation of OmpF trimers associated to one tightly bound LPS molecule. FFE-purified OmpF trimers that were loosely associated to LPS were repurified by FFE in the presence of decreasing concentrations of EDTA. This allowed the isolation of OmpF trimers with one, two, or eight molecules of loosely associated LPS molecules in addition to the one tightly bound LPS molecule. The strong

association of one LPS molecule with the functional unit of an OMP such as an OmpF trimer or a FhuA monomer suggests that all functional units of OMPs are capable of binding to one LPS molecule with high affinity. The equivalent association of Hib porin trimers with one LOS molecule is expected. Observation, however, of such association with Hib porin is difficult because the trimer readily dissociates. What is observed is the loose association of LOS with Hib porin monomers. SDS-PAGE analysis of samples from each step of Ni^{2+}-NTA purification identified the identical relative migration OmpP2.H6 in each lane. Such migration patterns indicate a weak interaction between OmpP2.H6 and LOS.

The deoxycholate- and high salt- wash steps were introduced into the POROS MC 20 chromatography protocol to deplete LOS in the preparations of OmpP2.H6. Examination of the flow-through fractions from high salt- and deoxycholate-wash steps' revealed only LOS indicating the efficiency and novelty of these steps.

Since deoxycholate is a denaturing detergent, single channel conductance experiments were undertaken on the high salt- and deoxycholate-washed protein preparations to assess the effect of deoxycholate exposure on OmpP2.H6(L8). Identical single channel conductance distribution was observed from OmpP2.H6(L8) purified with Ni^{2+}-NTA chromatography and from preparations additionally purified with POROS MC 20 chromatography. These measurements showed that exposure to deoxycholate does not alter the channel forming property of recombinant Hib porin. These preparations of OmpP2.H6(L8) rapidly precipitated when the NaCl concentration dropped below 150 mM. NaCl concentration in the buffer was increased to 200 mM to maintain protein in solution. The same NaCl concentration was used for crystallization buffer. Precipitation of LOS-depleted preparations of Hib porin suggests that LOS was interacting with OmpP2 in a stabilizing manner. However, the presence of LOS in a protein preparation would add considerable heterogeneity due to the variable number of O-antigen subunits covalently attached to each LOS molecule. Therefore, crystallization from these preparations was not expected to yield X-ray

quality crystals. Due to the heterogeneous nature of LOS, we determined that complete removal of LOS from the OmpP2.H6(L8) preparation was necessary prior to starting the crystallization trials. Since detergent-exchange chromatography required the protein preparations to be in buffer containing 50 mM NaCl, LOS was not completely removed in order to maintain protein stability. SDS-PAGE followed by silver staining for LOS showed that these preparations contained a LOS species that migrated as a sharp discrete band near the dye front. Although these preparations were not completely stripped of their LOS content, the appearance of a sharp discrete LOS band indicated the presence of one species of LOS in the protein preparation.

DLS analysis of OmpP2.H6(L4) and OmpP2.H6(L8) preparations showed a species with a molecular mass of 39 kDa indicative that porin monomers were purified. In contrast, analysis of a OmpP2.H6(L8) preparation purified exclusively with DDAO showed a major species with a molecular mass of 98 kDa and a minor species with a molecular mass of 1134 kDa. The 98 kDa species in the DDAO preparation of OmpP2.H6(L8) suggests that porin trimers were purified. The 1134 kDa species is predicted to reflect aggregates of DDAO in the protein preparation. These results imply that the larger detergent micelles corresponding to DDAO are unable to disrupt the intermolecular association between porin monomers necessary to maintain the trimeric organization of porins. The smaller detergent micelles corresponding to LDAO have the ability to disrupt the interactions between porin monomers that allow their association into trimers.

Preparations of OmpP2.H6(L8) not completely stripped of their LOS content produced crystals of hexagonal bipyramid and cubic morphology when screened against crystallization solution containing 30% PEG 400, 0.20M $MgCl_2$, and 0.10M N-2-Hydroxyethyl Piperazine N-2'-Ethanesulfonic acid (HEPES) pH 7.5. We predicted that the lack of X-ray diffraction by the hexagonal bipyramid crystals resulted from the preparations not being depleted of their LOS content. LPS was reported to interfere significantly with the crystallization of bacterial porins (Garavito and Rosenbusch, 1986). The heteregeneous nature of LOS is predicted to prevent the ordered lattice arrangement of porin molecules,

monomers or trimers. To eliminate any disordering effect of LOS, we decided to remove completely LOS from the protein preparations in a manner that maintained porin function as measured by single channel conductance. Crystallization trials were again attempted on LOS-depleted OmpP2.H6(L8) after exchange into buffers containing different detergents. Islands of crystallization were identified from preparations of OmpP2.H6(L8) detergent exchanged into DDAO or β-OG. Crystals of parallelpiped morphology were grown to sufficient size for X-ray radiation at a local source. Crystals were grown from the OmpP2.H6(L8) preparation, detergent exchanged into DDAO, using crystallization solution containing 12% PEG 6000, 0.10M $MgCl_2$, and 0.10M N-(2-Acetamido) iminodiacetic acid (ADA) pH 6.6 diffracted to 8Å resolution. The same crystals were irradiated at the synchrotron (Brookhaven National Laboratory, U.S.). Crystallographers take advantage of the stronger intensity X-ray beams generated at synchrotrons to obtain higher resolution data sets. The parallelpiped crystals of OmpP2.H6(L8) did not diffract X-rays to any resolution beyond 14Å at the synchrotron,. Reasons that might explain the poorer diffraction data from synchrotron radiation include the age of crystals and the transit conditions.

Use of non-ionic detergents in the protein purification protocol (see Methods and Materials) as compared to the detergent required in the wild type OmpP2 purification protocol was predicted to maintain the OmpP2.H6 in a conformation closer to its native conformation. Exposure to denaturing detergent and ethanol precipitation steps are known to denature proteins. Preparations of wild type OmpP2 that were believed to be denatured resulted in crystals unable to produce diffraction patterns beyond 4 Å by synchrotron (DESY, Hamburg, Germany) X-ray radiation. Our novel protocol for Hib porin purification employing hexahistidine affinity tags was designed to avoid exposure to denaturing detergents and precipitation steps. The purification protocol of OmpP2.H6 also spanned five days in comparison to a minimum of 10 days for the classical purification protocol of OmpP2. These modifications to the protocol for OmpP2.H6 purification were expected to maintain a maximum proportion of

proteins in their native conformation thus increasing the likelihood that better X-ray diffraction data would be derived from OmpP2.H6 crystals. DLS data indicated that trimers were purified when all steps of OmpP2.H6(L8) extraction and purification employed DDAO. Since the porin trimer is structurally more rigid than the monomer, crystallization trials of Hib porin preparations extracted and purified in DDAO are believed to promote growth of well ordered crystals.

Future plans to obtain X-ray quality crystals of Hib porin include rigidifying the extramembranous surface of Hib porin. Previous work showed that loop 4 was predicted to be 15 amino acids longer in Hib porin than the corresponding loop in OmpF of *E. coli* (Srikumar *et al.*, 1997). Since molecular modeling of Hib porin identified its structural similarities to OmpF, it is predicted that removal of amino acids from loop 4 of Hib thereby rendering the length of loop 4 comparable to loop 4 in OmpF may facilitate the growth of X-ray quality crystals. A strategy to increase possible crystal contacts employed site-directed mutagenesis of amino acids at the polar surfaces of OmpA171 and OmpX of *E. coli* (Pautsch *et al.*, 1999). Charged amino acids that can only bind to oppositely charged counter surfaces were mutated to polar amino acids that can bind various types of counter surfaces. Candidate regions of Hib porin that can be targeted in this manner include loops 2, 4, 5 and 8 and the periplasmic turns. The addition of 6 consecutive positively charged histidine residues in the surface-exposed region of loop 8 is expected to permit crystal contacts restricted to a negatively charged counter surface and preventing contact with positively charged counter surfaces. Since the membrane proximal location of the his6 tag in loop 4 of OmpP2.H6(L4) is not expected to participate in crystal contacts, employing OmpP2.H6(L4) in conjunction with site directed mutagenesis to neutralize charged amino acids at the surface is predicted to yield X-ray quality crystals.

References

Abrami, L., Capurro, C., Ibarra, C., Parisi, M., Buhler, J.M., and Ripoche, P. (1995). Distribution of mRNA encoding the FA-CHIP water channel in amphibian tissues: effects of salt adaptation. J. Membr. Biol. *143*, 199-205.

Agre, P., Bonhivers, M., and Borgnia, M.J. (1998). The aquaporins, blueprints for cellular plumbing systems. J. Biol. Chem. *273*, 14659-14662.

Allen, J.P., Feher, G., Yeates, T.O., Komiya, H., and Rees, D.C. (1987). Structure of the reaction center from *Rhodobacter sphaeroides* R-26: the protein subunits. Proc. Natl. Acad. Sci. U. S. A. *84*, 6162-6166.

Barcak, G.J., Chandler, M.S., Redfield, R.J., and Tomb, J.F. (1991). Genetic systems in *Haemophilus influenzae*. Methods Enzymol. *204:321-42*, 321-342.

Batley, M., Packer, N.H., and Redmond, J.W. (1982). Molecular analysis of the phospholipids of *Escherichia coli* k12. Biochim. Biophys. Acta *710*, 400-405.

Bauer, K., Struyve, M., Bosch, D., Benz, R., and Tommassen, J. (1989). One single lysine residue is responsible for the special interaction between polyphosphate and the outer membrane porin PhoE of *Escherichia coli*. J. Biol. Chem. *264*, 16393-16398.

Benz, R. (1994). Uptake of solutes through bacterial outer membranes. In Bacterial Cell Wall. J.-M. Ghuysen and R. Hakenback, eds. (Amsterdam: Elsevier Science B.V.), pp. 397-423.

Benz, R., Boehler-Kohler, B.A., Dieterle, R., and Boos, W. (1978). Porin activity in the osmotic shock fluid of *Escherichia coli*. J. Bacteriol. *135*, 1080-1090.

Benz, R., Janko, K., and Lauger, P. (1979). Ionic selectivity of pores formed by the matrix protein (porin) of *Escherichia coli*. Biochim. Biophys. Acta *551*, 238-247.

Beuron, F., Le Caherec, F., Guillam, M.T., Cavalier, A., Garret, A., Tassan, J.P., Delamarche, C., Schultz, P., Mallouh, V., and Rolland, J.P. (1995). Structural analysis of a MIP family protein from the digestive tract of *Cicadella viridis*. J. Biol. Chem. *270*, 17414-17422.

Braun, V. (1975). Covalent lipoprotein from the outer membrane of *Escherichia coli*. Biochim. Biophys. Acta *415*, 335-377.

Broome, C.V. (1987). Epidemiology of *Haemophilus influenzae* type b infections in the United States. Pediatr. Infect. Dis. J. *6*, 779-782.

Burroughs, M.H., Chang, Y.S., Gage, D.A., and Tuomanen, E.I. (1993). Composition of the peptidoglycan of *Haemophilus influenzae*. J. Biol. Chem. *268*, 11594-11598.

Calamita, G., Kempf, B., Bonhivers, M., Bishai, W.R., Bremer, E., and Agre, P. (1998). Regulation of the *Escherichia coli* water channel gene aqpZ. Proc. Natl. Acad. Sci. U. S. A. *95*, 3627-3631.

Capobianco, J.O. and Goldman, R.C. (1994). Macrolide transport in *Escherichia coli* strains having normal and altered OmpC and/or OmpF porins. International Journal of Antimicrobial Agents *4* , 183-189.

Charbit, A., Ronco, J., Michel, V., Werts, C., and Hofnung, M. (1991). Permissive sites and topology of an outer membrane protein with a reporter epitope. J. Bacteriol. *173*, 262-275.

Cope, L.D., Pelzel, S.E., Latimer, J.L., and Hansen, E.J. (1990). Characterization of a mutant of *Haemophilus influenzae* type b lacking the P2 major outer membrane protein. Infect. Immun. *58*, 3312-3318.

Cowan, S.W., Schirmer, T., Rummel, G., Steiert, M., Ghosh, R., Pauptit, R.A., Jansonius, J.N., and Rosenbusch, J.P. (1992). Crystal structures explain functional properties of two *E. coli* porins. Nature *358*, 727-733.

Dahan, D., Vachon, V., Laprade, R., and Coulton, J.W. (1994). Voltage gating of porins from *Haemophilus influenzae* type b. Biochim. Biophys. Acta *1189*, 204-211.

Dajani, A.S., Asmar, B.I., and Thirumoorthi, M.C. (1979). Systemic *Haemophilus influenzae* disease: an overview. J. Pediatr. *94*, 355-364.

Decker, M.D. and Edwards, K.M. (1998). *Haemophilus influenzae* type b vaccines: history, choice and comparisons. Pediatr. Infect. Dis. J. *17*, S113-S116

Deisenhofer, J., Epp, O., Miki, K., Huber, R., and Michel, H. (1984). X-ray structure analysis of a membrane protein complex. Electron density map at 3 A resolution and a model of the chromophores of the photosynthetic reaction center from *Rhodopseudomonas viridis*. J. Mol. Biol. *180*, 385-398.

Dominguez, M.A. and Pallares, R. (1998). Antibiotic resistance in respiratory pathogens. Curr. Opin. Pulm. Med. *4*, 173-179.

Eisele, J.L. and Rosenbusch, J.P. (1990). In vitro folding and oligomerization of a membrane protein. Transition of bacterial porin from random coil to native conformation. J. Biol. Chem. *265*, 10217-10220.

Ferguson, A.D., Breed, J., Diederichs, K., Welte, W., and Coulton, J.W. (1998). An internal affinity-tag for purification and crystallization of the siderophore receptor FhuA, integral outer membrane protein from *Escherichia coli* K-12. Protein Sci. *7*, 1636-1638.

Ferguson, A.D., Hofmann, E., Coulton, J.W., Diederichs, K., and Welte, W. (1998). Siderophore-mediated iron transport: crystal structure of FhuA with bound lipopolysaccharide. Science *282*, 2215-2220.

Ferré-D'Amaré, A.R. and Burley, S.K. (1994). Use of dynamic light scattering to assess crystallizability of macromolecules and macromolecular assemblies. Structure. *2*, 357-359.

Fischer, K., Weber, A., Brink, S., Arbinger, B., Schunemann, D., Borchert, S., Heldt, H.W., Popp, B., Benz, R., and Link, T.A. (1994). Porins from plants. Molecular cloning and functional characterization of two new members of the porin family. J. Biol. Chem. *269*, 25754-25760.

Fleischmann, R.D., Adams, M.D., White, O., Clayton, R.A., Kirkness, E.F., Kerlavage, A.R., Bult, C.J., Tomb, J.F., Dougherty, B.A., and Merrick, J.M. (1995). Whole-genome random sequencing and assembly of *Haemophilus influenzae* Rd. Science *269*, 496-512.

Forst, D., Welte, W., Wacker, T., and Diederichs, K. (1998). Structure of the sucrose-specific porin ScrY from *Salmonella typhimurium* and its complex with sucrose. Nat. Struct. Biol. *5*, 37-46.

Freundlieb, S., Ehmann, U., and Boos, W. (1988). Facilitated diffusion of p-nitrophenyl-alpha-D-maltohexaoside through the outer membrane of *Escherichia coli*. Characterization of LamB as a specific and saturable channel for maltooligosaccharides. J. Biol. Chem. *263*, 314-320.

Garavito, R.M., Jenkins, J., Jansonius, J.N., Karlsson, R., and Rosenbusch, J.P. (1983). X-ray diffraction analysis of matrix porin, an integral membrane protein from *Escherichia coli* outer membranes. J. Mol. Biol. *164*, 313-327.

Garavito, R.M. and Picot, D. (1991). Crystallization of membrane proteins: a minireview. Journal of Crystal Growth *110*, 89-95.

Garavito, R.M. and Rosenbusch, J.P. (1980). Three-dimensional crystals of an integral membrane protein: an initial x-ray analysis. J. Cell Biol. *86*, 327-329.

Garavito, R.M. and Rosenbusch, J.P. (1986). Isolation and crystallization of bacterial porin. Methods Enzymol. *125:309-28*, 309-328.

Gerbl-Rieger, S., Engelhardt, H., Peters, J., Kehl, M., Lottspeich, F., and Baumeister, W. (1992). Topology of the anion-selective porin Omp32 from *Comamonas acidovorans*. J. Struct. Biol. *108*, 14-24.

Goldshleger, R., Tal, D.M., and Karlish, S.J. (1995). Topology of the alpha-subunit of Na,K-ATPase based on proteolysis. Lability of the topological organization. Biochemistry *34*, 8668-8679.

Goldstein, F.W., Gutmann, L., Williamson, R., Collatz, E., and Acar, J.F. (1983). In vivo and in vitro emergence of simultaneous resistance to both beta- lactam and aminoglycoside antibiotics in a strain of Serratia marcescens. Ann. Microbiol. (Paris.) *134A*, 329-337.

Hancock, R.E. and Bell, A. (1988). Antibiotic uptake into gram-negative bacteria. Eur. J. Clin. Microbiol. Infect. Dis. *7*, 713-720.

Hancock, R.E., Farmer, S.W., Li, Z.S., and Poole, K. (1991). Interaction of aminoglycosides with the outer membranes and purified lipopolysaccharide and OmpF porin of *Escherichia coli*. Antimicrob. Agents Chemother. *35*, 1309-1314.

Hancock, R.E.W., Karunaratne D.N., and Bernegger-Egli C. (1994). Molecular organisation and structural role of outer membrane macromolecules. In Bacterial Cell Wall. J.-M. Ghuysen and R. Hakenback, eds. (Amsterdam: Elsevier Science B.V.), pp. 263-279.

Henderson, R. and Unwin, P.N. (1975). Three-dimensional model of purple membrane obtained by electron microscopy. Nature *257*, 28-32.

Hirsch, A., Breed, J., Saxena, K., Richter, O.M., Ludwig, B., Diederichs, K., and Welte, W. (1997). The structure of porin from *Paracoccus denitrificans* at 3.1 A resolution. FEBS Lett. *404*, 208-210.

Hirsch, A., Wacker, T., Weckesser, J., Diederichs, K., and Welte, W. (1995). Purification, characterization, crystallization, and preliminary X-ray results from *Paracoccus denitrificans* porin. Proteins *23*, 282-284.

Holzenburg, A., Engel, A., Kessler, R., Manz, H.J., Lustig, A., and Aebi, U. (1989). Rapid isolation of OmpF porin-LPS complexes suitable for structure- function studies. Biochemistry *28*, 4187-4193.

Jaffé, A., Chabbert, Y.A., and Derlot, E. (1983). Selection and characterization of beta-lactam-resistant *Escherichia coli* K-12 mutants. Antimicrob. Agents Chemother. *23*, 622-625.

Jap, B.K. and Walian, P.J. (1990). Biophysics of the structure and function of porins. Q. Rev. Biophys. *23*, 367-403.

Jap, B.K. and Walian, P.J. (1996). Structure and functional mechanism of porins. Physiol. Rev. *76*, 1073-1088.

Jeanteur, D., Schirmer, T., Fourel, D., Simonet, V., Rummel, G., Widmer, C., Rosenbusch, J.P., Pattus, F., and Pages, J.M. (1994). Structural and functional alterations of a colicin-resistant mutant of OmpF porin from *Escherichia coli.* Proc. Natl. Acad. Sci. U. S. A. *91*, 10675-10679.

Kim, H. (1998). Crystallization of OmpC osmoporin from *Escherichia coli.* Acta Crystallogr. D. Biol. Crystallogr. *54*, 1399-1400.

Klebba, P.E., Benson, S.A., Bala, S., Abdullah, T., Reid, J., Singh, S.P., and Nikaido, H. (1990). Determinants of OmpF porin antigenicity and structure. J. Biol. Chem. *265*, 6800-6810.

Koebnik, R. and Braun, V. (1993). Insertion derivatives containing segments of up to 16 amino acids identify surface- and periplasm-exposed regions of the FhuA outer membrane receptor of *Escherichia coli* K-12. J. Bacteriol. *175*, 826-839.

Kreusch, A., Neubuser, A., Schiltz, E., Weckesser, J., and Schulz, G.E. (1994). Structure of the membrane channel porin from *Rhodopseudomonas blastica* at 2.0 A resolution. Protein Sci. *3*, 58-63.

Kreusch, A. and Schulz, G.E. (1994). Refined structure of the porin from *Rhodopseudomonas blastica.* Comparison with the porin from *Rhodobacter capsulatus.* J. Mol. Biol. *243*, 891-905.

Laemmli, U.K. (1970). Cleavage of structural proteins during the assembly of the head of bacteriophage T4. Nature *227*, 680-685.

Locher, K.P., Rees, B., Koebnik, R., Mitschler, A., Moulinier, L., Rosenbusch, J.P., and Moras, D. (1998). Transmembrane signaling across the ligand-gated FhuA receptor: crystal structures of free and ferrichrome-bound states reveal allosteric changes. Cell *95*, 771-778.

Locher, K.P. and Rosenbusch, J.P. (1997). Oligomeric states and siderophore binding of the ligand-gated FhuA protein that forms channels across *Escherichia coli* outer membranes. Eur. J. Biochem. *247*, 770-775.

Loeb, M.R. and Smith, D.H. (1982). Properties and immunogenicity of *Haemophilus influenzae* outer membrane proteins. In *Haemophilus influenzae*: Epidemiology, Immunology, and Prevention of Disease. S.H. Sell and P.F. Wright, eds. (Amsterdam: Elsevier Scence Publishers),

Lugtenberg, B. and van Alphen, L. (1983). Molecular architecture and functioning of the outer membrane of *Escherichia coli* and other gram-negative bacteria. Biochim. Biophys. Acta *737*, 51-115.

Maier, C., Bremer, E., Schmid, A., and Benz, R. (1988). Pore-forming activity of the Tsx protein from the outer membrane of *Escherichia coli*. Demonstration of a nucleoside-specific binding site. J. Biol. Chem. *263*, 2493-2499.

Medeiros, A.A., O'Brien, T.F., Rosenberg, E.Y., and Nikaido, H. (1987). Loss of OmpC porin in a strain of *Salmonella typhimurium* causes increased resistance to cephalosporins during therapy. J. Infect. Dis. *156*, 751-757.

Michel, H. and Oesterhelt, D. (1980). Three-dimensional crystals of membrane proteins: bacteriorhodopsin. Proc. Natl. Acad. Sci. U. S. A. *77*, 1283-1285.

Moeck, G.S., Tawa, P., Xiang, H., Ismail, A.A., Turnbull, J.L., and Coulton, J.W. (1996). Ligand-induced conformational change in the ferrichrome-iron receptor of *Escherichia coli* K-12. Mol. Microbiol. *22*, 459-471.

Mohle-Boetani, J.C., Ajello, G., Breneman, E., Deaver, K.A., Harvey, C., Plikaytis, B.D., Farley, M.M., Stephens, D.S., and Wenger, J.D. (1993). Carriage of *Haemophilus influenzae* type b in children after widespread vaccination with conjugate *Haemophilus influenzae* type b vaccines. Pediatr. Infect. Dis. J. *12*, 589-593.

Morrissey, J.H. (1981). Silver stain for proteins in polyacrylamide gels: a modified procedure with enhanced uniform sensitivity. Anal. Biochem. *117*, 307-310.

Munson, R.J. and Tolan, R.W.J. (1989). Molecular cloning, expression, and primary sequence of outer membrane protein P2 of *Haemophilus influenzae* type b. Infect. Immun. *57*, 88-94.

Nabedryk, E., Garavito, R.M., and Breton, J. (1988). The orientation of beta-sheets in porin. A polarized Fourier transform infrared spectroscopic investigation. Biophys. J. *53*, 671-676.

Nakae, T. (1975). Outer membrane of *Salmonella typhimurium*: reconstitution of sucrose- permeable membrane vesicles. Biochem. Biophys. Res. Commun. *64*, 1224-1230.

Nestel, U., Wacker, T., Woitzik, D., Weckesser, J., Kreutz, W., and Welte, W. (1989). Crystallization and preliminary X-ray analysis of porin from *Rhodobacter capsulatus*. FEBS Lett. *242*, 405-408.

Nikaido, H. (1992). Porins and specific channels of bacterial outer membranes. Mol. Microbiol. *6*, 435-442.

Nikaido, H. (1993). Transport across the bacterial outer membrane. J. Bioenerg. Biomembr. *25*, 581-589.

Nikaido, H. (1994). Difussion of inhibitors across the cell wall. In Bacterial Cell Wall. J.-M. Ghuysen and R. Hakenback, eds. (Amsterdam: Elsevier Science B.V.), pp. 547-558.

Nikaido, H., Nikaido, K., and Harayama, S. (1991). Identification and characterization of porins in *Pseudomonas aeruginosa*. J. Biol. Chem. *266*, 770-779.

Nikaido, H. and Rosenberg, E.Y. (1983). Porin channels in *Escherichia coli*: studies with liposomes reconstituted from purified proteins. J. Bacteriol. *153*, 241-252.

Nikaido, H. and Vaara, M. (1985). Molecular basis of bacterial outer membrane permeability. Microbiol. Rev. *49*, 1-32.

Pautsch, A. and Schulz, G.E. (1998). Structure of the outer membrane protein A transmembrane domain. Nat. Struct. Biol. *5*, 1013-1017.

Pautsch, A., Vogt, J., Model, K., Siebold, C., and Schulz, G.E. (1999). Strategy for membrane protein crystallization exemplified with OmpA and OmpX. Proteins *34*, 167-172.

Przybylski, M., Glocker, M.O., Nestel, U., Schnaible, V., Bluggel, M., Diederichs, K., Weckesser, J., Schad, M., Schmid, A., Welte, W., and Benz, R. (1996). X-ray crystallographic and mass spectrometric structure determination and functional characterization of succinylated porin from *Rhodobacter capsulatus*: implications for ion selectivity and single-channel conductance. Protein Sci. *5*, 1477-1489.

Regelink, A.G., Dahan, D., Moller, L.V., Coulton, J.W., Eijk, P., van Ulsen, P., Dankert, J., and van Alphen, L. (1999). Variation in the composition and pore function of major outer membrane pore protein P2 of *Haemophilus influenzae* from cystic fibrosis patients. Antimicrob. Agents Chemother. *43*, 226-232.

Reid, J., Fung, H., Gehring, K., Klebba, P.E., and Nikaido, H. (1988). Targeting of porin to the outer membrane of *Escherichia coli*. Rate of trimer assembly and identification of a dimer intermediate. J. Biol. Chem. *263*, 7753-7759.

Renkin, E.M. (1954). Filtration, diffusion, and molecular sieving through cellulose membranes. Journal of General Physiology *38*, 225-243.

Sambrook, J., Fritsch, E.F., and Maniatis, T. (1989). Molecular Cloning (A laboratory manual (Cold Spring Harbor: Cold Spring Harbor Laboratory Press).

Schiltz, E., Kreusch, A., Nestel, U., and Schulz, G.E. (1991). Primary structure of porin from *Rhodobacter capsulatus*. Eur. J. Biochem. *199*, 587-594.

Schirmer, T. (1998). General and specific porins from bacterial outer membranes. J. Struct. Biol. *121*, 101-109.

Schirmer, T. and Cowan, S.W. (1993). Prediction of membrane-spanning beta-strands and its application to maltoporin. Protein Sci. *2*, 1361-1363.

Schirmer, T., Keller, T.A., Wang, Y.F., and Rosenbusch, J.P. (1995). Structural basis for sugar translocation through maltoporin channels at 3.1 A resolution. Science *267*, 512-514.

Schmid, K., Schupfner, M., and Schmitt, R. (1982). Plasmid-mediated uptake and metabolism of sucrose by *Escherichia coli* K- 12. J. Bacteriol. *151*, 68-76.

Schoffler, H. and Braun, V. (1989). Transport across the outer membrane of *Escherichia coli* K12 via the FhuA receptor is regulated by the TonB protein of the cytoplasmic membrane. Mol. Gen. Genet. *217*, 378-383.

Schulz, G.E. (1996). Porins: general to specific, native to engineered passive pores. Curr. Opin. Struct. Biol. *6*, 485-490.

Schweizer, M. and Henning, U. (1977). Action of a major outer cell envelope membrane protein in conjugation of *Escherichia coli* K-12. J. Bacteriol. *129*, 1651-1652.

Seki, H., Kasahara, Y., Ohta, K., Saikawa, Y., Sumita, R., Yachie, A., Fujita, S., and Koizumi, S. (1999). Increasing prevalence of ampicillin- resistant, non-beta-lactamase- producing strains of *Haemophilus influenzae* in children in Japan. Chemotherapy *45*, 15-21.

Setlow, J.K., Boling, M.E., Beattie, K.L., and Kimball, R.F. (1972). A complex of recombination and repair genes in *Haemophilus influenzae*. J. Mol. Biol. *68*, 361-378.

Siehnel, R.J., Worobec, E.A., and Hancock, R.E. (1988). Cloning of the *Pseudomonas aeruginosa* outer membrane porin protein P gene: evidence for a linked region of DNA homology. J. Bacteriol. *170*, 2312-2318.

Sikkema, D.J. and Murphy, T.F. (1992). Molecular analysis of the P2 porin protein of nontypeable *Haemophilus influenzae*. Infect. Immun. *60*, 5204-5211.

Sonntag, I., Schwarz, H., Hirota, Y., and Henning, U. (1978). Cell envelope and shape of *Escherichia coli*: multiple mutants missing the outer membrane lipoprotein and other major outer membrane proteins. J. Bacteriol. *136*, 280-285.

Srikumar, R., Dahan, D., Arhin, F.F., Tawa, P., Diederichs, K., and Coulton, J.W. (1997). Porins of *Haemophilus influenzae* type b mutated in loop 3 and in loop 4. J. Biol. Chem. *272*, 13614-13621.

Srikumar, R., Dahan, D., Gras, M.F., Ratcliffe, M.J., van Alphen, L., and Coulton, J.W. (1992). Antigenic sites on porin of *Haemophilus influenzae* type b: mapping with synthetic peptides and evaluation of structure predictions. J. Bacteriol. *174*, 4007-4016.

Sugawara, E. and Nikaido, H. (1992). Pore-forming activity of OmpA protein of *Escherichia coli*. J. Biol. Chem. *267*, 2507-2511.

Towbin, H., Staehelin, T., and Gordon, J. (1992). Electrophoretic transfer of proteins from polyacrylamide gels to nitrocellulose sheets: procedure and some applications. Biotechnology *24:145-9*, 145-149.

Trias, J., Dufresne, J., Levesque, R.C., and Nikaido, H. (1989). Decreased outer membrane permeability in imipenem-resistant mutants of *Pseudomonas aeruginosa*. Antimicrob. Agents Chemother. *33*, 1202-1206.

Tsai, C.M. and Frasch, C.E. (1982). A sensitive silver stain for detecting lipopolysaccharides in polyacrylamide gels. Anal. Biochem. *119*, 115-119.

Turk, D.C. (1982). Clinical importance of *Haemophilus influenzae*. In *Haemophilus influenzae*: Epidemiology, Immunology, and Prevention of Disease. S.H. Sell and P.F. Wright, eds. (Amsterdam: Elsevier Scence Publishers),

Vachon, V., Kristjanson, D.N., and Coulton, J.W. (1988). Outer membrane porin protein of *Haemophilus influenzae* type b: pore size and subunit structure. Can. J. Microbiol. *34*, 134-140.

Vachon, V., Laprade, R., and Coulton, J.W. (1986). Properties of the porin of *Haemophilus influenzae* type b in planar lipid bilayer membranes. Biochim. Biophys. Acta *861*, 74-82.

Vachon, V., Lyew, D.J., and Coulton, J.W. (1985). Transmembrane permeability channels across the outer membrane of *Haemophilus influenzae* type b. J. Bacteriol. *162*, 918-924.

Ward, J.L., Lum, M.K.W., and Bender, T.R. (1982). *Haemophilus influenzae* disease in Alaska: epidemiologic, clinical, and serologic studies of a population at high risk of invasive disease. In *Haemophilus influenzae*: Epidemiology, Immunology, and Prevention of Disease. S.H. Sell and P.F. Wright, eds. (Amsterdam: Elsevier Scence Publishers),

Weig, A., Deswarte, C., and Chrispeels, M.J. (1997). The major intrinsic protein family of *Arabidopsis* has 23 members that form three distinct groups with functional aquaporins in each group. Plant Physiol. *114*, 1347-1357.

Weiss, M.S., Abele, U., Weckesser, J., Welte, W., Schiltz, E., and Schulz, G.E. (1991). Molecular architecture and electrostatic properties of a bacterial porin. Science *254*, 1627-1630.

Weiss, M.S., Kreusch, A., Schiltz, E., Nestel, U., Welte, W., Weckesser, J., and Schulz, G.E. (1991). The structure of porin from *Rhodobacter capsulatus* at 1.8 A resolution. FEBS Lett. *280*, 379-382.

Welte, W., Nestel, U., Wacker, T., and Diederichs, K. (1995). Structure and function of the porin channel. Kidney Int. *48*, 930-940.

Wenger, J.D. (1998). Epidemiology of *Haemophilus influenzae* type b disease and impact of *Haemophilus influenzae* type b conjugate vaccines in the United States and Canada. Pediatr. Infect. Dis. J. *17*, S132-S136

Wenger, J.D., Hightower, A.W., Facklam, R.R., Gaventa, S., and Broome, C.V. (1990). Bacterial meningitis in the United States, 1986: report of a multistate surveillance study. The Bacterial Meningitis Study Group. J. Infect. Dis. *162*, 1316-1323.

Wojtczak, L. (1974). Permeability and other properties of the outer mitochondrial membrane. Rev. Roum. Physiol. *11*, 173-185.